学位論文

Universal scenario of transition to turbulence as an absorbing phase transition
(吸収状態転移として捉える乱流遷移の普遍的なシナリオ)

平成 29 年 12 月博士（理学）申請

東京大学大学院理学系研究科
物理学専攻
玉井 敬一

Ph.D. Thesis
Universal scenario of transition to turbulence as an absorbing phase transition

Keiichi Tamai
(Department of Physics, The University of Tokyo. Student ID: 35-157040)

Academic advisor: Masaki Sano

Thesis Committee:

Akira Ejiri (Chair)

Chikara Furusawa

Fujihiro Hamba

Seiji Miyashita

Hiroshi Noguchi

Submitted on December 20, 2017

Revised on February 1, 2018

Abstract

This dissertation is dedicated to the experimental studies on a transition to turbulence in channel flow, a simple open shear flow between two parallel plates. In open shear flows such as pipe flow and channel flow, laminar flow is known to become turbulent even though the laminar flow is stable against infinitesimal disturbance. Near the onset of sustained turbulence in these flows, the flow is in a state of spatiotemporal intermittency where spatially localized turbulent structure can decay into laminar flow or contaminate adjacent laminar flow to spread, and once the flow becomes completely laminar, it does not become turbulent unless additional disturbance is exerted to the flow. This process is qualitatively similar with the dynamics of the very simple stochastic model of the directed percolation (DP), which is one of the simplest model exhibiting a phase transition to an absorbing state (a state that systems can enter but cannot escape from). Indeed, it has long been conjectured that transitions to turbulence via spatiotemporal intermittency share the same universal features with DP (that is, the transitions fall into the DP universality class). A primary purpose of this dissertation is to directly examine, in a case of channel flow, whether the transition to turbulence falls into the DP universality class.

Keeping the primary purpose in mind, the former half of this thesis is devoted to clarify a suitable methodology to experimentally measure the critical exponents characterizing an absorbing phase transition. Given that the most earlier experimental works concerning a possible relation to the DP universality class have relied on probability distribution of lenghs/durations of intervals of local inactive state in steady state to estimate the correlation length/time of the system, we first numerically study the interval distribution in the contact process, one of the most well-known mathematical models in the DP universality class. We demonstrate that the conventional method may yield substantially biased results if one simply constructs a histogram from the data acquired within a short observation window to estimate the distribution. This is one of the possible reasons why experimental realizations of the DP universality class had been so rare despite the theoretical robustness of this class. We also employ an estimator for the interval distribution which properly takes account of censoring and sampling bias. As a result, we show that the interval distributions for various values of the control parameter, when estimated and rescaled in the suitable way, collapse onto a single curve.

In the latter half, we present the results of the characterization of a transition to turbulence in channel flow in terms of an absorbing phase transition. Since localized turbulent structures are advected by a mean flow and eventually goes out from the observation area, we drive the system at the boundary by a grid at the inlet. We first study how the critical phenomena of the DP universality class is affected by the advection and the boundary condition. A new model which whose advection strength can be arbitrarily controlled is introduced for this purpose. We demonstrate, through a combination of numerical simulation on the model and scaling argument, a correlation length and a correlation time can be respectively measured through a characteristic decay time of a temporal interval distribution and a characteristic decay length of an order parameter. Next we show the experimental results on the measurements of the critical exponents in the transitional channel flow, where all the exponents are found to be in a reasonable agreement with the spatially two-dimensional DP universality class. Furthermore, it turns out the interval distributions for various Reynolds number can be collapsed into a single universal curve if we rescale the data in a way required by the DP universality class. These findings constitute experimental evidences suggesting that the transition falls into the DP universality class.

Acknowledgement

First of all, the author offers his sincerest gratitude to Professor Masaki Sano for supervising the author for five years. None of the works presented in this thesis could have been accomplished without his deep insight into physics, experience with experimental techniques, warm support, patience and generosity.

The author is grateful to Professor Kazumasa A. Takeuchi, who kindly introduced the realm of the non-equilibrium scaling laws to the author. The author was substantially influenced by his way of thinking and of performing researches. The author also thank Professor Tetsuya Hiraiwa, who gave me many useful pieces of advice. His experience in theoretical physics and his vision considerably helped the author in various ways. The author takes this opportunity to thank his former and present colleagues in Sano Group for their fruitiful discussions, influence through their work and everyday conversations, which made the five years of his graduate school life enjoyable.

Financial support by the Japan Society for Promotion of Science (JSPS) is also gratefully acknowledged, enabling the author to buy equipments necessary for experiments and to travel in and outside the country to have a fruitiful interaction with researchers worldwide.

Last but not least, the author would like to thank my family for their continuing support, both financially and mentally.

Contents

List of Figures

List of Tables

Chapter 1

General Introduction

1.1 General background

Ultimate goal of physics as a branch of basic science is "to find a unified set of laws governing matter, motion, and energy at small (microscopic) subatomic distances, at the human (macroscopic) scale of everyday life, and out to the largest distances (e.g., those on the extragalactic scale)" [100]. Progress of modern physics has been made by repeatedly applying a paradigm which consists of (a) properly specifying a subset of natural phenomena to describe, (b) developing a theory which exploits an essense of the phenomena, and then (c) testing the theory by experiments. Owing to the remarkable progress, nowadays we can describe very wide variety of natural phenomena with modern physics in mind: At a microscopic scale, we know that the fundamental forces of the universe and properties of known elementary particles can be reasonably well described by the celebrated Standard Model (although it still falls short with being so-called *theory of everything*). At a macroscopic level, on the other hand, we are now able to directly observe black holes by making use of the gravitational waves.

Nevertheless, there are considerable amount of open problems which await for theoretical description. For example, studies on so-called complex systems (including biological ones) has still been at an early stage. One of key difficulties in complex systems is that a set of equations which is expected to describe such a system is typically non-linear (if known): Due to the non-linearity, it is difficult in general to describe how the solution behaves like.

1.1.1 Universal laws in non-linear systems

Physicists had spent very hard time with non-linear systems. The only way to systematically analyze highly non-linear systems had long been so-called perturbation theory: That is, one starts from linear, solvable model and then expand the quantities of interest in terms of formal power series. From the tedius (and sometimes inaccurate) calculation, it was

not obvious at all whether universal description insensitive to details of the system can be gained.

The situation drastically changed with seminal works by Wilson [101, 102] and subsequently by Feigenbaum [32]: Wilson applied the theory of renormalization group, which was originally invented as a tool to get rid of unphysical divergences, into critical phenomena, with self-similarity in his mind. Feigenbaum discovered that the universal constant, nowadays known as Feigenbaum constant, emerges as a system experiences a chain of period-doubling bifurcations to chaos. These works posed massive impact on the community at that time, as James Gleick, a famous historian of science, put it [37]:

> *"It was a very happy and shocking discovery that there were structures in non-linear systems that are always the same if you looked at them the right way."*

Nowadays these are some of the indispensable tools to deal with non-linear systems.

1.1.2 Transition to turbulence as a testbed of concepts

Studies on motion of fluids, in particular the transitions from laminar flow to turbulent flow has served as a great testbed for ideas in the study of non-linear systems, ever since the pioneering work by Reynolds (Fig. 1.1) [80]: Concepts in theoretical physics have consisderably helped understanding the transitions, and the complex motion of fluids has provided an inspiration for new general concepts. Examples of the relations in early ages include an enormous success in application of linear stability analysis to the flow between two cylinders by G. I. Taylor [96], and the discovery of chaos by E. N. Lorenz [65].

When the aforementioned universality in period-doubling bifurcations has been proposed, it took only 4 years to be experimentally tested in Rayleigh–Bénard convection (confined flow heated from below): Albert Libchaber and his coworkers performed a set of experiments on the convection in mercury and in liquid helium [63, 67], and they studied the onsets of period-doubling in time evolution of the temperature. As a result, the ratio of the Rayleigh number at the different onset is very close to the value predicted by Feigenbaum. Thus the universal route to turbulence in confined flow was identified as a period-doubling route to chaos.

Nearly at the same time, however, it has also been turned out that the situation is substantially more complex in shear flows such as pipe flow and channel flow. In these flows, transition to turbulence has been experimentally observed even though the laminar flow is linearly stable at the Reynolds number under investigation (Tab. 1.1). It means that the conventional scenario of transition to turbulence, which assumes linear instability of a regular flow, no longer seems to be very relevant.

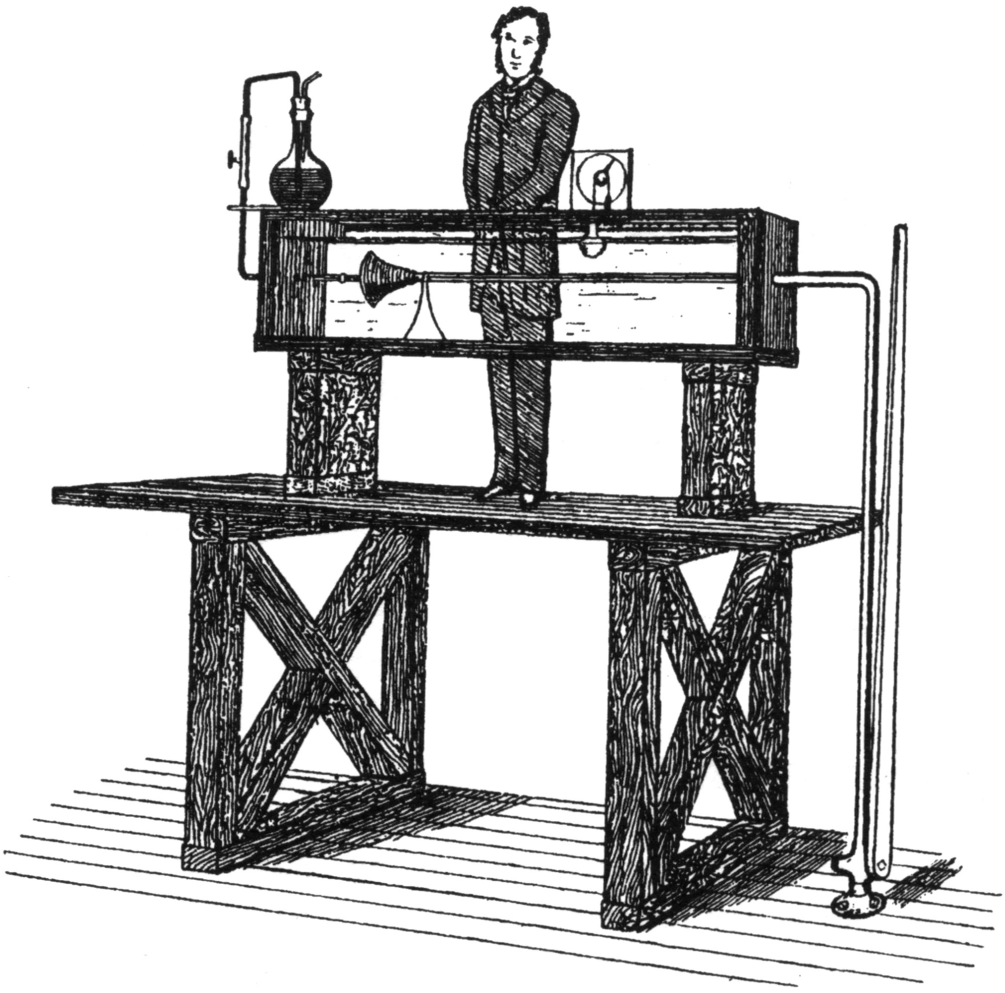

Figure 1.1: Pioneering work by Reynolds on transition to turbulence in pipe flow [80]. The picture is in a public domain.

Table 1.1: Critical Reynolds number for typical shear flow. Re_g is the empirically known threshold for the transition to turbulence, Re_c is the critical Reynolds number in terms of linear stability theory.

	Re_g	Re_c
Pipe flow	2,040 [3]	∞ [83]
Plane Couette flow	$\sim$325 [12]	∞ [81]
Plane Poiseuille flow	$\lesssim$1,000 [20]	5,772 [75]

Important progress was made in the beginning of the 21st century, by focusing on statistical properties of a localized turbulent structure in pipe flow. The localized turbulent structure (Fig. 1.2a), often called a "puff" in earlier literatures, can either decay or split as it propagates downstream. Although the puff itself had been recognized in as early as 1970s [103], it was not until 2010 that experiments and direct numerical simulation (DNS) with very long precise pipe and extensive accumulation of statistics enabled a group headed by Björn Hof to reveal that the probability $P_{\mathrm{d}}, P_{\mathrm{s}}$ for a puff to decay or split before time t obeys exponential distribution (Fig. 1.2b and Fig. 1.2c, [3, 4]):

$$P_{\mathrm{d}}(\mathrm{Re}, t) = 1 - \exp\left(-\frac{t - t_0}{\tau_{\mathrm{d}}(\mathrm{Re})}\right), \quad P_{\mathrm{s}}(\mathrm{Re}, t) = 1 - \exp\left(-\frac{t - t_0}{\tau_{\mathrm{s}}(\mathrm{Re})}\right). \tag{1.1}$$

The typical lifetime $\tau_{\mathrm{d}}, \tau_{\mathrm{s}}$ was found to coincide at the Reynolds number of 2,040 (Fig. 1.2d, [3]) , which is very close to the critical Reynolds number suggested in the 19th century. From their finding, one can gain an important insight into transition to sustained turbulence in pipe: Competition between a puff decaying and a puff splitting is relevant for describing the transition.

Meanwhile, the discovery by Avila *et al.* posed a difficult puzzle: The fact that spatial proliferation plays a relevant role means that one has to explicitly take spatial degree of freedom into account in order to properly describe the transition. In other words, one has to tackle a problem of transitions to *spatiotemporal* chaos. Is it, then, possible to consider a universal scenario on the transition?

1.1.3 Possible relation to absorbing phase transitions

A possible clue in quest of universal scenario of the transition to turbulence in open shear flow is an analogy to a simple stochastic process called the contact process [42]. In the contact process, each site can take either active or inactive state, and active site can deactivate or spread the activity to its neighbor. Then depending on the rate of spreading, activity may eventually die out or survive forever. In fact, theoretical studies and numerical simulation show that this model exhibits critical phenomena which are characterized by universal critical exponents. As it was the case with the Ising model, the set of universal critical exponents enables one to define a universality class, and the contact process is known to fall into the directed percolation (DP) universality class. The key feature of the DP universality class is that it has transition into an absorbing state, a state which systems can enter but cannot escape from. Recalling that a laminar flow is linearly stable and hence it has a good analogy to an absorbing state, one may naturally expect that the transition fall into the DP universality class, as conjectured by Yves Pomeau in 1986 [79].

It must be emphasized, however, that it is not obvious at all whether the transition indeed belongs to the DP universality class. First, the Navier–Stokes equation which governs the motion of fluids is a complex non-linear partial differential equation and hence it is totally

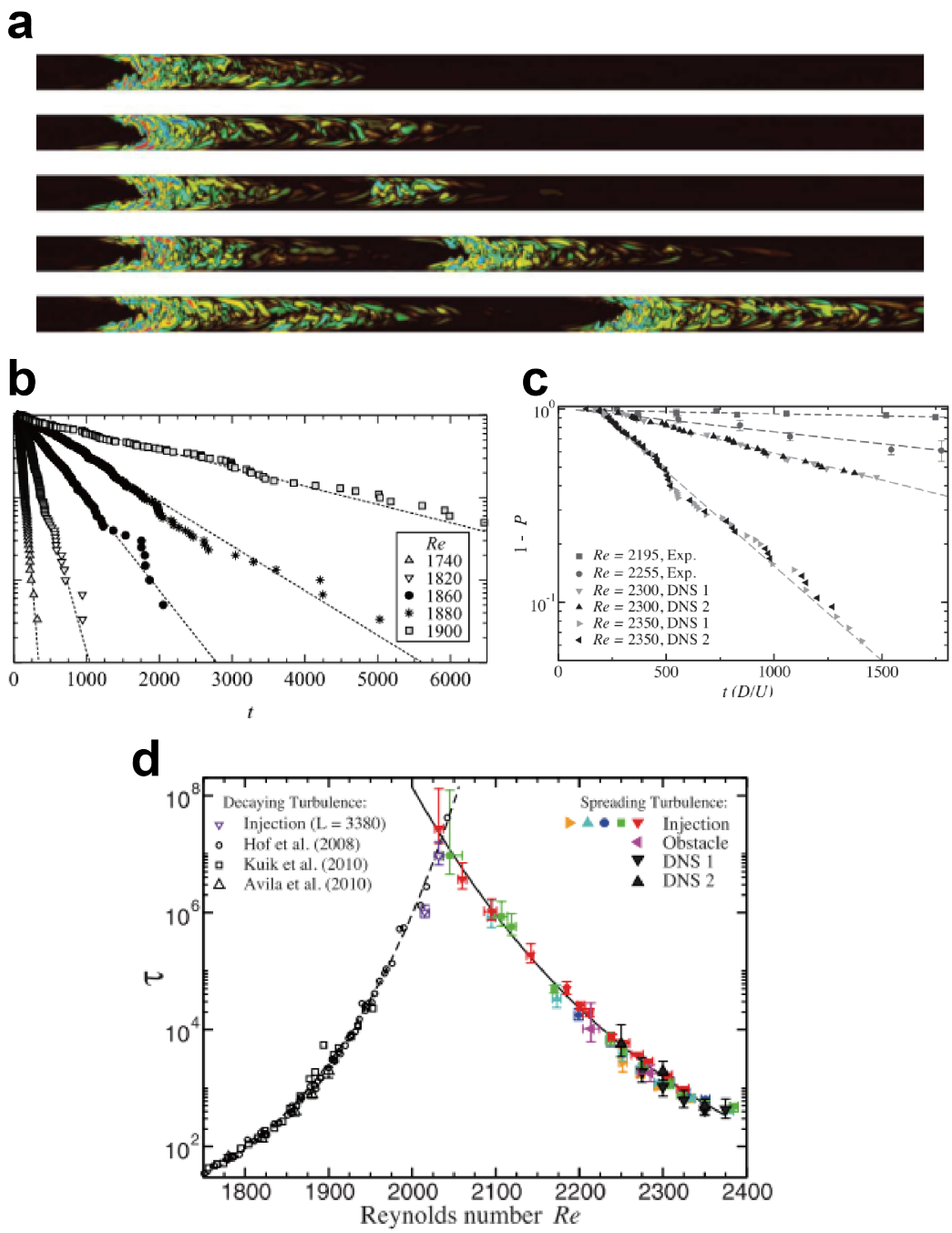

Figure 1.2: Turbulent puffs in pipe flow and their lifetime. **a**: Turbulent puff visualized in direct numerical simulation at $\mathrm{Re} = 2300$. Figure is adopted from Ref. [3]. **b**: The probability that a puff does not decay up to time t. Figure is adopted from Ref. [4]. **c**: The probability that a puff remains "in equilibrium". Figure is adopted from Ref. [3]. **d**: Lifetime of a puff with respect to Reynolds number. Figure is adopted from Ref. [3].

different from a simple stochastic model. Then it is possible that the dynamics which is not taken account of by the simple stochastic model affects the critical phenomena, although the DP universality class is believed to be extremely robust. Moreover, earlier experimental studies suggest that the DP universality class may be rather fragile in reality despite its robustness in theory: Many experimental works reported significant deviation from the DP universality class. Given this, one cannot tell *a priori* whether the transitions to turbulence in open shear flows indeed belong to the DP universality class, just because the phenomenology is similar with the contact process.

1.2 Objectives of this thesis

In the author's opinion, clarifying whether the transition possesses universal features is important for two reasons. If the transition is found to possess universal features, it implies that one can reasonably expect that one can describe the transition in terms of the universal scenario which does not depend on details of the system such as geometry of the flow. Conversely, if the universal scenario is ruled out by experimental results, it means that one has to rely on a system-specific approach to understand the transition. Hence examining the universal scenario provides us a significant clue on how one should understand the transition. Another reason for the significance of the examination of the universal scenario is that it gives a deeper insight into a question of how far one can expect the notion of universality in absorbing phase transitions to be relevant for describing natural phenomena. In other words, the examination poses an implication on whether the notion of universality is applicable for a wide variety of physical systems we observe in reality or it is just an oversimplified picture so that it is applicable only when some special conditions are met. Thus, the author believes that examining the universal scenario constitutes a significant step toward complete understanding of complex phenomena out of equilibrium, including transitions to turbulence.

That having said, one has to face with several difficulties when addressing the above issue. First, it has not been clear how one can put the concepts of critical phenomena in absorbing phase transitions into experimental test. Although the critical exponents are natural characterizers of the transition, one has to consider carefully about how one measures them correctly; as will be demonstrated in Chapter 3 of this thesis, one may obtain significantly biased results if one measures the exponents in a naïve way[1]. Second, one has to perform experiments or direct numerical simulation using very large system in order to make the system close to "thermodynamic limit." This requirement makes the direct measurements of the critical exponents costly. Presumably, these difficulties has been

[1]Note that, paraphrazing James Gleick (see Section 1.1.1), one cannot catch the sign of universality in non-linear systems unless one looks at them the right way.

keeping the universal scenario of transitions to turbulence from being directly examined for over 30 years.

In this thesis, we overcome the aforementioned difficulties and directly examine the universal scenario of transitions to turbulence by performing a series of experiments in a very large channel flow. In the former half of this thesis, we propose the method to experimentally measure the critical exponents. We point out that the conventional method does not properly take account of the fact that one is observing the system under a finite observation window in both space and time, and hence it is likely to produce biased results. We successfully avoid the bias by employing a technique of statistical analysis, which was originally proposed in a context of medical follow-ups. In the latter half, we present the results of the experimental characterization of the transition to turbulence in channel flow. We measured four critical exponents (three of which is independent from each other) and examined one universal scaling relation developed in the former half of this thesis, all in agreement in the spatially two-dimensional DP universality class. The experimental results presented in this thesis suggest that the transition to turbulence in channel flow indeed falls into the DP universality class.

1.3 Organization of this thesis

The rest of this thesis is organized as follows: In Chapter 2, universal features of the absorbing phase transitions are discussed. Particular emphasis is placed on similarity and difference in continuous phase transition at equilibrium, robustness of the universality class in absorbing phase transition, and experimental realizations. In Chapter 3, we discuss how the universal features of absorbing phase transitions can be probed numerically and experimentally. After seeing the substantial difference in these two, validity of the experimental method is validated numerically. In Chapter 4, we discuss how the critical phenomena of absorbing phase transitions can be affected by a combination of fixed boundary conditions and advection. In Chapter 5, we present our experimental results on a huge channel flow. We conclude the thesis with brief remark on future perspectives in Chapter 6.

Chapter 2

Universality of Absorbing Phase Transitions

Related publication by the author: None.

Primary purpose of this chapter is to provide readers prior knowledge about absorbing phase transitions necessary for reading the rest of this thesis. Since there are already thousands of publications related to this subject, exhaustive review on them is far beyond the scope of this thesis: See e.g. Refs. [44, 45] for more detailed overview.

2.1 Basic features of absorbing phase transitions

Theory of absorbing phase transitions mainly concerns transitions to an absorbing state, which systems can enter, but cannot escape from. Absorbing phase transitions are genuinely non-equilibrium in a sense that they do not obey the detailed balance condition

$$p_{\sigma_{\rm abs}\to\sigma}P_\infty(\sigma_{\rm abs}) \neq p_{\sigma\to\sigma_{\rm abs}}P_\infty(\sigma), \tag{2.1}$$

and therefore they cannot be associated with equilibrium models (here, σ, $\sigma_{\rm abs}$, $p_{\sigma\to\sigma'}$ and $P_\infty(\sigma)$ denote configuration, absorbing state, transition rate from the configuration σ to the configuration σ' and probability to find the configuration σ at the stationary state, respectively). Because of the non-equilibrium character of the transition, similarity and difference from phase transitions at equilibrium is of central interest in statistical mechanics.

Besides the conceptual interest, absorbing phase transitions are believed to be ubiquitous in Nature. Let us consider a wildfire for example: In a wildfire, some trees are on fire while others are not (left hand side of Fig. 2.1a), and fire may go out or spread to trees nearby. However, once fire becomes extinct (right hand side of Fig. 2.1a), a wildfire rarely ignites spontaneously, hence the forest in absence of fire naturally corresponds to an absorbing phase. One can find similar correspondence in various contexts such as synchronization of locally coupled oscillators [1, 6], spatiotemporal intermittency (spatial coexistence of

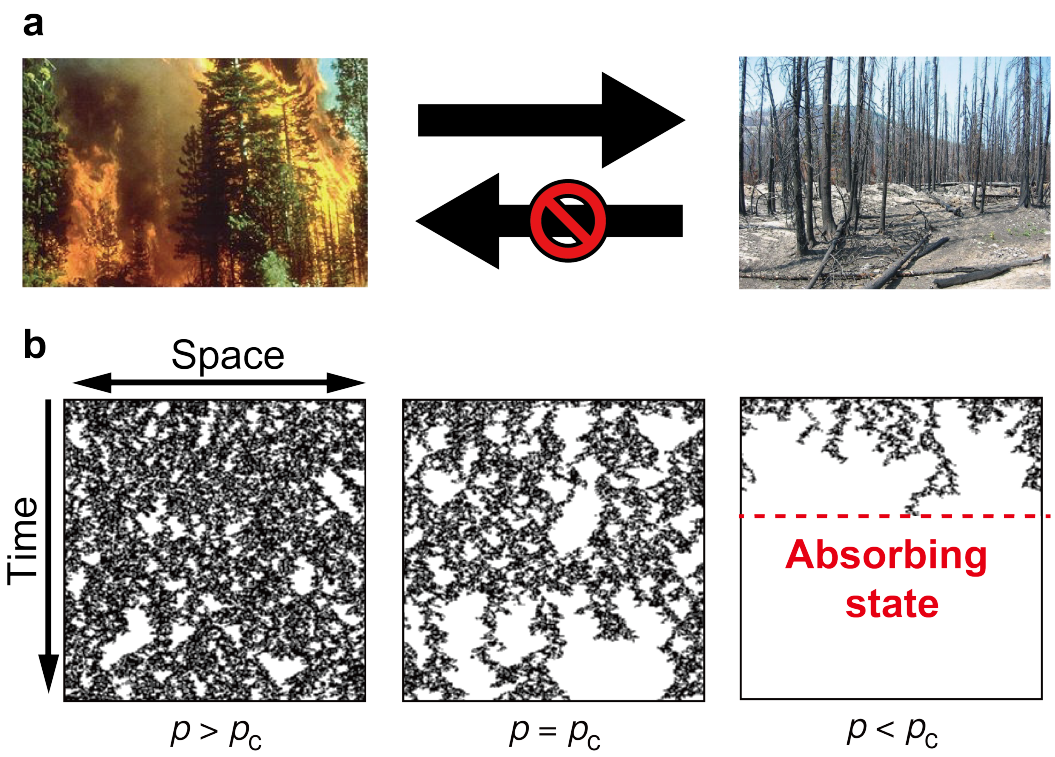

Figure 2.1: An example of absorbing phase transitions in Nature and mathematical models. **a**: Once fire becomes extinct (right hand side), a wildfire rarely ignites spontaneously, hence the forest in absence of fire naturally corresponds to an absorbing phase. Both pictures are in a public domain. **b**: Absorbing phase transition in a mathematical model (directed percolation).

local turbulent state and laminar one) [79] and even spreading of epidemics [42], and once formulated in mathematical models, the models also exhibit absorbing phase transitions (Fig. 2.1b). Thus, it is natural to believe that studying absorbing phase transition may provide useful insight into a wide subset of natural phenomena.

Vast theoretical and numerical efforts have revealed that absorbing phase transitions share many features in common with phase transitions in equilibrium. Considerable amount of models have been found to exhibit *continuous* transition to an absorbing state. Moreover, it also turns out that physical quantities such as order parameter and correlation length exhibit power-law behavior in a vicinity of the critical point. This is quite analogous to what one finds in the celebrated Ising model, where magnetization M and correlation length ξ exhibit a power-law behavior and its exponent is universal in a sense that it depends only on fundamental properties of a system such as number of dimensions and symmetry:

$$M \sim (T_c - T)^{\beta}, \quad \xi \sim |T_c - T|^{-\nu}. \tag{2.2}$$

As expected from the analogy, the exponents characterizing continuous transitions to ab-

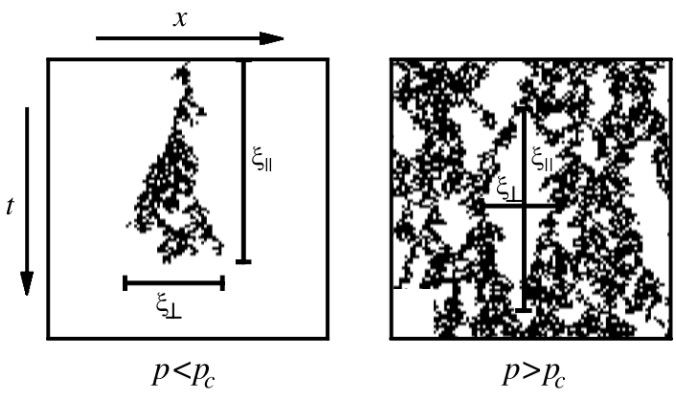

Figure 2.2: Physical meaning of a correlation length $\xi_\perp$ and a correlation time $\xi_{||}$. The figure is adopted from Ref. [45].

sorbing state turn out to be universal. This universality enables one to classify enormous number of systems exhibiting absorbing phase transitions into a rather small number of universality classes [74].

Nevertheless, absorbing phase transitions are indeed crucially different from equilibrium ones in some respects. The crucial differences stem from the fact that *time* is involved as an independent degree of freedom. First, stationary state of models with absorbing phase transitions are naturally characterized by two different scales, namely a correlation length $\xi_\perp$ and a correlation time $\xi_{||}$. Roughly speaking, the correlation length and the correlation time respectively represent typical lateral size and lifetime of a cluster originating from an initially isolated activity averaged over many independent realizations in a subcritical phase (where the system eventually falls into an absorbing state) whereas they represent typical size and duration of an inactive cluster in supercritical phase (Fig. 2.2). These lengthscales diverge close to criticality as

$$\xi_\perp \sim |p - p_c|^{-\nu_\perp}; \quad \xi_{||} \sim |p - p_c|^{-\nu_{||}} \tag{2.3}$$

and the associated critical exponent $\nu_\perp$ and $\nu_{||}$ are different in general (where p represents a control parameter of the system and p_c represents the critical point). Somewhat less obvious is that there are two essentially different ways to define an "order parameter" so that it takes non-zero value in an "active" phase and vanishes in an absorbing phase: On one hand, density of active sites at stationary state ρ_∞ corresponds to the probability that a site belongs to an infinite cluster which was generated in the past at $t = -\infty$ from a fully active state. On the other hand, one can also consider the probability $P_{\text{surv},\infty}$ that an isolated active site given at $t = 0$ will extend to $t = +\infty$. In other words, ρ_∞ probes the past whereas $P_{\text{surv},\infty}$ probes the future. Hence they behave differently unless the dynamic rules are symmetric under time reversal, and they are expected to exhibit a power-law scaling

$$\rho_\infty \sim (p - p_c)^\beta, \quad P_{\text{surv},\infty} \sim (p - p_c)^{\beta'}, \tag{2.4}$$

with generally different exponents β and β'. Thus stationary state of models with absorbing phase transitions are characterized by four independent critical exponents $(\beta, \beta', \nu_\perp, \nu_{||})$ without any further restrictions, in remarkable contrast with equilibrium phase transitions.

Regarding the difference of phase transitions out of equilibrium from those in equilibrium, it is interesting to note that absorbing phase transitions also share similar characteristics with *first-order* phase transitions in equilibrium. One prominent example is possible presence of hysteresis. To see this, let us consider gradually changing the control parameter from below the critical point to above. Ideally, the system never escapes from an absorbing state and hence the density of active sites remains to be zero during the whole procedure. In practice, however, small but non-vanishing disturbance which is experimentally inevitable may cause "spontaneous" nucleation of activity. Once the activity is nucleated above the critical point, it is likely to spread quickly over the entire system, eventually yielding the stationary value of the order parameter[1]. In other words, an absorbing state is metastable above the critical point, and hence absorbing phase transitions are rather similar to first-order phase transitions in equilibrium than second-order ones in that respect. Meanwhile, the order parameter decreases continuously to zero as the control parameter is changed from above the critical point to below (assuming (2.4) holds) and therefore absorbing phase transitions can be continuous. The argument given here may be interpreted as a warning not to give a statement about the order of a phase transition out of equilibrium based only on qualitative observation of it.

2.2 Theoretical treatment of absorbing phase transitions

2.2.1 Phenomenological scaling theory

One of the most remarkable results of the theory of equilibrium critical phenomena is that, once we have all the independent critical exponents within the universality class, then the critical behavior of the other physical quantities can be described in terms of those exponents through suitable scaling relations. For example, the critical behavior of the specific heat C and susceptibility χ above the critical temperature

$$C \sim (T - T_c)^{-\alpha}, \quad \chi \sim (T - T_c)^{-\gamma} \tag{2.5}$$

can be described in terms of the critical exponents β, δ associated with the critical phenomena of magnetization

$$M \sim (T_c - T)^{\beta} \; (T \leq T_c), \quad M \sim |H|^{1/\delta} \; (T = T_c) \tag{2.6}$$

[1]Indeed, a model exhibiting a continuous absorbing phase transition exhibits hysteresis when a small probability h that an inactive site turns active is assigned to the model [93].

(where H denotes the strength of external magnetic field) by the following scaling relations:

$$\alpha + 2\beta + \gamma = 2, \quad \gamma = \beta(\delta - 1). \tag{2.7}$$

Given this, it is tempting to consider how one can find similar scaling relations in critical phenomena of absorbing phase transitions. As we will see in the following, the phenomenological scaling theory provides us a general framework to accomplish this task.

The phenomenological scaling theory is based on an assumption that critical phenomena can be characterized in terms of only two diverging lengthscales, namely a correlation length $\xi_\perp$ and a correlation time $\xi_{||}$. As a starting point, we assume that multiplicative change of the deviation ε from the critical point

$$\varepsilon \mapsto \Lambda\varepsilon \tag{2.8}$$

rescales the order parameter and the correlation lengths by

$$\rho \mapsto \Lambda^\beta \rho; \quad P_{\text{surv}} \mapsto \Lambda^{\beta'} P_{\text{surv}}; \quad \xi_\perp \mapsto \Lambda^{-\nu_\perp}\xi_\perp; \quad \xi_{||} \mapsto \Lambda^{-\nu_{||}}\xi_{||}, \tag{2.9}$$

where ρ and P_{surv} respectively denote the density of active sites and survival probability of an active cluster generated from an isolated active site. The following, for instance, immediately follows from the assumption:

$$\rho(\Lambda^{-\nu_{||}}t, \Lambda^{-\nu_\perp}\boldsymbol{r}; \Lambda\varepsilon) = \Lambda^\beta \rho(t, \boldsymbol{r}; \varepsilon). \tag{2.10}$$

Since choice of the factor Λ is arbitrary, one can choose Λ so that one of the arguments becomes constant. For example, if we substitute $\Lambda = t^{1/\nu_{||}}$ into (2.10), we find

$$\rho(t, \boldsymbol{r}, \varepsilon) = t^{-\beta/\nu_{||}} f(\boldsymbol{r}/t^{1/z}, \varepsilon t^{1/\nu_{||}}) \quad \text{where} \quad z := \nu_{||}/\nu_\perp. \tag{2.11}$$

Likewise, we assume that all other physical quantities have to be rescaled by a power law with a suitable exponent. Key ingredient of the theory, then, is to determine the suitable exponent from *phenomenological* considerations. To see this, let us consider scaling properties of the two-point correlation function:

$$G(\Delta t, r, \tau) := \langle \rho(\boldsymbol{r}_1, t_1)\rho(\boldsymbol{r}_2, t_2)\rangle, \tag{2.12}$$

where $\Delta t = t_2 - t_1$, $r = |\boldsymbol{r}_2 - \boldsymbol{r}_1|$ and $\langle \cdots \rangle$ denotes the ensemble average. Although the correlation function $\langle \rho(\boldsymbol{r}_1, t_1)\rho(\boldsymbol{r}_2, t_2)\rangle$ depends on five parameters $(\boldsymbol{r}_1, \boldsymbol{r}_2, t_1, t_2, \tau)$ in general, translational invariance in space and time allows one to represent it in only three parameters. In the phenomenological scaling theory, the following scaling form for $G(\Delta t, r, \varepsilon)$ is assumed:

$$G(\Delta t, r, \varepsilon) = \Lambda^{-\kappa} G(\Lambda^{-\nu_{||}}\Delta t, \Lambda^{-\nu_\perp} r, \Lambda\varepsilon). \tag{2.13}$$

Substituting $\Lambda = \varepsilon^{-1}$ into (2.13), one finds

$$G(\Delta t, r, \varepsilon) = \varepsilon^{\kappa} G(t/\varepsilon^{-\nu_{||}}, r/\varepsilon^{-\nu_{\perp}}, 1). \tag{2.14}$$

Considering the active steady state and taking a limit of long distance $r \to \infty$, then the two points can be regarded as independent so that $\lim_{r\to\infty} G(\Delta t, r, \varepsilon) = \rho^2 \sim \varepsilon^{2\beta}$. Hence consistency with (2.14) requires

$$\kappa = 2\beta. \tag{2.15}$$

We employ the phenomenological scaling theory whenever necessary in what follows.

2.2.2 Field-theoretical methods

Field-theoretical renormalization group theory has been one of the most powerful analytical tool to study critical phenomena. As we will argue below, this is also the case for study of absorbing phase transitions. Although the field-theoretical approach does not give accurate predictions on critical exponents (and hence it is rather of limited interest from a quantitative viewpoint), it offers a deep insight into the origin of universality and justification of scaling relations [44].

A standard starting point for the field-theoretical methods is the effective Langevin equation describing time evolution of the order parameter $\rho(\boldsymbol{x}, t)$. The effective Langevin equation for a system with an absorbing phase transition typically consists of a deterministic part and a stochastic *multiplicative* noise term $\zeta(\boldsymbol{x}, t)$. Multiplicativity of the noise term ensures the presence of an absorbing state: Amplitude of the noise is zero if the system is in an absorbing state. For a given Langevin equation, one may first perform a dimensional analysis to clarify relevance of the noise. A key requirement in the dimensional analysis is that the system is invariant under the following dilation at the critical point:

$$x \mapsto \Lambda x; \quad t \mapsto \Lambda^z t; \quad \rho \mapsto \Lambda^{-\psi}\rho; \quad \text{where} \quad z = \nu_{||}/\nu_{\perp}, \psi = \beta/\nu_{\perp}. \tag{2.16}$$

Also the noise should be rescaled by a suitable exponent χ so that the noise is scale invariant.

$$\zeta \mapsto \Lambda^{\chi}\zeta. \tag{2.17}$$

Provided that z, β and χ are obtained, one can track how the coefficient of each term in the effective Langevin equation changes under the dilation in order to determine whether the noise term is relevant for the critical phenomena. Typically, there is a certain upper critical dimension d_c such that the noise is irrelevant if the spatial dimension d is larger than d_c ($d > d_c$) and relevant if $d < d_c$.

If the spatial dimension d of a system is below the upper critical dimension d_c, mean-field theory no longer provides quantitatively accurate predictions, and the critical exponents generally depend on d. In that case, perturbative expansion is usually performed to obtain the critical exponents in powers of $\epsilon(:= d_c - d)$ [50].

2.3 Directed percolation universality class

2.3.1 Basic features of directed percolation

Among the universality classes of absorbing phase transitions, the most fundamental one is that of *directed percolation*. Directed percolation (DP) was originally proposed by Broadbent and Hammersley in 1957 to study how the random properties of a porous medium influence the percolation of a fluid through it [14]. In this model, the medium is modelled by a regular lattice of interconnecting paths, each of which is independently assigned a probability p to be open (that is, to be wide enough for the fluid to pass through). Given the porous medium and a source, the fluid percolates through the media *in a permitted direction*. Interpretation of the direction is arbitrary: While this is naturally understood as the direction of gravity when considering the porous medium, it is often useful to regard the direction as that of time if one is interested in applying this framework to describe spatiotemporal dynamics (as we will see in Section 2.3.3, DP can also be interpreted as reaction-diffusion process). Each site is said to be *wet* if it is connected with source by open paths, and to be *dry* otherwise. Schematic representation of DP for square lattice is shown in Fig. 2.3.

Natural question is when and how the medium becomes permeable as p is gradually increased, although the medium is obviously impermeable when $p = 0$ and permeable when $p = 1$. Extensive numerical simulation suggested that the DP exhibits continuous phase transition at a highly non-trivial critical point ($p_c = 0.644700185(5)$ for a square lattice [55], for example): All the active clusters are finite below the critical point whereas there is non-vanishing probability $P_{\mathrm{surv},\infty}$ that wet sites constitute an infinite cluster, and the probability grows continuously from zero. Later, the continuity of the transition was rigorously established in 2002 [40].

While DP is quite similar with its "isotropic" counterpart in construction (only one difference being presence of a permitted direction), resulting cluster of wet sites is totally different. As expected from the construction, the cluster is characterized by two different lengthscales, one in a direction parallel with the permitted one, and the other in the perpendicular direction. Another important difference is whether it is related to phase transition in equilibrium: Isotropic percolation can be exactly mapped to the *equilibrium* q-state Potts model (generalization of the Ising model with q different values of the lattice variables) in a limit of $q \to 1$ [33, 34], but a layer with no wet site in DP corresponds to an absorbing phase and therefore DP cannot be mapped to any equilibrium models. As a natural consequence, the critical behavior of DP is characterized by different critical exponents from isotropic one. In particular, precise numerical estimations [54, 98] summarized in Tab. 2.1 suggest that the critical exponents of DP may be irrational, and hence that DP might be exactly unsolvable.

Nevertheless, one could extract some important properties in a rigorous way with a help

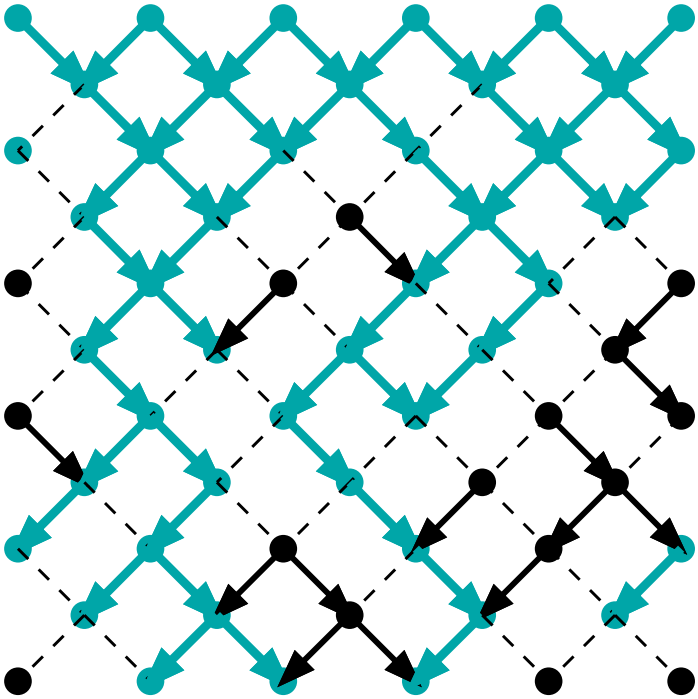

Figure 2.3: Schematic representation of DP in a square lattice. Open path is represented by a solid arrow whereas closed path is represented by a dashed line. Source is given at the top of the figure, and wet sites are colored in blue.

Table 2.1: Critical exponents of the DP universality class. Number in parentheses indicate uncertainty in the last digit claimed by the authors of each work. The column entitled "MF" shows respective critical exponent obtained via mean-field theory (See Section 2.3.3).

Spatial dimension d	$d = 1$ [54]	$d = 2$ [98]	$d = 3$ [98]	MF
β	0.276486(8)	0.580(4)	0.818(4)	1
$\nu_\perp$	1.096854(4)	0.729(1)	0.582(2)	1/2
$\nu_{\|\|}$	1.733847(6)	1.287(2)	1.106(3)	1

of a concept of duality [64], even if the system might be exactly unsolvable. In DP, the duality can be easily understood by simple geometrical argument. Important observation from Fig. 2.3 is that if a site A is connected with another site B through the directed paths, then they are still connected even when the direction of all the paths is reversed (physically this corresponds to time-reversed realization), and vice versa. Hence, if the time-reversed realization is started from fully wet initial condition, the resulting wet site at the bottom layer corresponds to the site which generate a cluster which percolates through the medium at the original realization, leading to the identity

$$\rho(t) = P_{\text{surv}}(t), \tag{2.18}$$

meaning that

$$\beta = \beta'. \tag{2.19}$$

It has to be noted, however, that the identity (2.18) is one of special properties of DP and hence does not necessarily hold for other models in the DP universality class. Nevertheless, concept of duality is still valid and the following asymptotic relation generically holds:

$$P_{\text{surv}}(t) \simeq \mu^2 \rho(t), \tag{2.20}$$

where μ^2 is a suitable (non-universal) proportionality factor between $P_{\text{surv}}(t)$ and $\rho(t)$. Thus the DP universality class is characterized by only three independent critical exponents instead of four as in absorbing phase transitions in general.

2.3.2 Other lattice models in the DP universality class

Recalling the notion of universality we have argued in Section 2.1, it is natural to expect that the same critical exponents can be found in different models as long as they are reasonably similar to DP. As we shall see below, more general models and some models proposed in a different context also fall into the DP universality class.

One of the most important generalization of DP was proposed by Domany and Kinzel [29]. Their automaton ("the DK automaton" hereafter) is of course similar to the original DP, but this time each site refers to the nearest neighbor in the above layer and the probability for the site to be wet depends on the number of wet sites (Fig. 2.4a):

$$P(1|0,0) = 0, \quad P(1|0,1) = P(1|1,0) = p_1, \quad P(1|1,1) = p_2 \tag{2.21}$$

with $P(0|i,j) = 1 - P(1|i,j)$ for $i,j \in \{0,1\}$. Note that the DK automaton includes the original DP as a special case of $(p_1, p_2) = (p, 2p - p^2)$. Since one has two independent control parameters (namely p_1 and p_2) in this automaton, one can draw a phase diagram for the automaton, as shown in Fig. 2.4b. Remarkably, strong numerical evidences suggest that the critical behavior *on this transition curve* (except the upper terminal, where the model has

two symmetric absorbing states) fall into the DP universality class. This is in a high contrast with a typical phase diagram in equilibrium phase transitions, where a critical "point" often appears in a phase diagram.

Another example of lattice models in the DP universality class indicates that a model does not need to be discretized in time to fall into DP. The most famous continuous-time Markov process in the DP universality class is the contact process [42] which was originally proposed as a model for epidemic spreading. In the contact process, each site s_i $(i = 1, 2, \cdots, N)$ is assigned either of the two states, namely active state $(s_i = 1)$ and inactive state $(s_i = 0)$. Active sites deactivate at a rate of unity while contaminates an activity to adjacent sites at a rate of λ. The contact process experiences a DP-class phase transition at a certain control parameter λ_c. Advantages of the contact process is that one can easily write down master equation associated with the contact process:

$$\frac{\partial P}{\partial t} = \sum_{s'} w_{s' \to s} P_t(s') - \sum_{s'} w_{s \to s'} P_t(s) \tag{2.22}$$

with

$$w_{0 \to 1, n} = n\lambda/2d, \quad w_{1 \to 0, n} = 1, \tag{2.23}$$

where n and d respectively denote the number of active neighbors and the spatial dimension of the model. This helps mathematicians to prove various results rigorously [13, 31].

Numerical evidences and theoretical considerations provide strong footings of robustness of the DP universality class; we will come back to this point in Section 2.3.4.

2.3.3 Mean-field theory of the DP universality class

Up to here we refrained from quantitative arguments, besides listing precise estimates of the critical exponents. In order to interpret the critical exponents from theoretical point of view, however, it is desirable to consider a theory which is analytically tractable. Mean-field theory we exploit in this Subsection provides us a simple framework to deal with this problem.

In order to consider the fraction of wet sites in a given layer $\rho(t)$, it is helpful to regard DP as reaction-diffusion system and the number of layer t as time. Associating wet sites with particles A and dry sites with vacancy é, one can see that DP consists of four elementary processes, as illustrated in Fig. 2.5:

$$\left.\begin{array}{ll} \text{self} - \text{destruction}: & A \to \text{é} \\ \text{diffusion}: & \text{é} + A \to A + \text{é} \\ \text{offspring production}: & A \to 2A \\ \text{coagulation}: & 2A \to A \end{array}\right\} \tag{2.24}$$

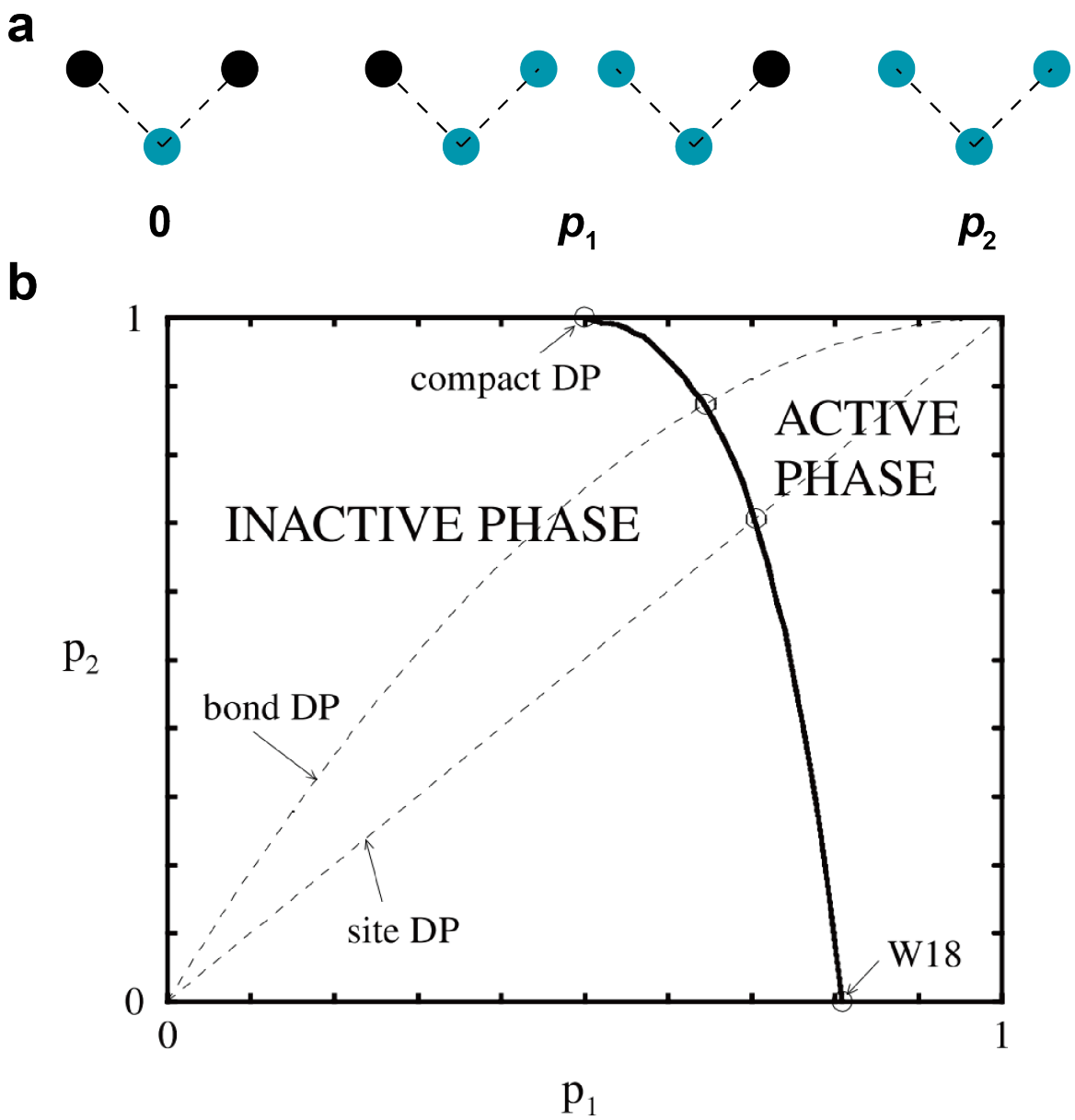

Figure 2.4: Domany–Kinzel automaton as a generalization of DP. **a**: Transition rule of the DK automaton. **b**: Phase diagram of the DK automaton. The figure is reproduced from Ref. [45].

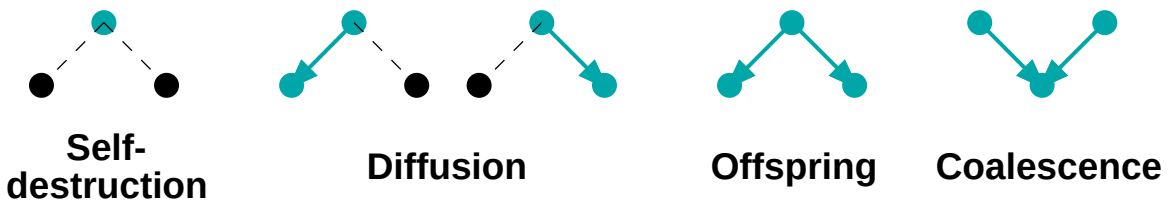

Figure 2.5: Interpretation of DP as a reaction-diffusion process.

The simplest mean-field theory consists of averaging the density of active sites over entire system. In this case, we may neglect a process which does not change the total number of active sites (that is, diffusion). Then, self-destruction and offspring production correspond to the linear term while coagulation gives rise to the quadratic term. Hence the generic mean-field theory for DP is represented by the following:

$$\frac{\mathrm{d}\rho_{\mathrm{MF}}(t)}{\mathrm{d}t} = \varepsilon\rho_{\mathrm{MF}}(t) - \lambda\rho_{\mathrm{MF}}^2(t), \tag{2.25}$$

where ε and λ are phenomenological parameters. This ordinary differential equation for given initial condition $\rho(t=0) = \rho_0$ can be exactly solved to yield

$$\rho_{\mathrm{MF}}(t) = \begin{cases} \dfrac{\rho_0\varepsilon e^{\varepsilon t}}{\rho_0\lambda e^{\varepsilon t} + (\varepsilon - \rho_0\lambda)} & \varepsilon \neq 0, \\ (\lambda t + \rho_0^{-1})^{-1} & \varepsilon = 0 \end{cases} \tag{2.26}$$

By taking the long-time limit of the solution (2.26), one finds

$$\lim_{t\to\infty} \rho_{\mathrm{MF}}(t) = \begin{cases} \varepsilon/\lambda & \varepsilon > 0, \\ 0 & \text{otherwise.} \end{cases} \tag{2.27}$$

From this, one can see that the theory exhibits continuous transition at the critical point $\varepsilon_c = 0$ and that the critical exponent β^{MF} associated with the order parameter is unity. Qualitative behavior of the time evolution also changes around the critical point, as demonstrated in Fig. 2.6: $\rho_{\mathrm{MF}}(t)$ decays exponentially below the critical point whereas it approaches a steady-state with non-zero stationary value of ρ_{MF}. Asymptotic behavior of the solution as $t \to \infty$ can be studied to explicitly see that

$$\rho_{\mathrm{MF}}(t) \simeq \begin{cases} -\varepsilon\left(\lambda - \frac{\varepsilon}{\rho_0}\right)^{-1} e^{-|\varepsilon|t} & \varepsilon < 0, \\ (\rho_0^{-1} + \lambda t)^{-1} & \varepsilon = 0, \\ \frac{\varepsilon}{\lambda} + \frac{\varepsilon}{\lambda^2}\left(\lambda - \frac{\varepsilon}{\rho_0}\right) e^{-\varepsilon t} & \varepsilon > 0. \end{cases} \tag{2.28}$$

In both $\varepsilon < 0$ and $\varepsilon > 0$, the solution approaches to its stationary value in an exponential manner with characteristic time of $|\varepsilon|^{-1}$, meaning that the critical exponent $\nu_{||}^{\mathrm{MF}}$ associated with the divergence of correlation time is unity.

In order to study divergence of the correlation length in mean-field theory, one has to take diffusion into account. This can be done by adding a diffusion term to the original mean-field theory:

$$\frac{\partial\rho}{\partial t} = \varepsilon\rho - \lambda\rho^2 + D\nabla^2\rho, \tag{2.29}$$

where D is a diffusion constant. Unfortunately, this nonlinear partial differential equation is hard to solve analytically. Nevertheless, one can determine the remaining exponent $\nu_{\perp}^{\mathrm{MF}}$ by considering the requirement that (2.29) is invariant under the rescaling

$$\boldsymbol{r} \to \Lambda\boldsymbol{r}, \quad t \to \Lambda^{\nu_{||}^{\mathrm{MF}}/\nu_{\perp}^{\mathrm{MF}}} t, \quad \rho(\boldsymbol{r}, t) \to \Lambda^{-\beta^{\mathrm{MF}}/\nu_{\perp}^{\mathrm{MF}}} \rho(\Lambda\boldsymbol{r}, \Lambda^{z^{\mathrm{MF}}} t). \tag{2.30}$$

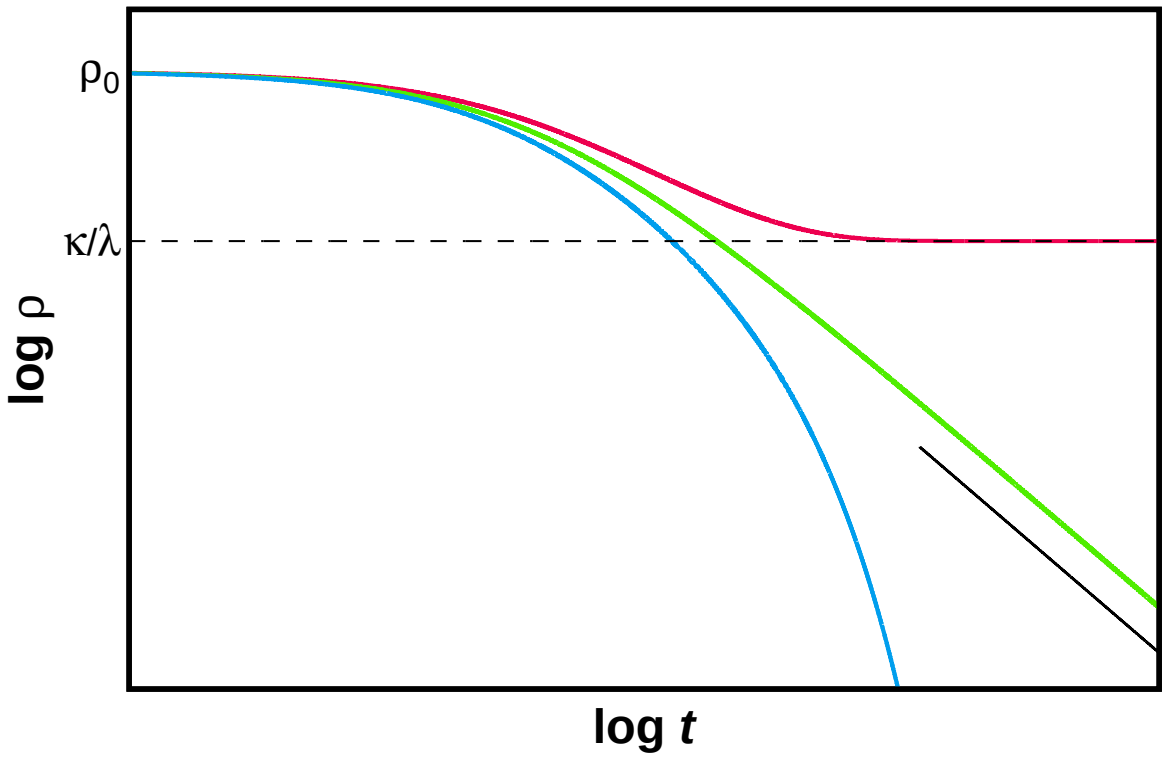

Figure 2.6: Solution of mean-field theory of DP (the Eq. (2.25) in the main text). The solution (2.26) is plotted for $\varepsilon = 0.3$ (magenta), $\varepsilon = 0$ (green) and $\varepsilon = -0.3$ (blue) in a logarithmic scale. Initial condition ρ_0 and a phenomenological parameter λ is respectively fixed to $\rho_0 = 1$ and $\lambda = 2$ for all the three cases. Black solid line is a guide-to-eye for t^{-1}.

at the critical point. Applying the scale transformation yields

$$\Lambda^{-(\beta^{\mathrm{MF}}+\nu_{||}^{\mathrm{MF}})/\nu_{\perp}^{\mathrm{MF}}}\frac{\partial\rho}{\partial t}=\Lambda^{-\beta^{\mathrm{MF}}/\nu_{\perp}^{\mathrm{MF}}}\varepsilon\rho-\Lambda^{-2\beta^{\mathrm{MF}}/\nu_{\perp}^{\mathrm{MF}}}\lambda\rho^2+\Lambda^{-(\beta^{\mathrm{MF}}/\nu_{\perp}^{\mathrm{MF}}+2)}D\nabla^2\rho \quad (2.31)$$

One can see that the requirement is fulfilled if $\varepsilon=0$ (this is the critical point) and $\beta^{\mathrm{MF}}+\nu_{||}^{\mathrm{MF}}=2\beta^{\mathrm{MF}}=\beta^{\mathrm{MF}}+2\nu_{\perp}^{\mathrm{MF}}$, meaning that $\nu_{\perp}^{\mathrm{MF}}=1/2$. To summarize, one can find a set of static critical exponents $(\beta^{\mathrm{MF}},\nu_{\perp}^{\mathrm{MF}},\nu_{||}^{\mathrm{MF}})$ in a framework of mean-field theory:

$$\beta^{\mathrm{MF}}=1,\quad \nu_{\perp}^{\mathrm{MF}}=1/2,\quad \nu_{||}^{\mathrm{MF}}=1. \quad (2.32)$$

Recalling theory of critical phenomena in equilibrium phase transitions [73], one may naturally be interested in number of upper critical dimension d_c above which the mean-field theory provides quantitatively correct predictions. To address this problem, one needs to start from master equation to derive phenomenological Langevin equation. This procedure can be performed in a case of the contact process [50], and the resulting Langevin equation highly resembles the mean-field theory with spatial degree of freedom (2.29) but is accompanied by multiplicative noise, reflecting the fact that fully inactive state ($\rho(\boldsymbol{x},t)=0$) is absorbing:

$$\frac{\partial\rho}{\partial t}=\varepsilon\rho-\lambda\rho^2+D\nabla^2\rho+\zeta \quad (2.33)$$

where

$$\langle\zeta(\boldsymbol{x},t)\rangle=0,\quad \langle\zeta(\boldsymbol{x},t)\zeta(\boldsymbol{x}',t')\rangle=\Gamma\rho(\boldsymbol{r},t)\delta(\boldsymbol{x}-\boldsymbol{x}')\delta(t-t'). \quad (2.34)$$

Here δ is a standard Dirac's delta function. Applying the same scale transformation as what we have done to obtain (2.31), it turns out that the noise term scales as $\Lambda^{-(\beta+d\nu_{\perp}+\nu_{||})/2\nu_{\perp}}\zeta$, where d denotes the spatial dimension. Recalling that $\Lambda>1$ implies the system approaches to the critical point (which can be seen from the rescaling of $\rho(\boldsymbol{r},t)$), the noise term is relevant if the scaling exponent of it is larger than that of other terms, that is,

$$-\frac{\beta^{\mathrm{MF}}+d\nu_{\perp}^{\mathrm{MF}}+\nu_{||}^{\mathrm{MF}}}{2\nu_{\perp}^{\mathrm{MF}}}>-\frac{\beta^{\mathrm{MF}}+\nu_{||}^{\mathrm{MF}}}{\nu_{\perp}^{\mathrm{MF}}}=-4. \quad (2.35)$$

This inequality can be readily solved to yield $d<4$, meaning that the noise term is relevant in $d<4$. Conversely, the noise is irrelevant in $d>4$, and marginal in $d=4$. It means that the upper critical dimension d_c of DP is 4.

The critical exponents below the upper critical dimension can be evaluated by means of field-theoretical renormalization group theory. Since we do not perform renormalization group analysis in the forthcoming Chapters, we do not exploit the procedure in detail, but we show some known results of the ϵ-expansion up to ϵ^2 (where $\epsilon=d_c-d$) [15, 16, 50]:

$$\beta=1-\frac{\epsilon}{6}\left[1-\left(\frac{11}{288}-\frac{53}{144}\log\frac{4}{3}\right)\epsilon+O(\epsilon^2)\right], \quad (2.36)$$

$$\nu_{\perp}=\frac{1}{2}+\frac{\epsilon}{16}\left[1+\left(\frac{107}{288}-\frac{17}{144}\log\frac{4}{3}\right)\epsilon+O(\epsilon^2)\right], \quad (2.37)$$

$$\nu_{||} = 1 + \frac{\epsilon}{12}\left[1 + \left(\frac{109}{288} - \frac{55}{144}\log\frac{4}{3}\right) + O(\epsilon^2)\right]. \tag{2.38}$$

Although these results are not very close to the numerical ones (shown in Tab. 2.1), they successfully capture qualitative trends of the exponents with respect to ϵ (as ϵ increases, β decreases while $\nu_\perp$ and $\nu_{||}$ increase).

2.3.4 Robustness of the DP universality class

What makes the DP universality class the most fundamental one in absorbing phase transitions is its robustness. As exemplified in Section 2.3.2, critical exponents of an absorbing phase transition in various models were found to be identical with the those of DP (within numerical accuracy, of course). Moreover, Cardy and Sugar pointed out [18] that the effective action of DP (which can be derived from the effective Langevin equation (2.33), (2.34)) coincides with that of the Reggeon field theory [70], which was originally proposed to describe interactions of hadrons at ultra-relativistic energies. This vast variety of examples is the source of the common belief that the DP universality class is very robust in theory.

The robustness of the DP universality class is informally expressed in a conjecture by Janssen and Grassberger: They conjectured that the model should generically fall into the DP universality class if it satisfies the following conditions [39, 50]:

1. The model displays a continuous phase transition from a fluctuating active phase into a unique absorbing state.
2. The transition is characterized by a positive one-component order parameter.
3. The dynamic rules involve only short-range processes.
4. The system has no unconventional attributes such as additional symmetries or quenched randomness.

Although this conjecture is yet to be established with rigorous footing, no counterexample has been proposed as of this writing. On the contrary, numerical evidences suggest that a model *does not* necessarily have to fulfill the above conditions to fall into the DP universality class. For example, a model with several absorbing states [71, 72] or with multicomponent order parameter [2, 41, 48, 57, 68, 76, 106] can also fall into the DP universality class in some cases. Thus it is empirically known that the DP universality class is extremely robust.

Field-theoretical methods provides further substantiation to the robustness of the DP universality class. To see this, one may consider adding higher-order terms (such as $\nabla^4\phi, \phi^3$) to the effective Langevin equation (2.33). By performing the dimensional analysis we have outlined in Section 2.3.3, one can show that such perturbations are irrelevant in a sense of renormalization group. In other words, even though higher-order corrections may be present in complex systems of physical interest, such corrections do not affect the critical phenomena of the system. This is the origin of the universality.

Table 2.2: Critical exponents measured in earlier experimental works, listed in chronological order. The row entitled "Theory" shows the theoretical value of the DP universality class up to the digit where comparison with experimental results is meaningful (see Tab. 2.1 for more precise value) and cells colored in gray indicate significant deviations from the theoretical value.

$d = 1$	β	$\nu_\perp$	$\nu_{\|\|}$
Annular Rayleigh–Bénard [23, 25]	($\lesssim$0.15)	0.5	0.5
Linear Rayleigh–Bénard [25]	0.30(5)	0.50(5)	0.50(5)
Taylor–Dean [26]	1.30(26)	∼0.64	∼0.73
Ferrofluidic spikes [82]	0.30(5)	1.2(1)	0.70(5)
Lateral heat convection in annulus [62]	0.27(3)	0.30(4)	0.75(3)
Theory	∼0.28	∼1.10	∼1.73

$d = 2$	β	$\nu_\perp$	$\nu_{\|\|}$
Turbulent liquid crystal [92, 95]	0.59(4)	0.75(6)	1.29(11)
Theory	∼0.58	∼0.73	∼1.30

Partial measurements	Results
Interface roughening ($d = 1$) [17]	$\nu_\perp/\nu_{\|\|} = 0.63(4)$ (cf. $\nu_\perp^{\mathrm{1DDP}}/\nu_{\|\|}^{\mathrm{1DDP}} \sim 0.63$)
Rayleigh–Taylor ($d = 2$) [78]	$\beta = 0.56(5)$ (cf. $\beta^{\mathrm{2DDP}} \sim 0.58$)

2.3.5 Experimental realization of DP universality class

One of the most surprising facts about the DP universality class is that it has been hard to observe experimentally in spite of its robustness we outlined previously: Although researchers have performed many experiments on a system where one would naïvely expect DP-class transition, some earlier works [17, 78] did not manage to measure all the three independent static critical exponents, and more importantly, many other works [23, 25, 26, 62, 82] reported considerably large deviation from DP in at least one exponent (results in earlier literatures are summarized in Tab. 2.2). This apparent contradiction was very surprising, as noted by Grassberger:

> *"... there is still no experiment where the critical behavior of DP was seen. This is a very strange situation in view of the vast and successive theoretical efforts made to understand it. Designing and performing such an experiment has thus top priority in my list of open problems."*

Some theoretical studies were performed to identify the likely cause of the difficulty in experimental realizations. One of the most fruitful directions for this purpose was to study the influence of the inhomogenity of the control parameter, which was likely to be present in experiments. Technically, taking inhomogenity into account corresponds to adding an

additional noise term $\chi(t, \boldsymbol{r})$ to the control parameter

$$\varepsilon \to \varepsilon + \chi(t, \boldsymbol{r}) \tag{2.39}$$

so that the minimal effective Langevin equation for DP is modified to

$$\frac{\partial \rho}{\partial t} = \varepsilon\rho - \lambda\rho^2 + D\nabla^2\rho + \rho\chi + \zeta \tag{2.40}$$

In this formulation, χ is quenched in a sense that physical quantities of interest (such as the density of the active sites) are averaged over independent realizations of the intrinsic noise ζ while the disorder field χ *is kept fixed*. For instance, the disorder field $\chi(\boldsymbol{r})$ for spatially quenched disorder is defined by the correlations

$$\overline{\chi(\boldsymbol{r})\chi(\boldsymbol{r}')} = \gamma\delta^d(\boldsymbol{r} - \boldsymbol{r}'), \tag{2.41}$$

where the bar denotes the average over independent realizations of the disorder field. Before field-theoretical consideration is provided, Moreira and Dickman studied two-dimensional contact process with spatially quenched disorder, and found that survival probability of active sites $P(t)$ and mean square radius of the cluster of active sites *does not* approach to power law but to non-universal logarithmic growth [69]. Later Janssen showed by field-theoretic analysis that the spatially quenched disorder is marginal and hence it can crucially disturb the critical behavior of the DP universality class [51].

Likewise, DP with temporally quenched disorder was also studied by Jensen [53]. The disorder field $\chi(t)$ for temporally quenched disorder is defined by the correlations

$$\overline{\chi(t)\chi(t')} = \gamma\delta(t - t'). \tag{2.42}$$

Jensen showed that the temporally quenched disorder is a relevant perturbation in a sense of renormalization group and therefore even weak disorder drastically affects the critical phenomena. These results demonstrate that the DP universality is indeed *fragile* to a certain kind of perturbations.

The aforementioned results of experiments and renormalization group might sound disheartening: They suggest that the DP universality class is too simple to give a quantitative prediction on realistic systems and one has to be equipped with detailed knowledge of the system (in particular possible presence of quenched disorder) to correctly describe it after all. Although one could also argue that the long absence of experimental realizations is not so surprising recalling the time it took for the Ising universality class to be realized experimentally since the discovery of the exact solution by Onsager and hence one should be optimistic [46], whether or not (and if yes, how far) quite simplified dynamics of DP is relevant for absorbing phase transition has been quite unclear.

This situation began to change in 2007: Takeuchi and his coworkers performed a set of experiments on electroconvection of nematic liquid crystal, and reported the first convincing

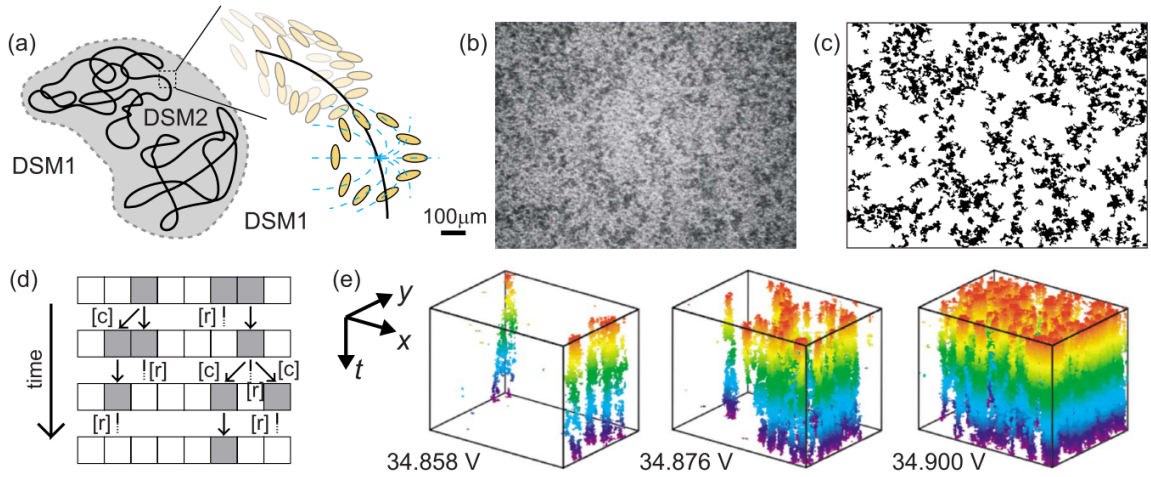

Figure 2.7: Spatiotemporal intermittency in turbulent liquid crystals. **a**: Sketch of a DSM2 domain with many entangled disclinations. **b**: Snapshot of the coexistence of DSM1 and DSM2. DSM2 appears darker than DSM1 when one observes light transmitted through the cell. **c**: Binarized image of **b**. **d**: Simplified model of the dynamics (essentially same as the contact process). A patch of DSM2 stochastically relax to DSM1 or contaminate neighboring DSM1 region. **e**: Spatiotemporal diagram of DSM2 patches. This figure is adopted from Ref. [95].

experimental realization of the DP universality class [92, 95]. In their work, they focused on the transition between two turbulent regime called dynamic scattering mode 1 and 2 (DSM1 and DSM2), which can be realized by applying strong AC electric field. A crucial difference between DSM1 and DSM2 lies in the density of topological defects: In DSM2, topological defects, often called disclinations in a study of liquid crystals, are present and they elongate and split constantly under the shear due to the fluctuating turbulent flow around, whereas they disappear immediately in DSM1 (Fig. 2.7a). This difference is important from both conceptual and practical points of view: Since disclinations are energetically unfavorable, fully DSM1 state naturally serves as an absorbing state in this system. Moreover, disclinations leads to the loss of light transmittance, and hence distinction between DSM1 and DSM2 is very easy (Fig. 2.7b and Fig. 2.7c). Using this system, Takeuchi and his coworkers successfully measured 12 critical exponents, 8 scaling relations and 5 scaling functions, all in agreement with the DP universality class in $2+1$ dimensions.

Why turbulent liquid crystals clearly exhibited universal critical phenomena of DP, despite many other experiments showed significant deviation from DP (apparently, at least)? Takeuchi *et al.* argued in Ref. [95] that there are three factors crucially different from earlier works:

- Experiments with large aspect ratio can be easily realized. Aspect ratio of the cell they used in their work is $3300h \times 3300h \times 2h$ (h represents half depth), which is larger in one order of magnitude than earlier works.

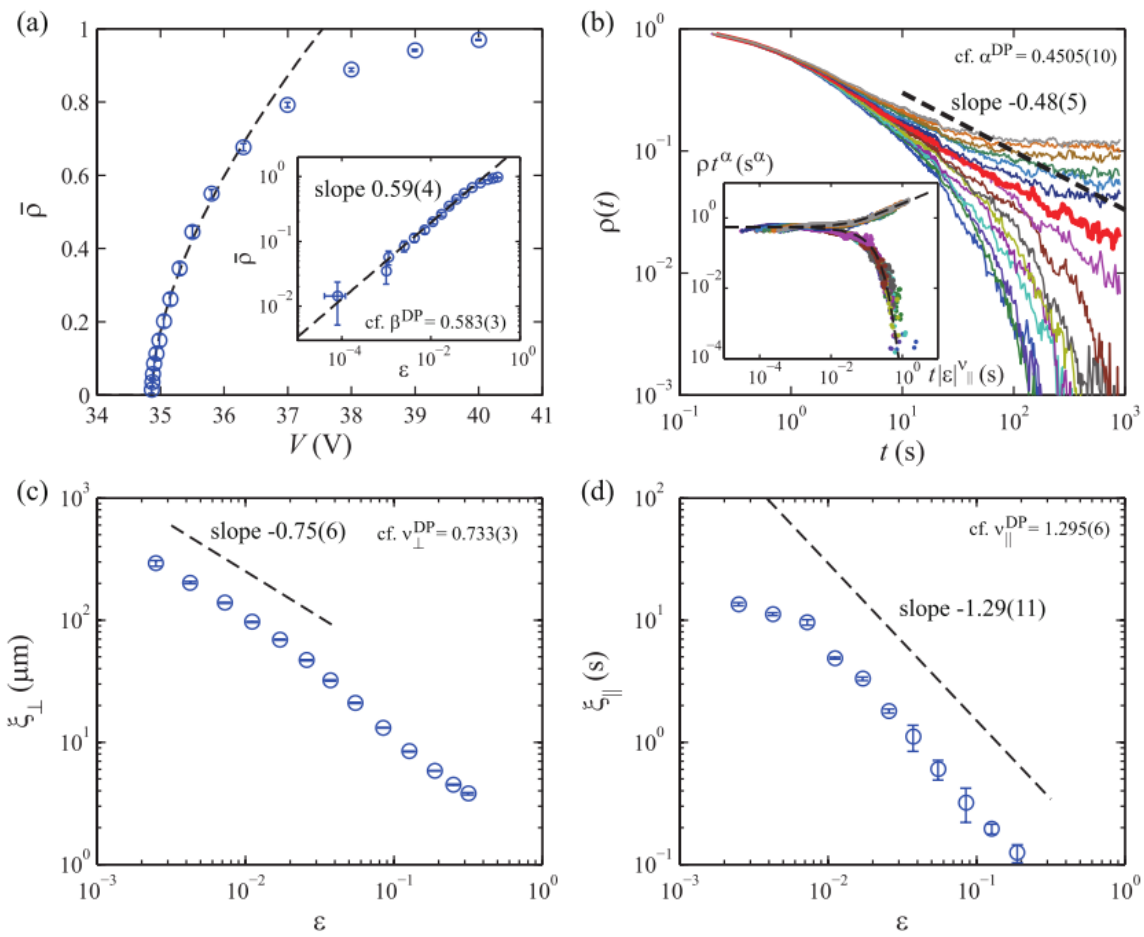

Figure 2.8: Critical phenomena in turbulent liquid crystal. **a**: Area fraction of DSM2 $\bar{\rho}$ averaged in time with respect to the applied voltage V. The inset shows the same data in a logarithmic scale as a function of $\varepsilon = (V^2 - V_c^2)/V_c^2$. **b**: Relaxation of ρ after quenching for various V. The inset shows the same data with rescaled axes $t|\varepsilon|^{\nu_{||}}$ and $t^{\beta/\nu_{||}}\rho(t)$ and the dashed curve indicates universal scaling function obtained through numerical simulation of the contact process. **c**: Correlation length in the steady state with respect to ε. **d**: Correlation time in the steady state with respect to ε. This figure is adopted from Ref. [94].

- Full DSM1 state has a very good analogy with absorbing state. As we described in the previous paragraph, spontaneous nucleation of DSM2 is energetically unfavorable and thus is very rare.

- Local turbulent fluctuation of DSM1 effectively kills long-range interaction. If one prepares laminar absorbing state, as many other works did, laminar state may introduce long-range effect through rigidity of their laminar patterns and/or propagation of soliton-like objects.

Since there are multiple different factors, the most crucial one is hard to tell from only a single experimental realization. While if the third one is the most crucial then the critical phenomena of DP may not be so ubiquitous in reality, otherwise it may be more robust than it had been considered to be. Hence experiments with other systems are needed to address the question of what the most crucial factor for experimental realizations of the DP universality class is.

Chapter 3

How to Probe Universal Features of Absorbing Phase Transitions

Related publication by the author: Section 2 of K. Tamai and M. Sano. How to experimentally probe universal features of absorbing phase transitions using steady state. Submitted to J. Stat Mech. (Preprint: arXiv, 1712.05789)
Contribution: The author (K.T.) conceived the project and performed numerical simulation, under advice and direction by the collaborator (M.S.).

In the previous Chapter, we focused on describing the basic universal features of absorbing phase transition expected theoretically and recent situation on robustness of the DP universality class in both theory and experiment. Meanwhile, the following question naturally arises: When a system with an absorbing phase transition is given, how can we examine the universal features? A primary purpose of this Chapter is to provide an extensive survey to address this question. As we will see in the following, the methods to do the job is massively different between numerical simulations and experiments. Furthermore, it turns out the conventional experimental methods can easily produce biased results unless one handles them with care, although the universal scaling ansatzs the experimental works have relied on is indeed valid in principle. Given these, we also propose a practical method to avoid the bias by employing a technique of statistical analysis which was originally proposed in a context of medical follow-ups.

3.1 Specific background

3.1.1 Numerical simulation of stochastic models

When one attempts to characterize an absorbing phase transition in a stochastic model, a critical spreading protocol where he/she introduces a localized active seed in an otherwise inactive system (as shown in Fig. 3.1) is regarded as one of the most reliable numerical

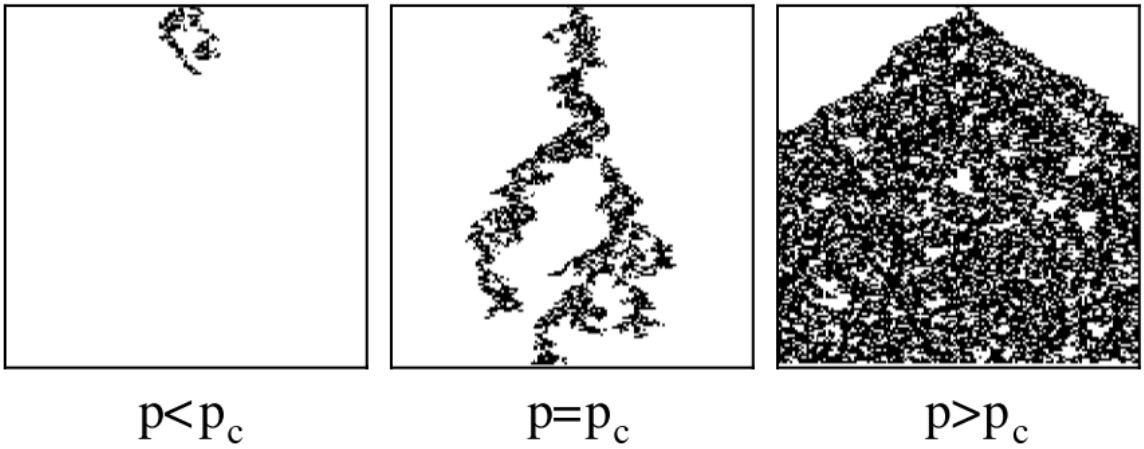

Figure 3.1: Schematic picture of a critical spreading protocol, showing the dynamics of an isolated active seed given at $t = 0$ in spatially one-dimensional DP. The vertical direction corresponds to the direction of time. The figure is adopted from [45].

techniques. This protocol, originally proposed by Grassberger and de la Torre [38], is concerned with time evolution of the probability of survival $P_{\rm surv}(t)$ for the seed, the number of active sites $V(t)$, and the average of mean square radius of the active cluster over surviving clusters $R_{\rm s}^2(t)$. These quantities are expected to obey the following scaling relations:

$$P_{\rm surv}(t;\varepsilon) \sim t^{-\delta}\tilde{P}_{\rm surv}(\varepsilon^{\nu_{||}}t), \tag{3.1}$$

$$V(t;\varepsilon) \sim t^{\Theta}\tilde{V}(\varepsilon^{\nu_{||}}t), \tag{3.2}$$

$$R^2(t;\varepsilon) \sim t^{\zeta}\tilde{R}(\varepsilon^{\nu_{||}}t), \tag{3.3}$$

where δ, Θ, ζ are the appropriate scaling exponents as usual.

As we will see in the following, the scaling exponents can be determined in a framework of phenomenological scaling theory. It follows by definition of the survival probability that $\lim_{t\to\infty} P_{\rm surv}(t) = \varepsilon^{\beta'}$, and hence

$$\delta = \beta'/\nu_{||} \tag{3.4}$$

so that the scaling relation (3.1) is consistent with this. In order to determine the other scaling exponents Θ, ζ, it is convenient to consider so-called the pair-connectedness function $C(r,t;\varepsilon)$ which represents the probability that an active seed at the origin ($r = 0, t = 0$) makes a site at r sites away from the origin active at time t[1]. Utility of the pair-connected function stems from the fact that $V(t;\varepsilon)$ and $R^2(t;\varepsilon)$ can be regarded as an integral of

[1]Historically, the pair-connected function has been a quantity of interest in estimating the theoretical value of the critical exponents of the directed percolation, because it can in principle be expanded as a finite polynomial of the percolation probability p from which the critical exponents is estimated quite accurately [54].

$C(r,t;\varepsilon)$ with respect to suitable weight:

$$V(t;\varepsilon) = \int \mathrm{d}\boldsymbol{r} C(|\boldsymbol{r}|,t;\varepsilon), \quad R^2(t;\varepsilon) = \frac{1}{V(t)} \int \mathrm{d}\boldsymbol{r} r^2 C(\boldsymbol{r},t;\varepsilon). \tag{3.5}$$

Now let us consider the scaling relation of the pair-connectedness function in a framework of phenomenological scaling theory. That is, we now assume the following scaling relation:

$$C(r,t;\varepsilon) = \Lambda^{-\kappa} C(\Lambda\varepsilon; \Lambda^{-\nu_\perp} r, \Lambda^{-\nu_{||}} t), \tag{3.6}$$

where κ is some suitable exponent and Λ is an arbitrary scaling factor. In the steady state (that is, $t \to \infty$), the probability that one finds any active sites is $\lim_{t\to\infty} P_{\mathrm{surv}}(\sim \varepsilon^{\beta'})$ by definition. Meanwhile, the probability that one finds an active site at a certain site $\boldsymbol{r}$ *given* that the cluster is still surviving is the steady area fraction ρ of active sites, and hence scales as ε^{β}. One can deduce from these observations that $C(r,t,\varepsilon)$ is rescaled by the following

$$\lim_{t\to\infty} C(r,t,\varepsilon) = \varepsilon^{\beta+\beta'}, \tag{3.7}$$

suggesting that

$$\kappa = \beta + \beta'. \tag{3.8}$$

Substituting (3.6) together with (3.8) into (3.5), one finds the following scaling relations:

$$\Theta = \frac{d\nu_\perp - (\beta+\beta')}{\nu_{||}}, \quad \zeta = \frac{2\nu_\perp}{\nu_{||}}. \tag{3.9}$$

This protocol has quickly become the *de facto* standard for measuring critical exponents [44, 45, 94], thanks to the three important advantages from a numerical point of view:

- The size of the system can be extended arbitrarily (by, e.g. reallocating memory accordingly) measurement is completely free from notorious finite-size effect and from impact of (usually periodic) boundary conditions.
- Since one only needs to evolve a few number of active sites for most runs, computation can be done very quickly.
- Especially if one is interested comparing the system with the DP universality class, one can directly check $\beta = \beta'$ by this protocol.

3.1.2 Deterministic models and experiments

Unfortunately, the critical spreading protocol is much less useful in experiments or in deterministic models, as pointed out by Takeuchi [94]. Major drawbacks of the critical spreading protocol in these situations are the following:

- One has to evolve the entire system for every time step. Hence, critical spreading protocol does not contribute to improve efficiency and consequently one suffers from lack of statistics in general.
- System is inevitably subject to finite-size effect and to impact of boundary conditions.
- Generating an active seed itself is not straightforward.

Given these, most experimental works in this context have relied on steady-state measurements [23, 25, 82].

In steady-state measurements, probability distribution of the lengths (or durations) of intervals of local inactive state (hereafter referred to as "spatial (temporal) interval distribution") has been quantity of central interest in earlier experimental studies. Extensive use of the distribution is based on a belief that critical behavior of absorbing phase transitions is characterized by only two diverging length scales, namely the correlation length and the correlation time. Local inactive state does not spontaneously turn active and the state in which entire system is inactive is absorbing, implying that characteristic length (time) of the decay of the distribution diverges at the critical point. Assuming that the belief is indeed the case, it is natural to expect that the characteristic length (time) of the distribution corresponds to the correlation length (time).

The interval distribution, however, is known to be hard to handle theoretically. As Henkel *et al.* pointed out in their book [44], the interval distribution should be regarded as multi-point correlation function in a sense that inactive interval between two spatially/temporally distant active sites requires that the activity must be absent *along a line* connecting them. This is in a sharp contrast with the ordinary two-point correlation function which probes correlated activity of the two points ignoring the sites in between. Hence it is not obvious *a priori* whether such a quantity obeys a simple scaling form. In earlier theoretical work [8], Ben-Naim and Krapivsky considered time evolution of a probability $E_n(t)$ that a randomly chosen string of n sites is inactive and $R_n(t)$ that a randomly chosen string of $n+1$ sites has n consecutive inactive sites with one active site at the extreme right-hand side, which are related to each other by

$$R_n = E_n - E_{n+1} \quad \text{or} \quad E_n = 1 - \sum_{i=0}^{n-1} R_i. \tag{3.10}$$

In this case, contamination of activity causes a loss of E_n whereas deactivation a creation of empty intervals, depending on the length of intervals of inactive sites next to the deactivated site. That is, if we denote the density of two neighboring intervals by $E_{l,m}$ then the time evolution of E_n can be (approximately) described by the following:

$$\frac{\mathrm{d}E_n}{\mathrm{d}t} = -R_n + \lambda \sum_{l=0}^{n-1} E_{l,n-1-l}. \tag{3.11}$$

Further approximating $E_{l,m}$ by $R_l R_m / R_0$ yields

$$\frac{\mathrm{d}E_n}{\mathrm{d}t} = -\sum_{i=0}^{n-1} \frac{\mathrm{d}R_i}{\mathrm{d}t} = -R_n + \frac{\lambda}{R_0} \sum_{l=0}^{n-1} R_l R_{n-l-1}. \tag{3.12}$$

which constitutes an infinite hierarchy of equations which is analytically intractable. Although E_n or R_n is not exactly identical to the interval distribution, the above consideration clearly illustrates the source of difficulty in rigorous consideration.

Nevertheless, simple phenomenological scaling argument may still be used to "derive" universal scaling *ansatz* which one can expect to hold at least to some approximation. Following the spirit of phenomenological scaling theory, let us postulate that inactive interval distributions have scaling properties analogous to that of ordinary two-point correlation function. That is, we put the following scaling ansatz with some unknown exponent $\kappa_{||}$:

$$P(\Delta t; \varepsilon) = \lambda^{-\kappa_{||}} P(\lambda^{-\nu_{||}} \Delta t; \lambda\varepsilon), \tag{3.13}$$

Substituting $\lambda = \Delta t^{1/\nu_{||}}$ to (3.13) yields

$$P(\Delta t; \varepsilon) = \Delta t^{-\kappa_{||}/\nu_{||}} g_{||}(\Delta t^{1/\nu_{||}} \varepsilon) \quad \text{where} \quad g_{||}(x) := P_{||}(1; x). \tag{3.14}$$

Then the average $\langle \Delta t \rangle$ of the inactive interval is evaluated as follows:

$$\begin{aligned} \langle \Delta t \rangle &:= \sum_{\Delta t=1}^{\infty} \Delta t P_{||}(\Delta t; \varepsilon) \\ &\sim \int_a^{\infty} \mathrm{d}\Delta t \Delta t \cdot P_{||}(\Delta t; \varepsilon) \\ &= \int_a^{\infty} \mathrm{d}\Delta t \cdot \Delta t^{1-\kappa_{||}/\nu_{||}} g(\Delta t^{1/\nu_{||}} \varepsilon) \\ &= \varepsilon^{\kappa_{||}-2\nu_{||}} \int_{\varepsilon^{\nu_{||}} a}^{\infty} \mathrm{d}T \cdot T^{1-\kappa_{||}/\nu_{||}} g(T) \\ &\sim \varepsilon^{\kappa_{||}-2\nu_{||}}, \end{aligned} \tag{3.15}$$

where a is a lower cutoff introduced to take the discreteness of the sum (in the first line) into account. Note that, when we obtain this from the second line from the bottom, we made use of the fact that $\kappa_{||}/\nu_{||} > 1$ which follows from the requirement that the distribution has to be normalized even in the limit of $\varepsilon \to +0$:

$$\sum_{\Delta t=1}^{\infty} P_{||}(\Delta t, \tau) = 1. \tag{3.16}$$

On the other hand, reciprocal ρ^{-1} of the order parameter is related to the mean of inactive intervals $\langle \Delta t \rangle$ and that of active ones $\langle \Delta t_{\mathrm{a}} \rangle$ by

$$\rho^{-1} = \frac{\langle \Delta t \rangle + \langle \Delta t_{\mathrm{a}} \rangle}{\langle \Delta t_{\mathrm{a}} \rangle} \sim \varepsilon^{-\beta}. \tag{3.17}$$

Since $\langle \Delta t_{\mathrm{a}} \rangle$ is not expected to diverge at the critical point, a manner in which ρ^{-1} diverges at the critical point is expected to be identical to that of $\langle \Delta t \rangle$, that is,

$$\langle \Delta t \rangle \sim \varepsilon^{-\beta}. \tag{3.18}$$

Comparison between Eqs. (3.15) and (3.18) yields $\kappa_{||} = 2\nu_{||} - \beta$, and hence we obtain the following scaling hypothesis:

$$P_{||}(\Delta t; \varepsilon) = \Delta t^{-(2-\beta/\nu_{||})} g_{||}(\Delta t^{1/\nu_{||}} \varepsilon). \tag{3.19}$$

where we assume $\beta < \nu_{||}$, which is indeed the case with DP universality class, as long as spatial dimension is not higher than 3. Essentially the same argument can be applied for spatial interval distributions, and we obtain the following as a result:

$$P_{\perp}(\Delta x; \tau) = \Delta x^{-(2-\beta/\nu_{\perp})} g_{\perp}(\Delta x^{1/\nu_{\perp}} \varepsilon). \tag{3.20}$$

If one is interested in considering complementary cumulative distribution function (CCDF) $R_l(\Delta l; \varepsilon)$ (where $l = ||, \perp$ and $\Delta l = \Delta t, \Delta x$) defined by

$$R_l(\Delta l; \varepsilon) := \int_{\Delta l}^{\infty} \mathrm{d}\Delta l' P(\Delta l'; \varepsilon), \tag{3.21}$$

it follows from (3.19) and (3.20) that

$$R_{||}(\Delta t; \varepsilon) \sim \varepsilon^{\nu_{||}-\beta} h_{||}(\varepsilon^{\nu_{||}} \Delta t), \tag{3.22}$$

$$R_{\perp}(\Delta x; \varepsilon) \sim \varepsilon^{\nu_{\perp}-\beta} h_{\perp}(\varepsilon^{\nu_{\perp}} \Delta x), \tag{3.23}$$

where $h_l(\Delta l; \varepsilon)$ is given as follows:

$$h_l(\Delta l^{1/\nu_l} \varepsilon) = \int_{\varepsilon(\Delta l)^{1/\nu_l}}^{\infty} \mathrm{d}x \nu_l x^{-(\nu_l+1-\beta)} g_l(x) \mathrm{d}x. \tag{3.24}$$

Let us emphasize again that (3.19) and (3.20) are nothing more than ansatzs: Although one can show that the possible scaling form of $P_{||}, P_{\perp}$ is limited to (3.19), (3.20) *if* we assume $P_{||}, P_{\perp}$ have scaling properties analogous to that of the ordinary two-point correlation functions, validity of the assumption is by no means obvious.

3.1.3 Objectives of the research

Given a lack of a rigorous theoretical footing and difficulty of analyzing the interval distribution, numerical validation of the scaling ansatz (3.19) and (3.20) is necessary in order to justify the experimental methodology to measure the critical exponents. However, there has been no published work which directly examined the ansatzs to the author's knowledge, besides the power-law decay of spatial interval distribution with the exponent $2 - \beta/\nu_{\perp}$ expected in the vicinity of the critical point [27]. Hence the aim of the study is to examine the universal scaling ansatzs (3.19) and (3.20) through the numerical simulation on the contact process.

3.2 Methods

3.2.1 Numerical simulation of the contact process

Let us recall that the master equation of the contact process is given by a master equation

$$\frac{\partial P}{\partial t} = \sum_{s'} w_{s' \to s} P_t(s') - \sum_{s'} w_{s \to s'} P_t(s) \tag{3.25}$$

with

$$w_{0 \to 1,n} = n\lambda/2d, \quad w_{1 \to 0,n} = 1, \tag{3.26}$$

where n and d respectively denote the number of active neighbors and the spatial dimension of the model. Although the contact process is continuous in time, discrete-time formulation is very often used in numerical simulations [66].

1. Choose one active site randomly.
2. Deactivate the site with probability $1/(1+\lambda)$. Otherwise, choose one of the nearest neighbors randomly and activate it (if inactive).
3. Increment the time by $1/N_{\text{act}}$, where N_{act} is a number of active sites. Then go back to 1.

We performed Monte–Carlo simulation on the contact process in spatially one-dimensional ring (lattice system with periodic boundary condition) with length of 1,024 sites. In a case of $d = 1$, the critical point has been very precisely estimated to be $\lambda_c = 3.297848(20)$ [56]. We varied the control parameter λ in a range of $10^{-3}\lambda_c < \lambda - \lambda_c < 3 \times 10^{-1}\lambda_c$ and we performed $n = 50$ realizations for each λ. In each realization, the system was initially set to the state where all sites are active, and we evolved the system according to the standard discrete-time formulation [66] for 10^7 steps (first 10^6 steps were discarded in a course of analysis to ensure that the quasi-steady state is measured).

In order to acquire ensemble of configurations, we adopted the method by Dickman and Martins de Oliveira [27]: We first saved the $M_s = 2,000$ samples of configuration for each time step during the first M_s steps, and then the list was updated with probability $p_{srep} = 0.005$ by replacing a randomly chosen configuration on the list by the current one whenever the time step was increased by unity. In this way, 100,000 configurations were recorded. Time series of a certain site with length of W time steps was also accumulated in a similar manner: Time series of randomly chosen M_t sites were saved during the first W steps, and the list was updated with probability $p_{trep} = 0.05$ by replacing a randomly chosen time series on the list by the most recent time series obtained at a randomly chosen site for each W time steps. Thus we collected 25,000 time series for each λ. These samples of configuration and time series were used to obtain the interval distributions.

3.2.2 How to estimate the interval distributions from data

Since one does not have an infinite resource to record the configuration or time series, one has to *estimate* the distribution from data acquired within some finite observation window. Although extensive consideration on this problem has not been given in earlier literatures concerning experimental realization of the DP universality class (besides a brief remark given in Ref. [95]), the problem is much more delicate than one might expect it to be.

The simplest way to estimate the distribution $P_l(\Delta l)$ is just to count the number of completely observed intervals $N(\Delta l)$ of length Δl and normalize the resulting "histogram" to unity. If one has n independent realizations of the configuration or time series (we assume this situation in the following unless otherwise stated), this idea can be represented formally by the following:

$$\hat{P}_l(\Delta l) := \frac{\sum_{i=1}^{n} N_i(\Delta l)}{\sum_{i=1}^{n} S_i}, \tag{3.27}$$

where $N_i(\Delta l)$ represents the number of completely observed intervals of length Δl within the ith realization and S_i the sum of $N_i(\Delta l)$ over Δl:

$$S_i := \sum_{\Delta l} N_i(\Delta l). \tag{3.28}$$

the total number of completely observed intervals within the ith realization. Although equivalent, it is often convenient to consider the complementary cumulative distribution function (CCDF) $R_l(\Delta t)$

$$R_l(\Delta l) := \sum_{\Delta l' \geq \Delta l}^{\infty} P_l(\Delta l'), \tag{3.29}$$

because then one does not have to bother from selecting the size of the bin. Hereafter, we concentrate on constructing an estimator for CCDF unless otherwise stated. Replacing $P_l(\Delta l')$ with the empirical estimator $\hat{P}_l(\Delta l')$ (3.27) yields the following empirical estimator $\hat{R}_l(\Delta l)$ for CCDF, that is,

$$\hat{R}_l(\Delta l) := \sum_{\Delta l' \geq \Delta l} \hat{P}_l(\Delta l') = \frac{\sum_{i=1}^{n} \sum_{\Delta l' \geq \Delta l} N_i(\Delta l')}{\sum_{i=1}^{n} S_i}. \tag{3.30}$$

As expected, it can be shown that the empirical estimator is consistent in a limit of infinite observation window W [5]:

$$\lim_{W \to \infty} \hat{R}_l(\Delta l) = R_l(\Delta l). \tag{3.31}$$

Since this estimator $\hat{P}_l$ is easy to construct and it converges to the intrinsic interval distribution $P_l(\Delta l)$ of the system in a limit of $W \to \infty$ by construction, it may be tempting to rely on it.

Unfortunately, the empirical estimator is likely to produce biased results if one use it when only finite observation is available, as is always the case in experiments. When the observation is performed under a finite observation window, the first and the last interval is

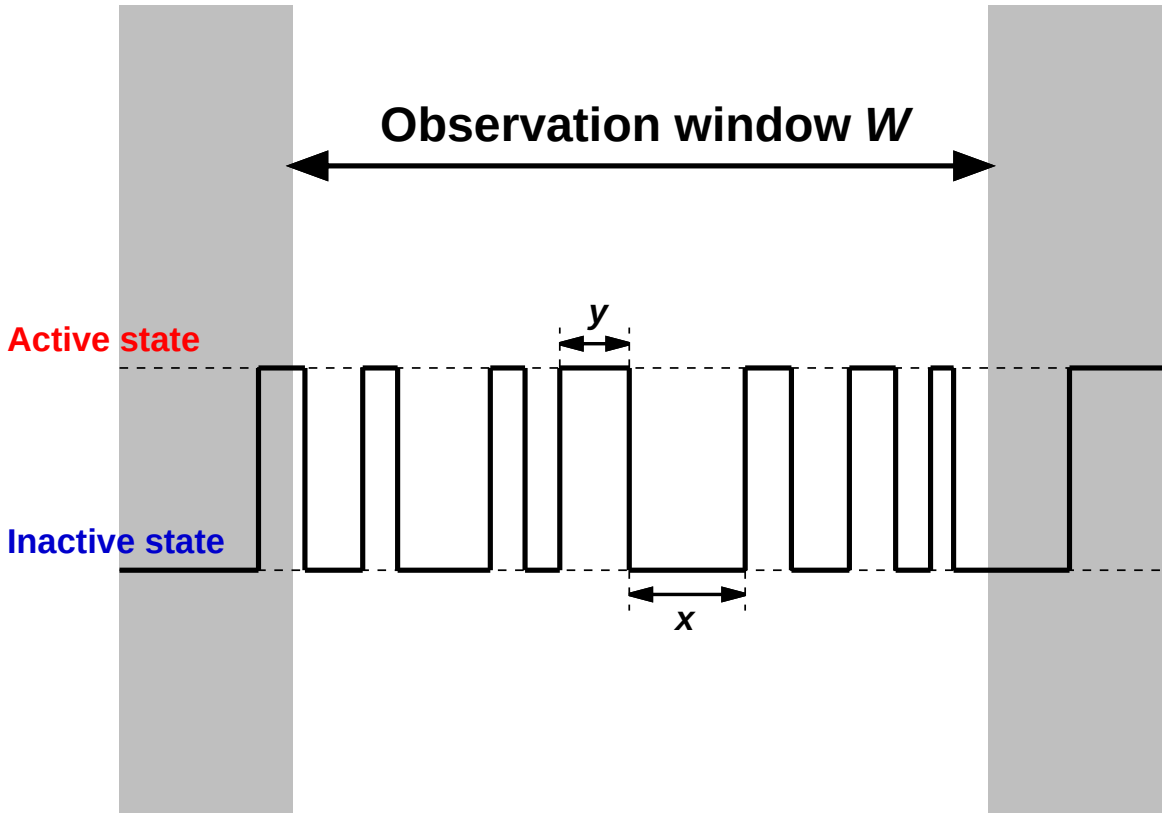

Figure 3.2: Schematic picture of censoring by finite observation window. The gray region is out of the observation window and hence not observed. In this observation window, the leftmost interval of active state and the rightmost interval of inactive state is not completely observed.

censored by the edge of the window (as illustrated in Fig. 3.2). This censoring makes the situation complicated in two ways [105]:

- Dependence between adjacent intervals is "induced" even if originally independent from each other. For example, the longer the first interval is, the more likely the second interval is censored by the edge of the observation window (and so on).

- Obviously the distribution $R(t)$ is not estimable for $t > W$ where W is the size of the window. Moreover, the distribution for the second interval is not estimable if $t > W - \tau_1$, where τ_1 is a minimum value of t' such that $R(t') = 0$ (and so on). Thus, one has to find some quantity which is identifiable and meaningful.

Due to these difficulties, unified appropriate approach has not been emerged up to date despite extensive effort in literatures, but rather a case-specific approach is needed.

One of the most well-known non-parametric estimator for possibly censored time series is the Kaplan–Meier estimator [58]. The Kaplan–Meier estimator, named after Edward L. Kaplan and Paul Meier, was originally proposed to estimate the probability for the event of

interest occurs later than time t, and is defined by the following:

$$\hat{R}_{\mathrm{KM}}(t) := \prod_{t' \le t} \left(1 - \frac{D_{\mathrm{KM}}(t')}{M_{\mathrm{KM}}(t')}\right); \tag{3.32}$$

where M_{KM} is the number of subjects "at risk" (neither have experienced the event nor are censored) and D_{KM} is the number of events observed at time t, and t' is the ordered and distinct uncensored times. Key assumption behind this estimator is that the censoring time is independent from the individual lifetime t. The same assumption is also employed in other estimators of this (product-limit) form. Fortunately, this is indeed the case in our study, although one should check the validity of the assumption carefully in more general situations (e.g. in a medical follow-up where censoring can occur because of a competing risk and hence a censoring may be informative to a lifetime of a patient).

However, one runs into difficulty when one attempts to apply the Kaplan–Meier estimator to recurrent data: If one constructs a variant of the Kaplan–Meier estimator (3.32) for pooled recurrence times by

$$\hat{R}_{\mathrm{PKM}}(t) := \prod_{t' \le t} \left(1 - \frac{D_{\mathrm{PKM}}(t')}{M_{\mathrm{PKM}}(t')}\right); \tag{3.33}$$

(where $M_{\mathrm{PKM}}(t)$ denotes the total number of observed intervals no shorter than t (be it partially censored or not) and $D_{\mathrm{PKM}}(t)$ denotes the total number of completely observed intervals of length t), the estimator is generally biased because the last (possibly censored) interval for each realization is subject to biased sampling. Of course one could work around the issue by constructing the standard Kaplan–Meier estimator (3.32) using only the first recurrence time, but this implies that one just discards all the other observed intervals and hence the measurement is very inefficient. Thus the key issue is how one can *efficiently* estimate the distribution of interest without causing systematic bias.

The above considerations motivate us to look for an alternative way to estimate interval distributions. Here we employ the estimator proposed by Wang and Chang [99]. Representing it in a somewhat informal style for practical purposes, the estimator by Wang and Chang is given by the following[2]:

$$\hat{R}_{\mathrm{WC}}(t) := \prod_{t' \le t} \left(1 - \frac{D_{\mathrm{WC}}(t')}{M_{\mathrm{WC}}(t')}\right); \tag{3.34}$$

$$D_{\mathrm{WC}}(t) := \sum_{i=1}^{n} \Theta(S_i - 1) \cdot \frac{N_i(t)}{S_i}, \tag{3.35}$$

$$M_{\mathrm{WC}}(t) := \sum_{i=1}^{n} M_i(t) \quad \text{with} \quad M_i(t) = \begin{cases} \Theta(W - t) & S_i = 0 \\ \sum_{t'=t}^{W} N_i(t')/S_i & \text{otherwise} \end{cases}, \tag{3.36}$$

[2]Strictly speaking, this is a special case of the Wang–Chang estimator where all the realizations are given the same weight in estimating the distribution.

where Θ is the standard Heaviside step function with $\Theta(0) = 1$, $N_i(t)$ represents the number of completely observed intervals of length t within the ith realization, $S_i(= \sum_{t'} N_i(t'))$ represents the total number of completely observed intervals within the ith realization, and t' is the ordered and distinct uncensored times. Although time series of current interest is not univariate but consists of two states observed alternately, we can still apply this technique provided that we begin our observation from a left edge of the inactive interval (that is, from a point where the observed state turns from active to inactive) [49]. Nice thing about this estimator is that, assuming conditional independence and independent censoring, one can theoretically show that the estimator weakly converges to the intrinsic conditional probability of the system, in a limit of infinite number of realizations (not the infinite size of the window) [99]. Hence we employ the estimator by Wang and Chang when necessary.

3.3 Results

We first studied the spatial interval distribution where the expected power-law decay has been already reported [27]: We estimated the CCDF $\hat{R}_\perp(\Delta x)$ using the empirical estimator (3.30) under the observation window of $W = 1,000$. As shown in Fig. 3.3a, the resulting CCDF $\hat{R}_\perp(\Delta x)$ exhibited an exponential decay for sufficiently large Δx, through which one can define a correlation length $\xi_\perp$ of the system. The correlation length $\xi_\perp$, which can be estimated from the exponential decay of the distriution

$$\hat{R}_\perp(\Delta x) \sim \exp(-\Delta x/\xi_\perp) \quad \text{for} \quad \Delta x \gg 1, \tag{3.37}$$

was found to diverge as $\xi_\perp \sim \varepsilon^{-\nu_\perp}$, as expected from the phenomenological scaling argument (Fig. 3.3b). This result encouraged us to rescale $\hat{R}_\perp(\Delta x)$ according to the scaling ansatz (3.23), and we obtained a reasonably good collapse as shown in the inset of Fig. 3.3a.

Given the issue of censoring by a finite observation window outlined in Section 3.2.2, one might wonder why the empirical estimator worked reasonably well in this case. Comparison between the correlation length of the system and the finite observation window provides us a reasonable explanation to this: Within the range of our study, the correlation length of the system was about 60 sites at the longest, which is shorter than the observation window by about one order of magnitude. Hence the window is long enough for the system so that the empirical estimator under this window reasonably well approximates the result expected for $W \to \infty$.

Now we turn our attention to the temporal interval distribution: We estimated the CCDF $\hat{R}_{||}(\Delta t)$ by an empirical estimator under the observation window of $W = 500$ and $W = 5,000$. We found that the result is very sensitive to the choice of W especially near the critical point (Fig. 3.4a). Moreover, even if we estimate the correlation time $\xi_{||}$ through an exponential decay of the distribution estimated under $W = 5,000$, the resulting $\xi_{||}$ as a

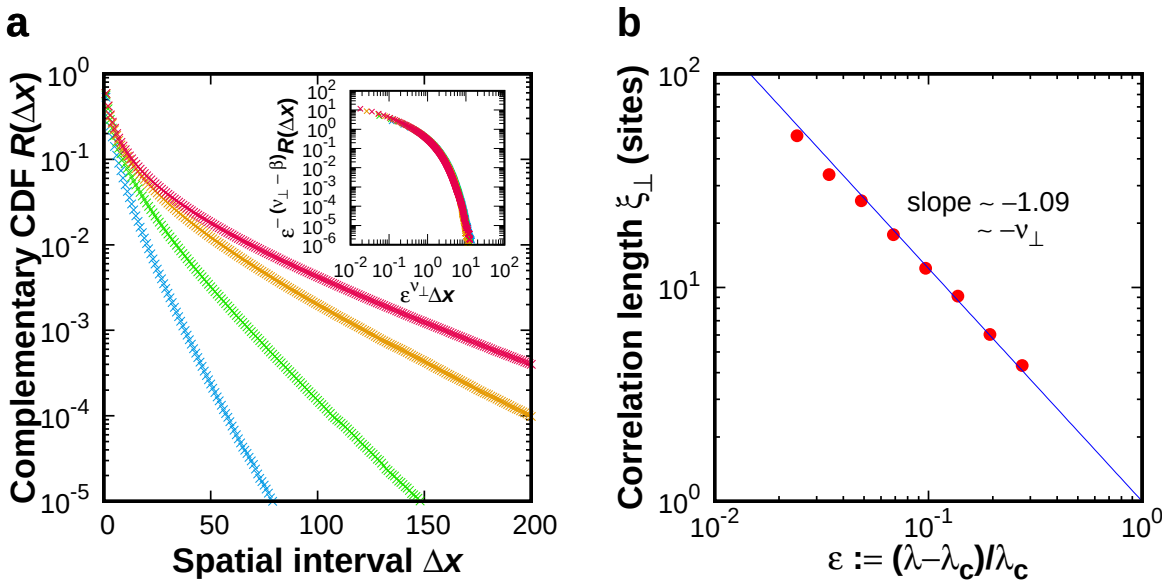

Figure 3.3: Spatial interval distribution estimated by the empirical estimator. **a**: Spatial interval distributions for $\lambda = 3.33785$ (magenta, $\varepsilon := (\lambda - \lambda_c)/\lambda_c \sim 1.2 \times 10^{-2}$), $\lambda = 3.41098$ (orange, $\varepsilon \sim 3.4 \times 10^{-2}$), $\lambda = 3.52412$ (green, $\varepsilon \sim 6.9 \times 10^{-2}$), and $\lambda = 3.75039$ (blue, $\varepsilon \sim 1.4 \times 10^{-1}$) are shown ($\lambda_c = 3.297848(20)$ [56]). The inset shows the result of rescaling of the plot according to the scaling hypothesis (3.23). Note that the theoretical value $\beta, \nu_\perp$ of the DP universality class was used to rescale the data. **b**: The correlation length $\xi_\perp$ as a function of ε. The blue line is a guide-to-eye for the expected power-law divergence with exponent $-\nu_\perp$.

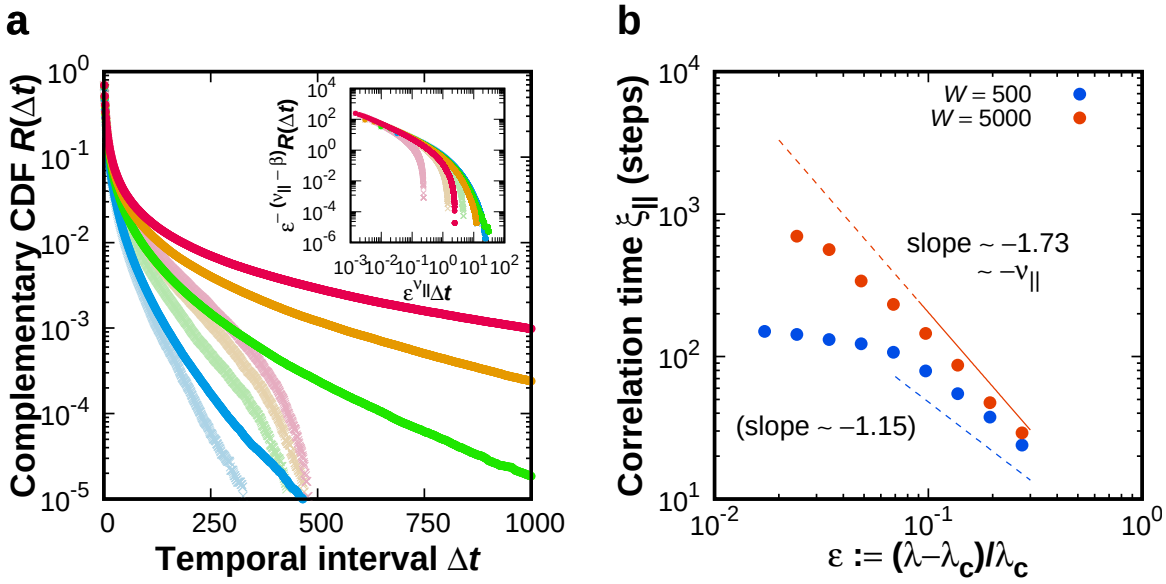

Figure 3.4: Temporal interval distribution estimated by the empirical estimator. **a**: Temporal interval distributions for $\lambda = 3.33785$ (magenta, $\varepsilon := (\lambda - \lambda_c)/\lambda_c \sim 1.2 \times 10^{-2}$), $\lambda = 3.41098$ (orange, $\varepsilon \sim 3.4 \times 10^{-2}$), $\lambda = 3.52412$ (green, $\varepsilon \sim 6.9 \times 10^{-2}$), and $\lambda = 3.75039$ (blue, $\varepsilon \sim 1.4 \times 10^{-1}$) are shown. Results of the estimation under the window of $W = 500$ is painted in light color whereas ones under the window of $W = 5,000$ is painted in vivid color. The inset shows the result of rescaling of the plot according to the scaling hypothesis (3.22). Note that the theoretical value $\beta, \nu_{||}$ of the DP universality class was used to rescale the data. **b**: The correlation time $\xi_{||}$ as a function of $\varepsilon = (\lambda - \lambda_c)/\lambda_c$. The orange solid line is a guide-to-eye for the expected power-law divergence with exponent $-\nu_{||}$, and is extended outside the region where the reasonable agreement was found (orange dashed line). Blue dashed line shows a guide-to-eye whose slope well approximates the apparent power-law behavior.

function of ε does not exhibit a clear power-law divergence with the expected exponent $-\nu_{||}$, as shown in Fig. 3.4b. As expected from these observations, the rescaled complementary CDFs for various control parameter λ do not overlap in general, as shown in the inset of Fig. 3.4a, although the scaling collapse is observed at far away from the critical point for $W = 5,000$. Extrapolation from the "scaling regime" ($\varepsilon \gtrsim 0.1$) suggests that the correlation time grows up to about 3,000 steps at $\varepsilon \sim 0.02$, which is comparable to the size of the window. Hence it is natural that the deviation from the expected power-law divergence is observed even for $W = 5,000$.

This contrast of the results between the spatial interval distribution and the temporal one is worth emphasizing. Since $\nu_\perp < \nu_{||}$ holds in the DP universality class (as well as in other universality classes of absorbing phase transitions known so far [44]), a correlation length grows much slower than a correlation time as getting close to the critical point. Suppose, for example, one performs a set of experimental measurements in spatially one-dimensional

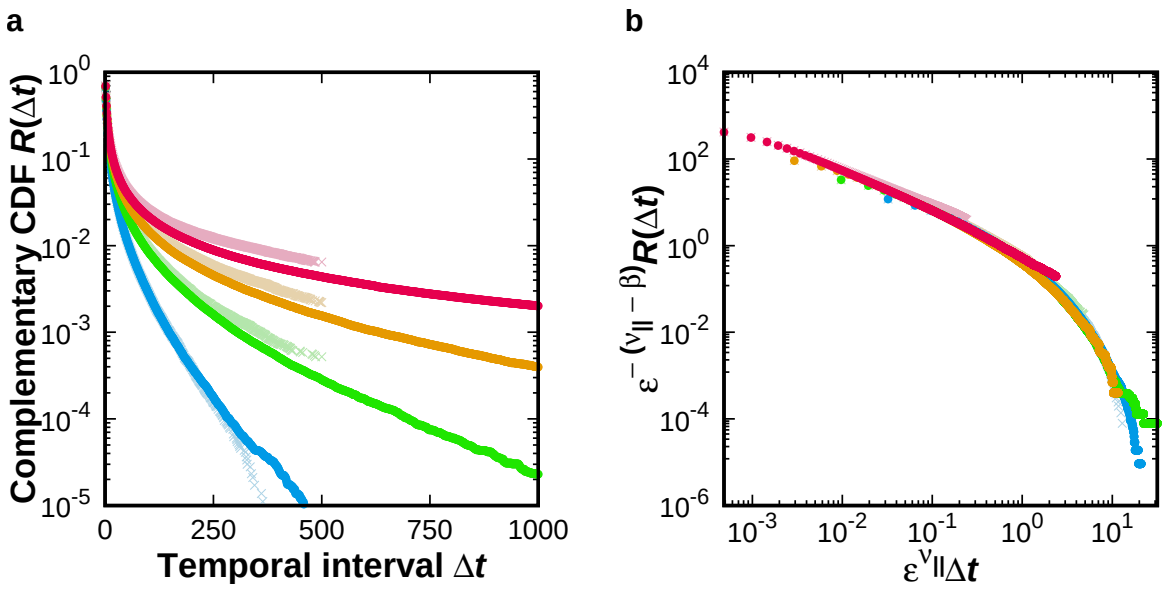

Figure 3.5: Temporal interval distribution estimated by the Wang–Chang estimator. **a**: Temporal inactive interval distribution of spatially one-dimensional contact process for $\lambda = 3.37785$ (magenta, $\varepsilon := (\lambda - \lambda_c)/\lambda_c \sim 1.2 \times 10^{-2}$), $\lambda = 3.41098$ (orange, $\varepsilon \sim 3.4 \times 10^{-2}$), $\lambda = 3.52412$ (green, $\varepsilon \sim 6.9 \times 10^{-2}$), and $\lambda = 3.75039$ (blue, $\varepsilon \sim 1.4 \times 10^{-1}$). The results of the estimation under the window of $W = 500$ is painted in light color whereas ones under the window of $W = 5,000$ is painted in vivid color. **b**: Same data as **a**, but the data was rescaled according to the universal scaling ansatz The inset shows the result of rescaling of the plot according to the scaling hypothesis (3.22). Note that the theoretical value $\beta, \nu_{||}$ of the DP universality class was used to rescale the data.

system with control parameter ε varied over two orders of magnitude to provide reliable estimates of the critical exponents (in accordance with a critical remark by Stumpf and Porter [91]). Then, the correlation length of the system grows about 150 times in a course of measurements whereas the correlation time grows about 3,000 times(!), if the system does fall into the DP universality class. This difference of one digit drastically changes the difficulty in measuring critical exponents through interval distributions especially considering the experiments, although one should also consider the difficulty of performing experiments with large systems carefully when designing the projects.

Having seen that the empirical estimator yields massively biased results for the temporal interval distributions, let us employ the aforementioned the Wang–Chang estimator (3.34). We estimated the CCDF $\hat{R}_{||}(\Delta t)$ by the Wang–Chang estimator under the observation window of $W = 500$ and $W = 5,000$. As a result, we found that the result is much less sensitive to the choice of the value of W than the empirical estimator is, although slight difference is still present (Fig. 3.5a). We also tested the scaling ansatz (3.22) and we obtained a reasonable collapse both for $W = 500$ and $W = 5,000$ (Fig. 3.5b).

Provided that the problem of estimation is moderated, the inactive interval distribution

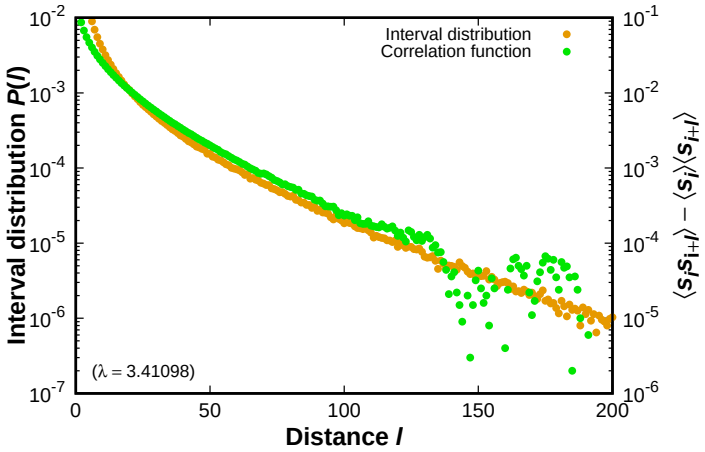

Figure 3.6: Comparison between the interval distribution and the two-point correlation function. Spatial interval distribution and the two-point correlation function for $\lambda = 3.41098$ ($\varepsilon \sim 3 \times 10^{-2}$) are compared.

serves as a very useful tool to characterize collective dynamics off the critical point. The utility of inactive interval distribution can be seen by comparing it with the static correlation function $C_s(l) := \langle s_i s_{i+l} \rangle - \langle s_i \rangle \langle s_{i+l} \rangle$: The spatial interval distribution $P_\perp(l)$ and the static spatial correlation function at $\lambda = 3.41098$ (that is, $\varepsilon \sim 3 \times 10^{-2}$) is shown in Fig. 3.6 as an example. The results suggest that both interval distribution function and static correlation function decay exponentially, and that the characteristic lengths of the decay coincide with each other[3]. Significant difference can be found for $l \sim 130$, where the correlation function begins to scatter presumably due to lack of statistics. Thus, the severe demand of statistics makes the measurement of correlation function impracticable in typical experiments, and interval distribution function is an attractive alternative in that case.

3.4 Discussions

Given the results we outlined in this work, now let us discuss on interpretation of the results of experimental literatures concerning possible relation to the DP universality class. The experimental results prior to Takeuchi *et al.* [92, 95] have two features in common: First, as is also pointed out by Henkel *et al.* [44], the largest deviation from the theoretical value of DP was found for estimate of the critical exponent $\nu_{||}$ associated with divergence of a correlation time. Second, the estimated critical exponent $\nu_{||}, \nu_\perp$ are smaller than the theoretical value. Our work suggests a likely explanation to this situation: If we measure the interval distribution using the empirical estimator (3.27) under a short observation window, estimated correlation length/time saturates near the critical point (Fig. 3.4a), which leads

[3]Note that the behavior of $C_s(l)$ and $P_\perp(l)$ are significantly different from each other for small l just as expected: It follows from (2.13) and (2.15) that $C_s(l)$ decays as $l^{-2\beta/\nu_\perp}$ whereas it follows from (3.20) that $P_\perp(l)$ decays as $l^{-(2-\beta/\nu_\perp)}$.

one to significant underestimation of the critical exponents. Recalling that effectiveness of the empirical estimator is a matter of comparison between the size of the window and the intrinsic correlation length/time of the system, it is reasonable that the estimation of $\nu_{||}$ is more strongly subject to the impact of a finite observation window than that of $\nu_{\perp}$ is.

To further substantiate our argument, let us revisit an earlier experimental work by Rupp *et al.* [82] as an example. In their work, the authors estimated the correlation length (time) through the distribution of spatial (temporal) interval and the resulting critical exponent $\nu_{\perp}$ was consistent with theoretical value, whereas $\nu_{||}$ was massively smaller. However, at $\varepsilon \sim 3 \times 10^{-2}$ or less, the estimated correlation time is comparable or longer than a one-tenth of the observation window, and qualitatively consistent behavior can be seen if one neglects that region as unreliable. Hence, it could be that the correlation time of the system indeed diverged in a same manner as predicted by the DP universality class but that the authors gave a biased estimate of the correlation time near the critical point due to a finite observation window. Thus, one should be cautious when performing and interpreting the measurements on a correlation time and a correlation length through the interval distributions.

Although the theoretical outcome of the present study (namely validation of the universal scaling ansatz for interval distributions) itself is not very surprising if one assumes the phenomenological scaling theory is correct, it can be considered as a lesson: Even if the physical factor which makes the situation complicated (e.g. quenched disorder) is not present at all, one may literally fail to capture universal features of absorbing phase transitions if he/she does this naïvely with limited resources. The present study provides a practical remedy to the difficulty and demonstrates the utility of the method, which can be utilized for measurements in other physical (also possibly ecological or social) systems.

Chapter 4

Impact of Active Wall and Advection on DP-Class Transitions

Related publication by the author: Section 3 of K. Tamai and M. Sano. How to experimentally probe universal features of absorbing phase transitions using steady state. Submitted to J. Stat Mech. (Preprint: arXiv 1712.05789), and Supplementary Information of M. Sano and K. Tamai, A universal transition to turbulence in channel flow. Nat. Phys. **12**, 249-253 (2016).
Contribution: The author (K.T.) conceived the project and performed numerical simulation, under advice and direction by the collaborator (M.S.).

When one attempts to characterize transitions to turbulence in shear flow as phase transitions out of equilibrium, one has an additional factor to concern: A localized turbulent structure is advected by mean flow. In this case, localized active (turbulent) state travels downstream and eventually the activity goes out of the observation area. In order to prevent the system from falling into an absorbing state, one needs to drive the system at the boundary, but then the effect of advection is no longer negligible because the advection cannot be transformed away by Galilean transformation. Then, how does the combination of the active boundary condition and the advection affect the critical phenomena of the DP-class transitions? A primary purpose of this Chapter is to perform a systematic study on this question.

4.1 Specific background

4.1.1 Impact of an active wall

Impact of boundary conditions on critical phenomena has been a topic of considerable interest in the field of statistical mechanics. While the standard theoretical framework of critical phenomena usually assumes thermodynamic limit where the system is infinitely large (although one can employ finite-size scaling to analyze the data for finite-size systems

[73]), materials in reality always possess boundaries. Moreover, extensive studies on critical phenomena in equilibrium show that physical quantities measured close to the boundary may behave differently than in the bulk [28]. In order to successfully apply the theory of critical phenomena to real physical systems, therefore, it is desirable to clarify how the presence of boundaries affect critical phenomena.

In contrast with equilibrium statistical mechanics, where progress in experimental works and the extension of the conformal field theory [7, 43] to systems with boundaries [19] substantially boosted systematic studies on the subject, studies on impacts of boundaries on non-equilibrium critical phenomena have still been in a much more primitive stage. Rather, the situation may be compared with that of surface equilibrium critical phenomena in 1970s: Lacking with both experimental realizations and powerful analytical frameworks, the subject has has not been paid very much attention, although there indeed exist some theoretical works [35, 47].

Still, an active boundary condition in which sites at the boundary are always forced to be active is one of the simplest boundary conditions, and it can be studied in a framework of mean-field theory and phenomenological scaling [44]. To see this, let us consider the mean-field theory of DP (2.29)

$$\frac{\partial \rho}{\partial t} = \varepsilon\rho - \lambda\rho^2 + D\nabla^2\rho$$

supplemented with an active boundary condition

$$\lim_{r_\perp \to +0} \rho(t, \boldsymbol{r}) = \infty \quad \text{for} \quad \forall t, \tag{4.1}$$

where $r_\perp$ denotes the coordinate perpendicular to the boundary condition (hereafter we refer to the boundary condition as "the wall"). Note that the third term of the right hand side of the mean-field theory can no longer be neglected because of the breakdown of Galilean invariance due to the wall. The stationary solution ρ_∞ of the mean-field theory can be found by observing that ρ_∞ depends only on $r_\perp$ (and hence $\nabla^2\rho_\infty = \partial^2_{r_\perp}\rho_\infty$) and thereby solving the following ordinary differential equation:

$$0 = \varepsilon\rho_\infty - \lambda\rho_\infty^2 + D\frac{\mathrm{d}^2\rho_\infty}{\mathrm{d}r_\perp^2}. \tag{4.2}$$

In particular, note that ρ_∞ is of the form $\rho_\infty(r_\perp) \sim r_\perp^{-2}$ if $\varepsilon = 0$ (that is, the system is exactly on the critical point). Phenomenological scaling theory provides us a way to interpret the exponent of -2. Recall the phenomenological scaling (2.11) of $\rho(t, \boldsymbol{r})$, that is,

$$\rho(t, \boldsymbol{r}, \varepsilon) = t^{-\beta/\nu_{||}} f(\boldsymbol{r}/t^{1/z}, \varepsilon t^{1/\nu_{||}}) \quad \text{where} \quad z := \nu_{||}/\nu_\perp.$$

Assuming that $r_\perp$ rescales like a length and averaging over a hyperplane parallel to the wall yields

$$\bar{\rho}(t, r_\perp, \varepsilon) = t^{-\beta/\nu_{||}} \tilde{f}(r_\perp/t^{1/z}, \varepsilon t^{1/\nu_{||}}), \tag{4.3}$$

where $\bar{\rho}$ denotes the average of ρ. Clearly, $\bar{\rho}$ in close proximity will become constant after only a short time (more specifically, as long as $r_\perp/t^{1/z} \ll 1$). In particular, it follows from the stationarity of $\bar{\rho}$ near the wall for $\varepsilon = 0$ that

$$\tilde{f}(y, 0) \sim y^{-\beta/\nu_\perp} \quad \text{for} \quad y \ll 1 \tag{4.4}$$

and consequently

$$\rho_\infty(r_\perp; \varepsilon = 0) \sim r_\perp^{-\beta/\nu_\perp}, \tag{4.5}$$

which indeed agrees with the results of the mean-field theory (recall $\beta^{\mathrm{MF}} = 1, \nu_\perp^{\mathrm{MF}} = 1/2$; see Section 2.3.3).

4.1.2 Combination of active wall and advection

The next question to ask is how the system with an active wall is affected in the presence of the advection. It is important to note that the advection can no longer be transformed away by a suitable Galilean transformation due to the wall, and hence advection may affect the system in a non-trivial manner.

To address this question, Blythe studied the totally asymmetric contact process (a special case of the contact process where active sites are not allowed to activate the adjecent inactive site against the direction of the given bias [97]) driven by an active boundary condition [10]: He numerically studied mean occupancy $\rho(x)$ at the steady state as a function of the distance x from the active wall, and he found that the $\rho(x)$ obeys the following scaling form:

$$\rho(x) \sim x^{-\beta/\nu_{||}} f(\varepsilon^{\nu_{||}} x). \tag{4.6}$$

This result implies that the correlation length $\xi_\perp$ cannot be observed in the steady-state density profile $\rho(x)$ of the driven asymmetric contact process (hereafter we will refer to it as DACP). As argued by Blythe, this implication is reasonable because the decay length L of the occupancy $\rho(x)$ can no longer be represented by a correlation length alone, but instead by a combination of the two different lengthscales in general:

$$L \sim \xi_{||} \cos\theta + \xi_\perp \sin\theta, \tag{4.7}$$

where θ represents the strength of the advection. Since the critical exponent $\nu_{||}$ is larger than $\nu_\perp$, the contribution from the first term becomes dominant near the critical point.

How can the exponent $\nu_\perp$ be measured? As an alternative strategy, Costa *et al.* studied the velocity v of the wave (Fig. 4.1) of the activity [24]. Their idea was that since there is a single lengthscale and a single timescale, the characteristic velocity of the system should be given by their ratio:

$$v \sim \xi_\perp/\xi_{||} \sim \varepsilon^{\nu_{||} - \nu_\perp}. \tag{4.8}$$

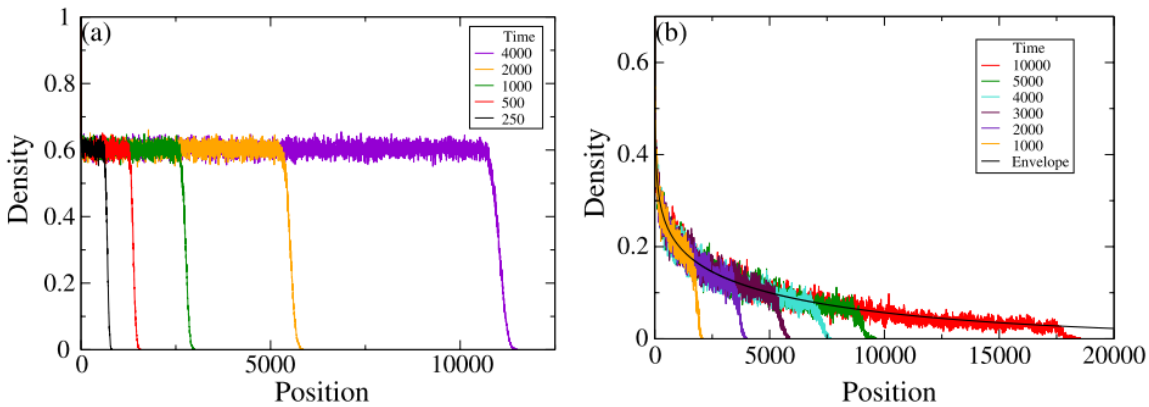

Figure 4.1: Wave of the activity in DACP. **a**: Occupancy averaged over 500 realizations at high-density regime. **b**: Occupancy averaged over 500 realizations at low-density regime. The figure is adopted from Ref. [24].

To substantiate their idea, they studied the mean-field theory of DACP. Within our notation, the mean-field theory is represented by the following:

$$\frac{\partial \rho}{\partial t} = \varepsilon\rho - \lambda\rho^2 - v_x\frac{\partial \rho}{\partial x} + D\frac{\partial^2 \rho}{\partial x^2}, \tag{4.9}$$

where the third term in the right hand side is introduced to take the advection into account and v_x denotes the velocity of the advection. Note that the mean-field theory possesses a distinct transition at $\varepsilon = 0$. Assuming that $\rho(t, x)$ can be described by $\rho(t, x) = \rho_\infty(x)f(t, x)$ with a suitable function f (where ρ_∞ denotes the stationary solution of the mean-field theory), one finds the following differential equation for f:

$$\frac{\partial f}{\partial x} = \lambda\rho_\infty f(1-f) - \left(v_x - \frac{2D\rho'_\infty}{\rho_\infty}\right)\frac{\partial f}{\partial x} + D\frac{\partial^2 f}{\partial x^2}. \tag{4.10}$$

If $\varepsilon > 0$, one can make use of the fact that $\rho_\infty \to \varepsilon/\lambda$ and $\rho'_\infty \to 0$ as $x \to \infty$ to obtain the following Fisher wave equation far away from the wall:

$$\frac{\partial f}{\partial t} = \varepsilon f(1-f) - v_x\frac{\partial f}{\partial x} + D\frac{\partial^2 f}{\partial x^2}. \tag{4.11}$$

Assuming a travelling wave $f(t, x) = f(x - vt)$, one eventually arrives at the following expression for the velocity v of the travelling wave:

$$v = v_x + \sqrt{4D\varepsilon}. \tag{4.12}$$

Thus the velocity of the wave indeed exhibits a power-law behavior, and the exponent of $1/2$ coincides with $\nu_{||}^{\mathrm{MF}} - \nu_{\perp}^{\mathrm{MF}}$ (recall $\nu_{||}^{\mathrm{MF}} = 1, \nu_{\perp}^{\mathrm{MF}} = 1/2$; see Section 2.3.3).

4.1.3 Objectives of the research

The method to measure the critical exponent $\nu_\perp$ proposed by Costa *et al.* is unsatisfactory for our purpose because of the following reasons:

- The numerical result of the velocity of the travelling wave in DACP by Costa *et al.* shows systematic deviation from the expected power law (Fig. 4.2). This suggests that subleading corrections may be prominent.
- Even if the argument by Costa *et al.* were correct, this protocol suffers from the same drawbacks as the critical spreading protocol we have seen in Section 3: One has to track the time evolution of the wave and hence one typically suffers from lack of statistics.

Also it is important to note that the speed of the advection and the control parameter cannot be varied independently in DACP, forbidding one from systematically studying the impact of advection on the system.

Given these, a main purpose of the present study is to study the impact of advection in a more systematic way by introducing a new model which allows us to accomplish the task. By numerically measuring physical quantities which are experimentally accessible (namely, the steady-state density $\rho_\infty(x)$ and the inactive interval distribution), we aim to clarify how the quantities are affected in the presence of the advection, and thereby how one can measure the critical exponents in this case.

4.2 Methods

4.2.1 Monte–Carlo simulation on a model

The model in the present study consists of a spatially one-dimensional string $\{s_i\}_{i=0}^{L-1}$ of L sites each of which can take either of two states, namely an active state ($s_i = 1$) or an inactive state ($s_i = 0$). In order to mimic the effect of advection, we introduce a new parameter θ: If the integer part of $t \tan\theta$, which indicates the position of a probe initially placed at the wall, does not change after the increment of t by 1, we evolve the system according to the standard rule of directed bond percolation (Fig. 4.3a) and otherwise we apply an advection by introducing transition rules which are asymmetric in streamwise direction (Fig. 4.3b):

$$\begin{aligned}
\mathrm{Prob}(s_i(t+1/2) = 1 | s_i(t) = 1, s_{i-1}(t) = 1) &= 1 - (1-p)^2, \\
\mathrm{Prob}(s_i(t+1/2) = 1 | s_i(t) = 1, s_{i-1}(t) = 0) &= p, \\
\mathrm{Prob}(s_i(t+1/2) = 1 | s_i(t) = 0, s_{i-1}(t) = 1) &= p, \\
\mathrm{Prob}(s_i(t+1/2) = 1 | s_i(t) = s_{i-1}(t) = 0) &= 0.
\end{aligned} \tag{4.13}$$

In other words, the speed of the advection is given by $\tan\theta$. We impose an active boundary condition at the wall:

$$s_0(t) = 1 \quad \text{for} \quad \forall t. \tag{4.14}$$

Note that the system no longer possesses unique absorbing state, and hence that a non-trivial steady state is well-defined even for finite system [10, 47]. This is in a sharp contrast with

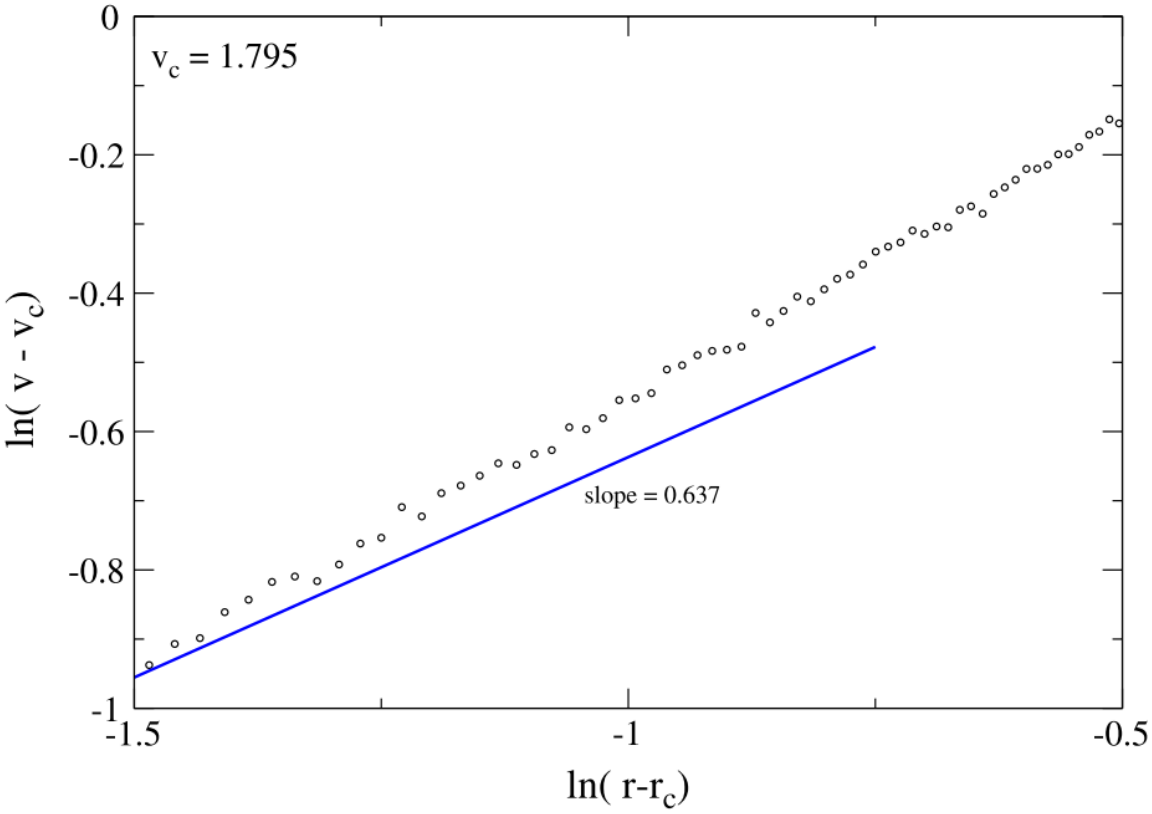

Figure 4.2: Velocity of the travelling wave in DACP. Velocity of the wave v is plotted as a function of the control parameter r (which corresponds to ε in our notation of the mean-field theory). The solid line is a guide-to-eye for $v - v_c = (r - r_c)^{\nu_{||}^{1\mathrm{DDP}} - \nu_{\perp}^{1\mathrm{DDP}}}$. The figures is adopted from Ref. [24].

the ordinary setup we discussed in the previous Chapter, where, for finite system, true steady state is always absorbing and one is often forced to consider *quasi*-steady state.

Our model is more advantageous than DACP in a sense that it allows us to tune both percolation probability and speed of advection independently. In DACP, the effective diffusion coefficient is coupled with a speed of advection, and hence one cannot study the dynamics with non-vanishing but weak advection. Price to pay for this advantage is that correspondence between the behavior for the finite system with N sites and that for the first N sites are not exact (unless $\theta = \pi/4$, where the state of the ith site from the wall is independent from that of the jth site for $i < j$). However, as we will see in the following, clear scaling behavior can be seen even in the present model, and hence we do not consider the price to be expensive for our purpose.

We performed a Monte–Carlo simulation on a lattice of the size N. Unless otherwise stated, we set $N = 8,192$. We started our simulation with the system whose site in the wall is active and other sites are inactive. In order to study the steady state of the model, we first performed the simulation for $W_{\rm warm}$ timesteps and then the statistics were accumulated over another $W_{\rm sample}$ timesteps. Unless otherwise stated, we fixed $W_{\rm warm}$ and $W_{\rm sample}$ to be $W_{\rm warm} = 15 \times 10^4$ and $W_{\rm sample} = 85 \times 10^4$, respectively. The simulation was repeated over 16 times to further improve statistics.

4.3 Results – Order parameter

4.3.1 Numerical results

First, we shall see that the model has two distinct phases by studying the order parameter. Due to the breakdown of Galilean invariance we mentioned above, order parameter ρ has to be measured with respect to the distance x from the wall. We defined the order parameter $\rho(x)$ as a fraction of time that the xth site from the wall is active during the stationary simulation. The results shown in Fig. 4.4a shows that $\rho(x)$ decays exponentially when the percolation probability p is small whereas it saturates to a finite value when $p > p_c$. This suggests that the model has a distinct transition from so-called a low-density phase to a high-density phase, despite the fact that absorbing state is no longer present. Although the critical point p_c is expected to be identical with the original directed bond percolation for a square lattice ($p_c = 0.644700185(5)$ [55]), location of the critical point can be determined *a posteriori* by using the power law decay of the order parameter which is expected near the critical point: At the critical point, the order parameter is expected to decay in a power law with exponent of $-\beta/\nu_{||}$ (the inset of Fig. 4.4a), as expected from (4.6).

The exponential decay in the low-density phase allows us to define a decay length L as

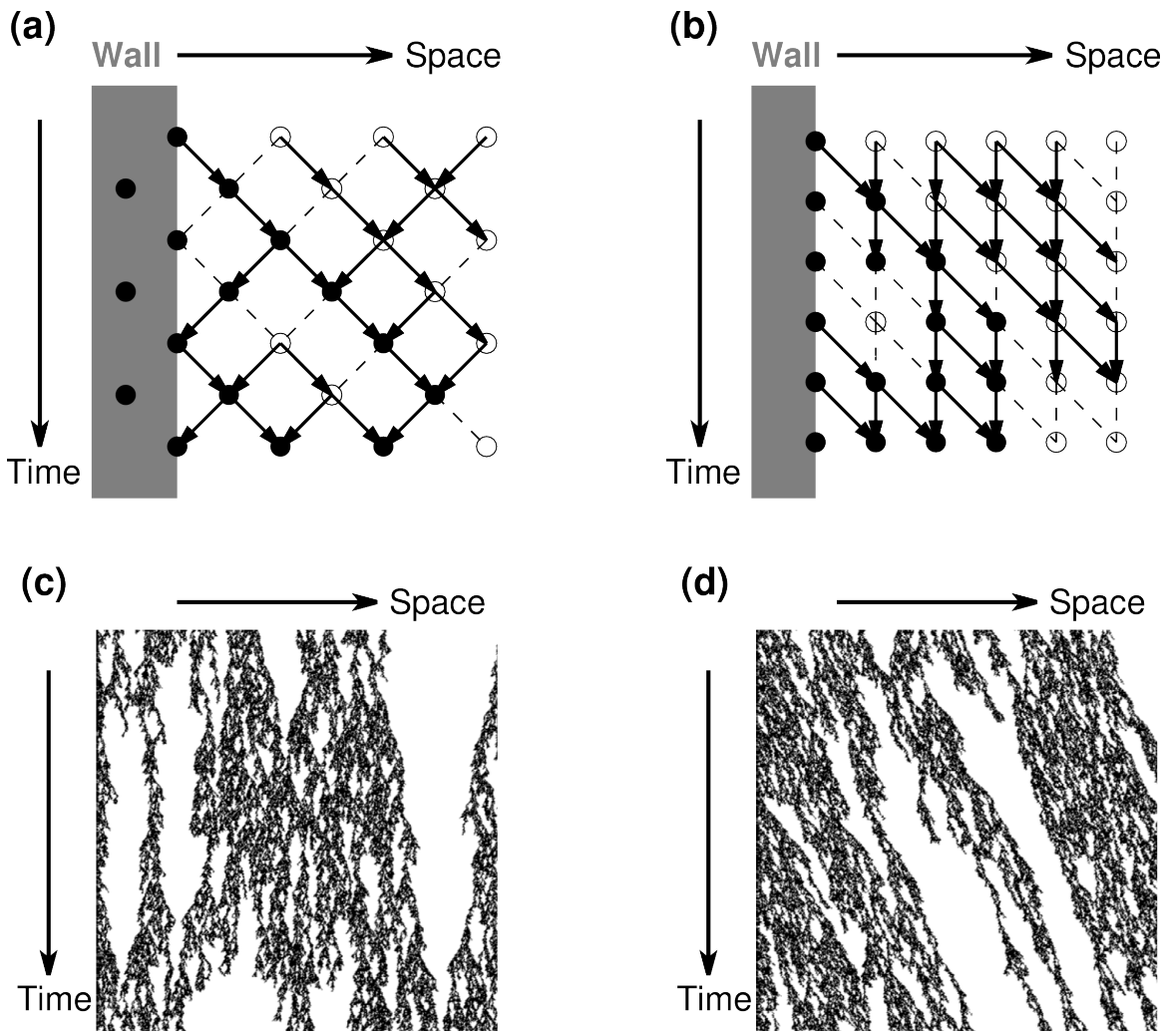

Figure 4.3: Schematic representation of the model. **a**: Dynamic rules without advection. **b**: Dynamic rules with advection ((4.13) in text). **c**: Typical spatiotemporal dynamics near the wall for $\theta = 0$. **d**: Typical spatiotemporal dynamics near the wall for $\theta = 2\pi/9$. For **c** and **d**, a case with $p = 0.64807$ ($\varepsilon := (p - p_c)/p_c \sim 5 \times 10^{-3}$) is shown.

a characteristic length of the decay at $p < p_c$, that is,

$$\rho(x) \sim \exp(-x/L(p;\theta)) \quad \text{for} \quad p < p_c, x \gg 1 \tag{4.15}$$

As shown in Fig. 4.4b, we found that L as a function of $p - p_c$ shows a power-law behavior in the vicinity of the critical point, and the exponent of the power-law behavior coincides with the critical exponent $\nu_{||}$ of DP associated with divergence of the correlation time, as long as advection is sufficiently strong (that is, θ is large). These results are consistent with those reported by Costa *et al.* [24], where a heuristic argument for this result is also given. Indeed, one can see, from the inset of Fig. 4.4b, that $L(p;\theta)/\tan\theta$ takes very similar value among various θ provided that p is same, suggesting that $L(p;\theta)/\tan\theta$ corresponds to the correlation time of the system. This implies that one can use $\rho(x)$ instead of interval distribution to probe divergence of correlation time, allowing him/her to effectively sidestep the difficulty we described in the previous Chapter.

Price to pay for the ability to measure correlation time using the spatial decay of the order parameter $\rho(x)$ is difficulty in measuring critical exponent β from stationary value of $\rho(x)$ which is expected for sufficiently large x. Since the decay length L diverges in a same manner as the correlation time, there is a considerable fraction of time in which the site is active even in the low-density phase unless one measures ρ at extremely far away from the wall. We demonstrate this effect by showing the results of the measurement of the order parameter ρ at the fixed observation point (8,000th site from the active wall) for $\theta = \pi/4$, as shown in Fig. 4.4c. One can see a significant round-off at the onset of the high-density phase. However, we are still able to plot the stationary value with respect to ε by making use of the knowledge of the location of the critical point we can obtain through $\rho(x)$, and power-law behavior with the exponent of β can be confirmed.

Having seen how the critical exponents β and $\nu_{||}$ can be measured using the steady state of this model, let us now study how $\rho(x)$ experiences crossover from a case without advection (just a simple active boundary condition, as mentioned in e.g. [35, 47]) to a case with advection. To address this issue, we measured $\rho(x)$ in a vicinity of the critical point ($p = 0.644710$, that is, $\varepsilon \sim 1.5 \times 10^{-5}$) for various θ. Since the correlation length and the correlation time of the system is expected to be very large, we performed the simulation on a setup which is larger in both space and time: We set N, W_{warm} and W_{sample} respectively to be $N = 32,768$, $W_{\text{warm}} = 10^6$ and $W_{\text{sample}} = 3 \times 10^6$ in this case. As one can see from the results shown in Fig. 4.4d, we observe a power law decay whose exponent is different from $\beta/\nu_{||}$ that we have seen previously: Actually, the exponent coincides with $\beta/\nu_{\perp}$ which is expected from a phenomenological scaling argument in a case without advection [44]. Beyond a certain lengthscale, the power-law decay with the exponent $-\beta/\nu_{||}$ is recovered, although deviation from the expected behavior is present due to an inactive boundary condition placed at the other side of the system. We will come back to this point after giving theoretical interpretations of the numerical results in terms of a mean-field theory.

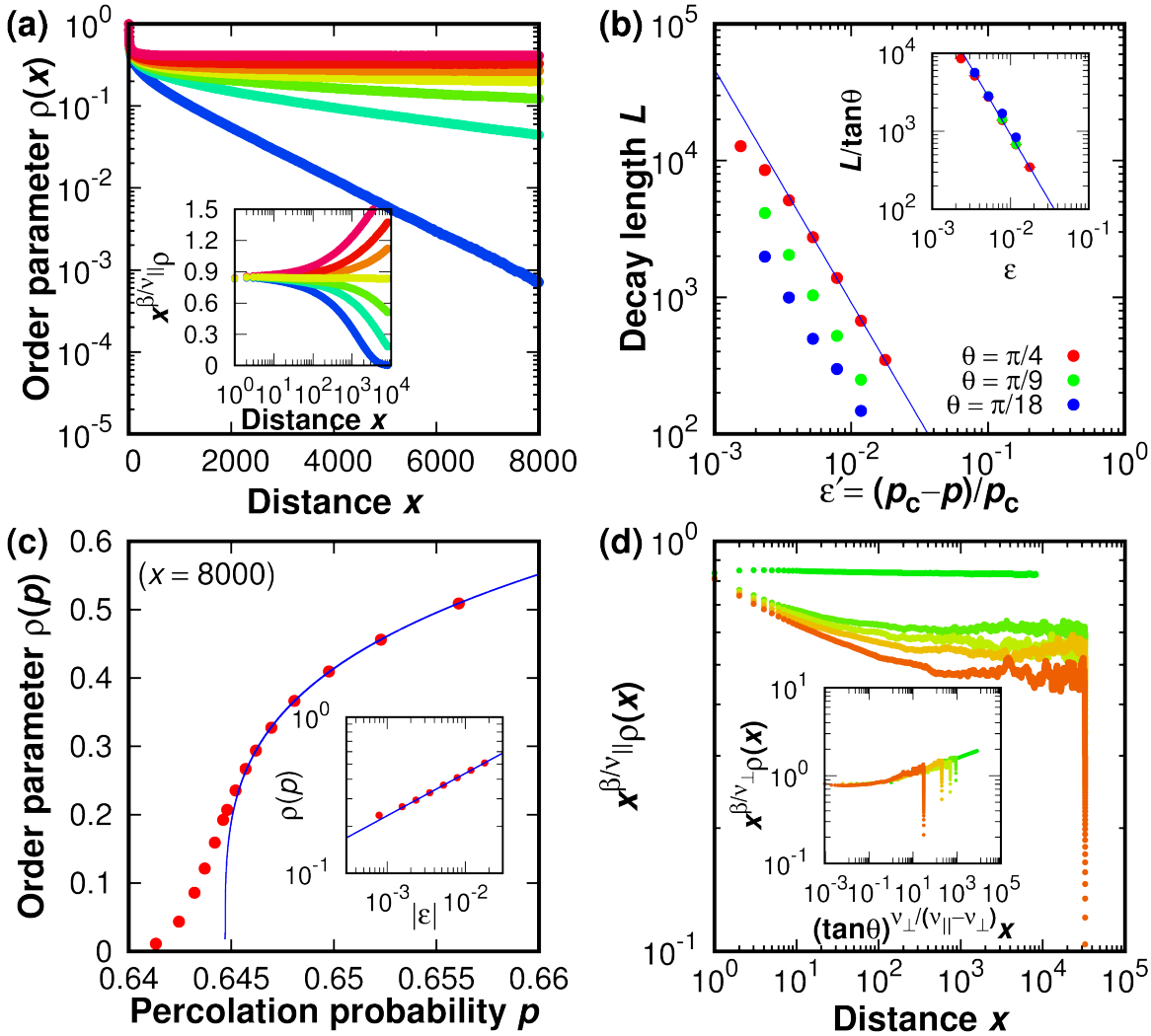

Figure 4.4: Order parameter of the directed percolation model with active wall and asymmetric connection. **a**: Spatial dependence of the order parameter $\rho(x)$ for $p-p_c = (1.5)^{2k}\times 10^{-3}$ $(k = 2, 1, 0)$, $p = p_c$ and $p - p_c = -(1.5)^{2k} \times 10^{-3}$ $(k = 0, 1, 2)$, from top to bottom. A case with $\theta = \pi/4$ is shown as an example. Inset shows the same data, but the vertical axis is rescaled by $x^{\beta/\nu_{||}}$. **b**: Decay length L (see text) of the order parameter for various θ. The blue line is a guide-to-eye for $L \sim \varepsilon^{-\nu_{||}}$. The inset shows $L/\tan\theta$ as a function of ε. **c**: Order parameter ρ measured at $x = 8,000$ for various $\theta = \pi/4$. Solid curve represents a guide to eye for $\rho \sim (p - p_c)^{\beta}$. **d**: $\rho(x)$ in a vicinity of the critical point ($p = 0.644710$) for $\theta = \pi/4$ and $\theta = (7 - 2k)\pi/180$ $(k = 0, 1, 2, 3)$, from top to bottom. Here, we performed a longer numerical simulation in both space and time (except for $\theta = \pi/4$): $N = 32,768$, $W_{\text{warm}} = 10^6$ and $W_{\text{sample}} = 3 \times 10^6$, and statistics were acquired over 8 realizations. Inset shows the same data, but both the horizontal axis and the vertical axis are rescaled as $(\tan\theta)^{\frac{\nu_\perp}{\nu_{||}-\nu_\perp}} x$ and $x^{\beta/\nu_\perp}\rho(x)$, respectively. Note that the theoretical value $\beta, \nu_{||}, \nu_\perp$ of the DP universality class was used to rescale the data.

4.3.2 Mean-field theory

A mean-field theory provides a useful way to interpret the crossover we have seen above. Although the mean-field theory is not exact in d-dimensional system with $d \leq 3$, it successfully captures essential features of our results. Let us recall the mean-field theory of DACP (4.9)

$$\frac{\partial \rho}{\partial t} = \varepsilon\rho - \lambda\rho^2 - v_x \frac{\partial \rho}{\partial x} + D\frac{\partial^2 \rho}{\partial x^2}$$

with an active boundary condition

$$\lim_{x \to +0} \rho(x) = \infty.$$

As long as one is interested in the steady state, one may put $\partial\rho/\partial t = 0$, and since Galilean invariance is expected to hold except for streamwise direction, one may also put $\nabla^2\rho = \partial_x^2\rho$. As a result, we obtain the following Fisher–Kolmogorov–Petrovskii–Piskunov (FKPP) equation:

$$\varepsilon\rho - \lambda\rho^2 - v_x \frac{\mathrm{d}\rho}{\mathrm{d}x} + D\frac{\mathrm{d}^2\rho}{\mathrm{d}x^2} = 0. \tag{4.16}$$

As shown by Costa *et al.* [24], the asymptotic solution of (4.16) for large x takes several forms depending on ε. For $\varepsilon < 0$, which we will refer to as the low-density phase, we have

$$\rho(x) \simeq \exp(-x/\xi) \text{ where } \xi = \frac{2D}{\sqrt{v_x^2 + 4|\varepsilon|D} - v_x}. \tag{4.17}$$

For sufficiently small $|\varepsilon|$, ξ diverges as $|\varepsilon|^{-1}$ for $v_x' > 0$ and thus the exponent 1 coincides with the mean-field DP exponent of $\nu_{||}$. If $v_x = 0$, ξ diverges as $|\varepsilon|^{-\frac{1}{2}}$, and the exponent $1/2$ coincides with the mean-field DP exponent of $\nu_\perp$. On the other hand, we have $\rho(x) \simeq \varepsilon/\lambda$ for $\varepsilon > 0$ and the exponent 1 coincides with the mean-field DP exponent of β. Note that the asymptotic behavior of $\rho(x)$ for $v_x > 0$ does not change even if $v_x = 0$.

To focus on our purpose with the simplest case, we concentrate on a case with $\varepsilon = 0$, that is, when the system is exactly on a critical point (asymptotic solutions for large x in both the high-density and the low-density phase has already given [24]). If the advection is absent ($v_x = 0$), we can easily solve (4.16) to find $\rho(x) = 6Dx^{-2}/\lambda$. The exponent of 2 coincides with the mean-field DP exponent of $\beta/\nu_\perp$. Meanwhile, we find $\rho(x) = v_x x^{-1}/\lambda$ if the effect of advection is so large ($v_x \gg 1$) that the diffusive (fourth) term of (4.16) is negligible compared to the advective (third) term. The exponent of unity coincides with the mean-field DP exponent of $\beta/\nu_{||}$.

Given that which solution can be found is a matter of comparison between the second term and the third term, it is natural to ask for lengthscale x_* at which the second term and the third term becomes comparable. To address this question, we check the ratio of the terms which are assumed to be dominant over one assumed to be negligible [9]. If we substitute $\rho(x) = 6Dx^{-2}/\lambda$ (the solution of the (4.16) for $v_x = 0$) to the advection term and

take a ratio over the diffusion term, we obtain the following:

$$v_x \frac{\mathrm{d}}{\mathrm{d}x} \frac{6D}{\lambda} x^{-2} / \left(D \frac{\mathrm{d}^2}{\mathrm{d}x^2} \left(\frac{6D}{\lambda} x^{-2} \right) \right) = \frac{v_x}{2D} x. \tag{4.18}$$

Thus, the assumption that the advection term is negligible compared to the diffusion term is valid for $x \to 0$. Conversely, a similar argument leads us to find that the the assumption that the diffusion term is negligible to advection term is valid for $x \to \infty$. As a result, we have the following asymptotic solutions of (4.16):

$$\rho(x) \sim \begin{cases} \dfrac{6D}{\lambda} x^{-2}; & x \to 0, \\ \dfrac{v_x}{\lambda} x^{-1}; & x \to \infty. \end{cases} \tag{4.19}$$

The distance x_* which satisfies $6Dx_*^{-2}/\beta = v_x x_*^{-1}/\beta$, that is,

$$x_* = 6D/v_x, \tag{4.20}$$

gives an approximate lengthscale at which $\rho(x)$ experiences the crossover from $\rho(x) \sim 6Dx^{-2}/\lambda$ to $\rho(x) \sim v_x x^{-1}/\lambda$. As expected, x_* diverges to infinity as $v_x \to +0$.

4.3.3 Numerical results revisited

Even though the mean-field theory cannot be directly applied when the spatial dimension d is less than 4, one can give a heuristic argument to estimate the typical lengthscale at which $\rho(x)$ experiences crossover, albeit more roughly. Repeating the similar argument as what we gave above, one is led to

$$\rho(x) \sim \begin{cases} x^{-\delta_\perp}; & x \to 0, \\ (x/v_x)^{-\delta_{||}}; & x \to \infty, \end{cases} \tag{4.21}$$

where $\delta_\perp = \beta/\nu_\perp$ and $\delta_{||} = \beta/\nu_{||}$. Then one can deduce, from a parallel argument to the mean-field theory, that

$$x_* \sim v_x^{-\frac{\nu_\perp}{\nu_{||} - \nu_\perp}}. \tag{4.22}$$

It is worthwhile to note that the value of $\nu_\perp/(\nu_{||} - \nu_\perp)$ is unity in $d \geq 4$, so that it coincides with what we have obtained in the mean-field theory (4.20). Recalling the empirical observation in Fig. 4.4d that the coefficient of the power-law decay with the exponent $\beta/\nu_\perp$ is not sensitive to the value of θ, we arrive at the following scaling ansatz:

$$\rho(x; \theta) \sim x^{-\beta/\nu_\perp} f((\tan\theta)^{\frac{\nu_\perp}{\nu_{||} - \nu_\perp}} x), \tag{4.23}$$

where f is the universal scaling function. We rescaled the data in Fig. 4.4d according to this ansatz, and we found a reasonably good collapse as a result, as shown in the inset of Fig. 4.4d (besides the artifact due to the inactive boundary condition).

4.3.4 Remarks on some preceding studies

A few comments are in order before closing this Section: Statistical property of the decay length L is different from the curtain width introduced by Chen *et al.* [22], although the intuitive meaning of these quantities are similar to each other. In Ref. [22], the authors considered probability $P_w(n)$ that active state is present until $n\xi_\perp$ in the low-density phase, and mode w of the distribution $P_w(n)$ was defined as the curtain width. In that case, $P_w(n)$ is equivalent to the probability that the *longest-surviving* cluster which we observe at time t was generated at $t - n\xi_\perp/v$, where v is the velocity of the advection. Thus, $P_w(n)$ actually probes extreme value of lifetime of a cluster of active sites in a sense, and it is reasonable that the resulting curtain width w could be longer than the typical distance for which an individual cluster can travel from the active wall. As clarified by Chen *et al.*, the curtain width w does not obey a pure power law, but is affected by the additional logarithmic factor:

$$w \simeq A\varepsilon^{-\nu_{||}} \log\left(\frac{\varepsilon_0}{\varepsilon}\right). \tag{4.24}$$

On the other hand, the order parameter $\rho(x)$ in present work directly probes the survival probability of individual cluster, and so such an additional factor is absent.

Another comment concerns with apparent contradiction with Costa *et al.*, who claimed that the exponent $\nu_\perp$ cannot be accessed from steady-state density profile. In the driven asymmetric contact process (DACP) proposed by Costa *et al.* [24], the velocity v_x of the advection and the diffusion constant D are coupled with the activation rate r by the following:

$$v_x = r(1-\rho), \quad D = v_x/2. \tag{4.25}$$

This implies that the velocity v_x of the advection is almost fixed near the critical point, and v_x is not close to zero (recall that $r_c = 3.3055(5)$). Also, assuming (4.22) gives a good approximation of the lengthscale of the crossover, the typical lengthscale x_* of the crossover decreases very rapidly with v_x. This makes the observation of the crossover near the criticality in DACP practically impossible. However, the activation rate and the velocity of the advection may be safely regarded as independent from each other in some cases (e.g. applying shear flow to electroconvection of liquid crystals), and the crossover could be observed in that case. Thus, our claim and that made by Costa *et al.* are not incompatible to each other, but the apparent contradiction stems from specific selection of the model.

4.4 Results – Inactive interval distribution

Since the crossover of the order parameter is not clearly observed unless the advection is sufficiently weak, it is desirable to find an alternative way to measure the remaining static critical exponent $\nu_\perp$. In the following, we demonstrate that $\nu_\perp$ can be measured via probability distribution of *duration* of interval measured at far away from the wall. Although

the temporal interval distribution generally depends on the distance x from the active wall due to the breakdown of Galilean invariance, choice of x does not make noticeable difference as long as the saturation of $\rho(x)$ is achieved. We measured the complementary cumulative distribution function $R(\tau)$ for the temporal interval distribution using the empirical estimator (3.30). The use of the empirical estimator is justified because the correlation time of the system is about 10^4 time steps at the longest within the range of p in the present study (recall the inset of Fig. 4.4b), and hence W_{sample} is about 100 times longer than the correlation time.

Just like the ordinary case we have seen in the previous Chapter, we observed a crossover to an exponential decay for sufficiently large τ (Fig. 4.5a), enabling us to investigate a characteristic time ξ of the decay:

$$R(\tau) \sim \exp(-\tau/\xi) \quad \text{for} \quad \tau \gg 1. \tag{4.26}$$

The characteristic time diverges in a power law with exponent $-\nu_{||}$ when $\theta = 0$ as expected. As we increase the velocity $\tan\theta$, however, we observe that ξ deviates from the expected power law, but exhibits power-law divergence with different exponent: In fact, the results shown in Fig. 4.5b suggest that the new exponent is close to the critical exponent $\nu_\perp$ of the DP universality class. The larger a value of θ is, the larger a value of ε_* at which ξ experiences the crossover becomes.

Simple heuristics provides clear interpretation on the results, even though analytical treatment of the interval distribution is substantially more difficult than the order parameter due to the fact that the distribution should be regarded as a multi-point correlation function (see Section 3.1.2). Typical spatiotemporal dynamics of DP with advection at far away from the active wall is shown in Fig. 4.6a. If the distance from an active wall is sufficiently large, correlation between the local state at the probe and active wall is negligible, and hence the dynamics looks similar to each other if we apply suitable Galilean transformation (Fig. 4.6b), although active wall is still needed to sustain the high-density phase. Then, in this coordinate system, measuring the temporal intervals at the fixed position corresponds to measure the length of the inactive cluster along a tilted line. Here, we apply a somewhat rough approximation where we regard each cluster of inactive state as an ellipse which has a major axis of length $l_{||}$ and a minor axis of length $l_\perp$. Choice of the major axis is based on the fact that $\nu_{||} > \nu_\perp$ in the DP universality class and so that the correlation time diverges more rapidly than the correlation length. Then, the length L of the longest line across the ellipse gives the characteristic time for decay of the distribution of the inactive intervals. Simple geometric argument gives

$$L \sim \sqrt{\frac{2\xi_{||}^2\xi_\perp^2}{v^2\xi_{||}^2 + \xi_\perp^2}}. \tag{4.27}$$

Important consequence of (4.27) is that, in the presence of the advection, L is expected to

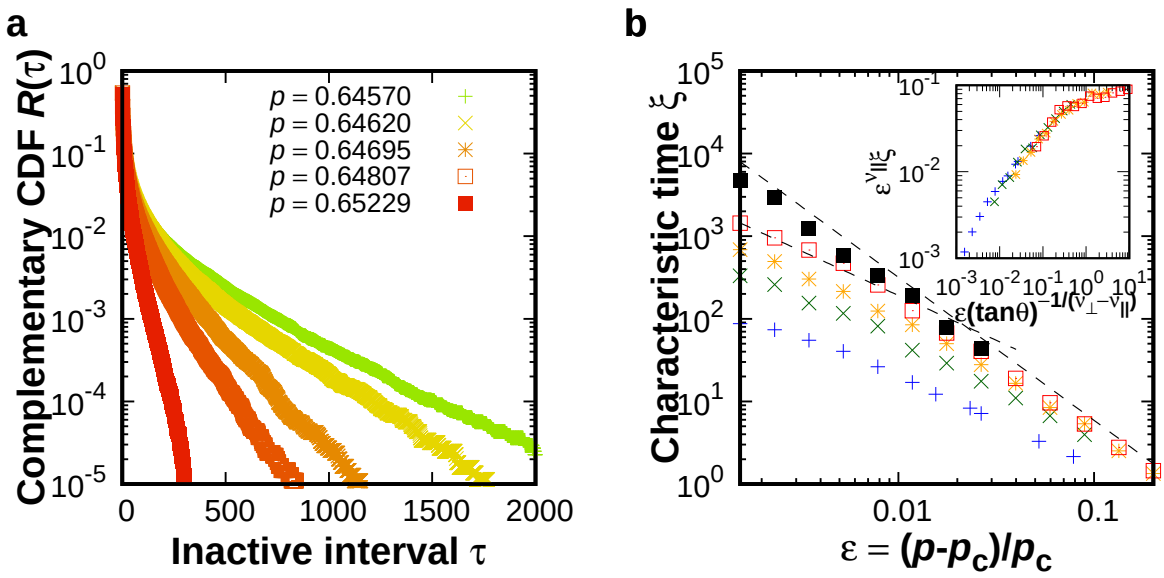

Figure 4.5: Temporal interval distribution of the directed percolation model with active wall and asymmetric connection. **a**: Temporal interval distributions for various p is shown for $\theta = \pi/9$ as an example. **b**: Dependence on the distance to the criticality ε of characteristic time ξ for $\theta = 0$ (black), $\theta = \pi/36$ (red), $\theta = \pi/18$ (orange), $\theta = \pi/9$ (green) and $\theta = \pi/4$ (blue). The steeper dashed line shows a guide-to-eye for the power-law behavior with exponent $\nu_{||}$, and the other line for $\nu_{\perp}$. The inset shows the same data, but the horizontal axis and the vertical axis is rescaled as $\varepsilon(\tan\theta)^{-\frac{1}{\nu_{||}-\nu_{\perp}}}$ and $\varepsilon^{\nu_{||}}\xi$, respectively. Note that the theoretical value $\nu_{||}, \nu_{\perp}$ of the DP universality class was used to rescale the data.

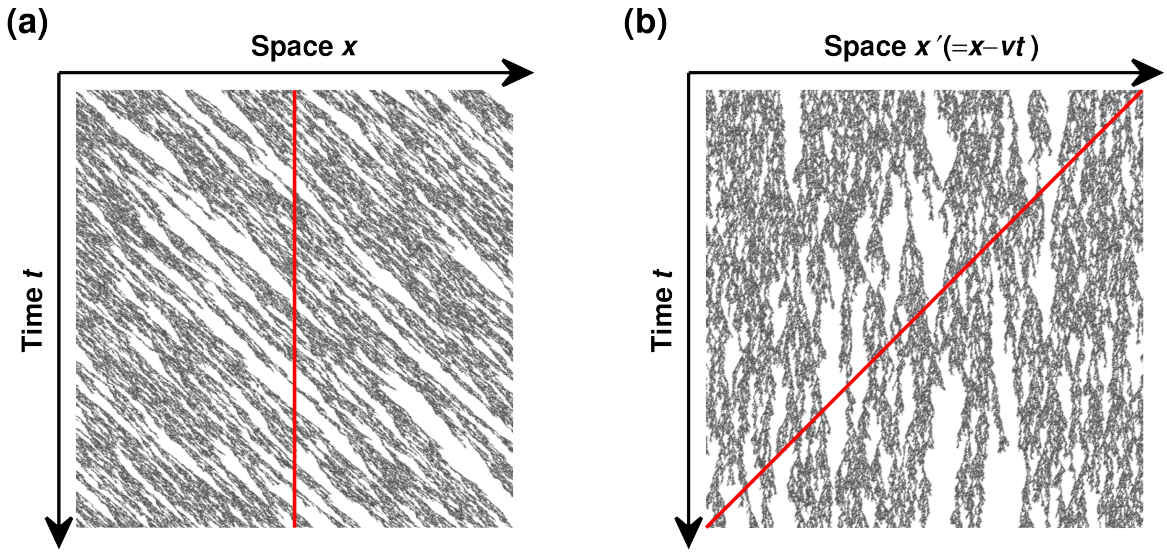

Figure 4.6: Typical spatiotemporal dynamics of DP with advection in the high-density regime. Active sites and inactive sites are depicted in gray and white, respectively. **a**: In original coordinate system, measuring inactive intervals at fixed position corresponds to measure inactive intervals along a vertical line (red line is shown as an example). **b**: Same dynamics as **a**, but Galilean transformation is applied. The resulting picture is very similar to ordinary DP. In this coordinate system, the red line is tilted, whose angle depends on the velocity v of the advection.

exhibit power-law divergence with exponent $\nu_\perp$ near the critical point. The crossover is expected for ε_* such that $v^2\xi_{||}^2 \sim \xi_\perp^2$, that is,

$$\varepsilon_* \sim v_x^{\frac{1}{\nu_{||}-\nu_\perp}}. \tag{4.28}$$

Parallel argument to what we gave for deriving (4.23) leads us to the following universal scaling ansatz for the characteristic time ξ:

$$\xi(\varepsilon; \tan\theta) \sim \varepsilon^{\nu_{||}} g((\tan\theta)^{-\frac{1}{\nu_{||}-\nu_\perp}}\varepsilon), \tag{4.29}$$

where g is the universal scaling function. We rescaled the data in Fig. 4.5b according to this ansatz, and we again found a reasonably good collapse as a result, as shown in the inset of Fig. 4.5b. This suggests that the aforementioned simple argument captures the essence of the numerical results. Note that, if one would like to consider spatially d-dimensional systems, repeating the geometric argument in a case of ellipsoids instead of ellipses suffices, although the essential result is not expected to change.

Recalling the phenomenological scaling argument given in Section 3.1.2, it is natural to speculate that the universal scaling ansatz (3.22)

$$R(\tau; \varepsilon) \sim \varepsilon^{\nu_{||}-\beta} h_{||}(\varepsilon^{\nu_{||}}\tau)$$

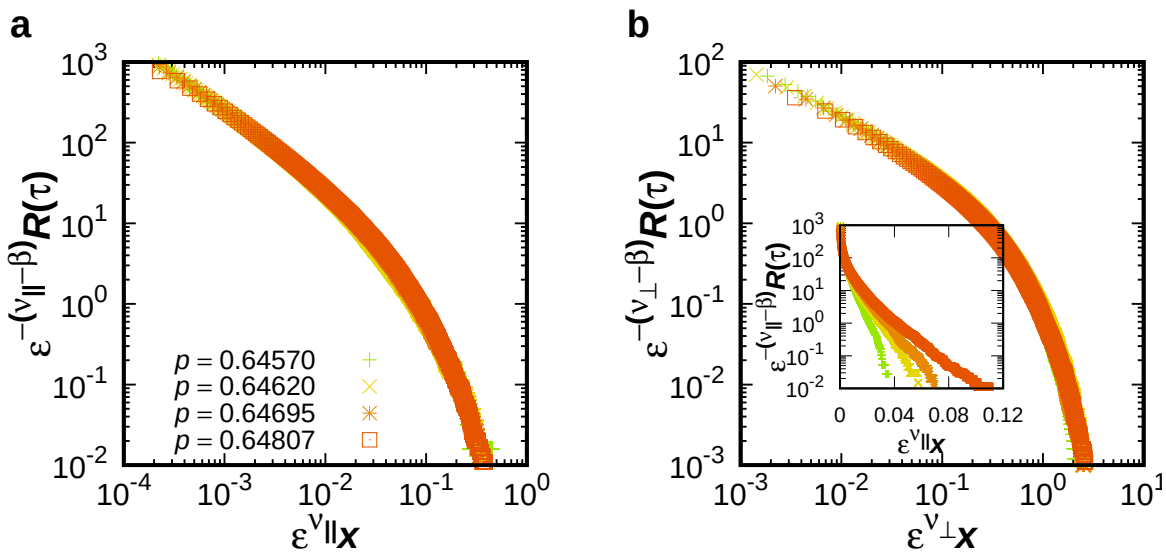

Figure 4.7: Universal scaling of the temporal interval distribution of the directed percolation model with active wall and asymmetric connection. **a**: Temporal interval distributions for $\theta = 0$, rescaled according to the scaling ansatz (3.22). **b**: Temporal interval distributions for $\theta = \pi/9$ (original data is shown in Fig. 4.5a), rescaled according to the scaling ansatz (3.23). Inset shows the same data rescaled according to (3.22). Note that the theoretical value $\beta, \nu_{||}, \nu_{\perp}$ of the DP universality class was used to rescale the data.

may hold in a case without advection whereas (3.23)

$$R(\tau;\varepsilon) \sim \varepsilon^{\nu_\perp - \beta} h_\perp(\varepsilon^{\nu_\perp}\tau)$$

with advection, as long as the system is sufficiently close to the critical point. To examine this speculation, we rescaled the data for $\theta = 0$ and $\theta = \pi/9$ (as an example) according to the universal scaling ansatz (3.22) and (3.23), respectively. The results shown in Fig. 4.7a and 4.7b indicates this is indeed the case (It is important to note that, if the advection is present, the interval distribution for various p does not overlap under rescaling with respect to the scaling ansatz (3.22), as shown in the inset of Fig. 4.7b). From these observations, one can safely conclude that the critical exponent $\nu_\perp$ in this case can be measured through temporal interval distributions at the steady state, even if the advection is too strong for the crossover of $\rho(x)$ to be observed clearly. Hence we no longer need to rely on measuring the velocity of the activity wave [24] which suffers from the same drawbacks as the critical spreading protocol.

4.5 Discussions

To conclude this Chapter, let us summarize how one can measure the critical exponents in a system with an active wall and advection:

- Even though the system no longer possesses an absorbing state, qualitative behavior of the density $\rho(x)$ as a function of the distance from the active wall x is expected to change across a certain critical point p_c. Below the critical point, $\rho(x)$ is expected to decay exponentially whereas to saturate at some non-zero value above the critical point. Near the critical point, a power-law decay of $\rho(x)$ may be observed.

- The critical exponent $\nu_{||}$ associated with the divergence of the correlation time can be measured through the decay length L of $\rho(x)$ in the low-density phase: $L \sim (p_c - p)^{-\nu_{||}}$ is expected near the critical point (where p denotes the control parameter of the system).

- The critical exponent β associated with the order parameter can be measured through $\rho(x)$ at sufficiently far away from the wall in the high-density phase: $\rho \sim (p - p_c)^{\beta}$ is expected. Although the round-off is expected near the critical point (especially for spatially one-dimensional systems, where L is expected to change very rapidly), reasonable estimate of the exponent can be obtained provided that the scaling regime is wide enough. One could also consider making use of the power-law decay in the vicinity of the critical point (with exponent $-\beta/\nu_{||}$) and checking consistency.

- The most secure way to measure the critical exponent $\nu_{\perp}$ associated with the divergence of the correlation length is to study the temporal interval distribution and to estimate the characteristic time ξ of the decay: $\xi \sim (p - p_c)^{-\nu_{\perp}}$ is expected near the critical point, although the crossover to $-\nu_{||}$ is possible for large $p - p_c$. If the advection is sufficiently weak, one may observe a crossover between two different power laws (namely, $x^{-\beta/\nu_{\perp}}$ for small x and $x^{-\beta/\nu_{||}}$ for large x) for $\rho(x)$ in the vicinity of the critical point p_c.

Thus, the complete set of the static critical exponents $(\beta, \nu_{||}, \nu_{\perp})$ can be observed by steady-state measurements. In particular, it is worthwhile to emphasize that one does not have to rely on interval distributions to obtain $\nu_{||}$ and hence one is practically free from considering rather sophisticated data analysis we have seen in Chapter 3, although intentionally applying advection in a controlled manner might be more difficult in some systems.

While we concentrated on presenting the numerical results in spatially one-dimensional systems, the results are expected to be also applicable for higher dimensions, because the results can be interpreted in terms of the phenomenological scaling theory, which does not assume specific number of spatial dimensions. Note that we have numerically seen in Ref. [84] that the essential results does not change in $d = 2$.

Chapter 5

A Universal Transition to Turbulence in Channel Flow

Related publication by the author: M. Sano and K. Tamai. A universal transition to turbulence in channel flow. Nat. Phys. **12**, 249-253 (2016).
Contribution: The author (K.T.) set up the system to visualize and record the dynamics of the transitional channel flow, and performed a series of experiment with his collaborator (M.S.). The author performed an image analysis independently from the collaborator and checked the consistency of the results each other. Also, the author devised a method to measure the critical exponents from the binarized data, which was later developed to a more systematic study, as reported in Chapter 3 and Chapter 4 in this thesis.

In the previous Chapter, we have seen that the critical exponents of the DP universality class $\beta, \nu_{||}, \nu_{\perp}$ can be measured respectively through order parameter at far away from the wall in high-density phase, decay length of the order parameter ρ in low-density phase and temporal interval distribution in high-density phase respectively, when DP is subject to an active boundary condition and advection. We are now on a stage where we carry on the experiments and examine whether the transition indeed falls into the DP universality class or not.

5.1 Specific backgrounds

5.1.1 Spatiotemporal intermittency and the DP universality class

By the late 1980s, the process of transition to temporal chaos in strongly confined systems has been reasonably understood, due to the extensive studies on low-dimensional dissipative dynamical systems and to rapid progress in experimental works. Remarkable results in the studies along this line include the discovery of the universality for period-doubling route to chaos [32] and experimental observation of it [63, 67]: A group headed by Libchaber

performed a series of experiments on Rayleigh–Bénard convection in liquid helium and mercury. In their experiments, the working fluids were strongly confined (in other words, the aspect ratio of the cell was very small) so that only a small number of convective rolls were formed, and temperature oscillations were measured using local bolometers. As the temperature difference ΔT between the top and the bottom part of the fluid (which is proportional to the Rayleigh number) was increased, the period-doubling cascade was observed. Precise measurements near the onset of each bifurcation allowed Libchaber and his colleagues to determine the ratio δ of the difference of the Rayleigh number between the adjacent bifurcations to be $\delta = 4.4(1)$, which was found to be close to the celebrated Feigenbaum constant $\delta = 4.669\cdots$.

In many systems of practical interest, however, the system is only weakly confined. In that case, one may be forced to deal with *spatiotemporal* chaos where chaos has both a spatial and a temporal meaning, and hence the situation is much less advanced than that in strongly confined systems. It has been a challenging question whether universal description can be obtained for spatiotemporal chaos, especially for subcritical bifurcations where the transition can happen (as a response to strong disturbance) even though the regular (laminar) state of the system is stable against infinitesimal disturbance.

The possible relation between subcritical transitions to turbulence and the DP universality class was first explicitly conjectured by Yves Pomeau in 1986 [79]. The idea behind this conjecture is to focus on randomness of turbulent fluctuation when trying to understand the behavior of fronts separating turbulent regions to laminar ones: Due to the randomness, turbulent fluctuation (which may be localized in space) may either relax spontaneously into laminar state or contaminate its neighbor, and the competition between the two processes is highly analogous to the dynamics of the models in the DP universality class. More specifically, the conjecture can be stated like the following: Transitions to turbulence via spatiotemporal intermittency (intermittent spatial coexsistence of laminar state and turbulent state) may fall into the DP universality class. This conjecture suggests that the universal description for subcritical transition to spatiotemporal chaos may be available.

For careful readers who may have confused, let us emphasize here that subcritical nature of the transition and continuity of it in a sense of statistical mechanics do not contradict with each other. Indeed, subcritical nature of the transition implies that one expects to observe hysteresis as one continuously varies the control parameter of the system, which is one of the prominent characteristics of first-order (discontinuous) phase transitions in equilibrium. However, as we have already argued in Section 2.1, an absorbing state in a continuous absorbing phase transition is not completely unstable but metastable, and hence the expected hysteresis does not necessarily imply that the transition is discontinuous. Another point to concern is that the localized chaotic (turbulent) state may have the minimal size below which it cannot be sustained. However, such a presence of the minimal size does

not constitute a discontinuous jump of the order parameter (which can be typically defined as an area fraction of a localized chaotic (turbulent) state) in the thermodynamic limit, provided that the minimal size is not proportional to the aspect ratio of the system. In summary, it is possible in principle that a system exhibits a subcritical transition to spatiotemporal chaos which is continuous in a sense of statistical mechanics, although one should be careful not to confuse with notions in studies of dynamical systems.

Having seen that a continuous transition to spatiotemporal intermittency may fall into the DP universality class *in principle*, the next natural question is whether this is indeed the case *in reality*. This question led to extensive experimental studies on Rayleigh–Bénard convection [23, 25] in a system with higher aspect ratio than that of Libchaber's. As a result, the researchers reported significant deviation from the conjectured DP universality class, although $\beta = 0.30(5)$ in a linear cell is in a reasonable agreement with the spatially one-dimensional DP (see Tab. 2.2). This suggests that the conjecture by Pomeau is incorrect at least in a case of Rayleigh–Bénard convection. However, as we have seen in Chapter 3, measurements of the critical exponents $\nu_{||}, \nu_{\perp}$ with a limited resources is a delicate issue (note that the efficient and non-biased estimator of the interval distribution had not been studied until the late 1990s [99]), it should be said that it has still been unclear whether the conjecture is indeed incorrect at this stage.

5.1.2 Transitions to turbulence via spatiotemporal intermittency in shear flow

Earlier works on transitions to turbulence in shear flow suggest that the transitions are discontinuous. To the author's knowledge, the first experimental work in light of the conjecture by Pomeau has been performed by Bottin and her coworkers [11, 12]: They conducted experiments on plane Couette flow (simple shear flow between two parallel plates moving at the same speed but in opposite directions) with an apparatus of moderate aspect ratio (about $70h$ in span-wise direction and $380h$ in stream-wise, where h denotes the half width of the gap), and their experimental results suggested that the transition is discontinuous. Similar observation was obtained numerically by Duguet *et al.* [30] However, neither of the authors did not manage to study the transition very close to the critical Reynolds number, presumably due to the huge system size and very long observation time required to study the flow in that case. This makes drawing a convincing conclusion about the nature of the transition difficult, especially when there is a considerable possibility that the system exhibits continuous transition characterized by a power-law onset with a rather small exponent.

On the contrary, extensive studies on pipe flow performed in the 21st century suggest that spatiotemporal intermittency observed in pipe flow is highly analogous to DP: It has been turned out that lifetime of a turbulent puff shares a same characteristics as a memoryless

process and that the competition between the decaying process and the splitting one is the crucial factor for transitions to turbulence in pipe flow [3]. This suggests that the transition to turbulence in pipe flow is highly analogous to the phase transition in DP. More recently, numerical evidence that Couette flow exhibits scale invariance at the onset of turbulence [88], which is often interpreted as a sign of a continuous transition, although they made a tricky selection on a computational domain and hence it is not clear whether the scale invariance that Shi *et al.* is observable in reality.

5.1.3 Objectives of the research

As we have seen in the previous Subsection, there is a considerable dispute about whether the transition to turbulence in shear flow exhibits universal features as conjectured by Pomeau. Although indirect evidences have been reported from both sides of the opinion, there has been no published work which directly measured the critical exponents. Hence, the aim of the present work is to perform a series of systematic experimental studies on transitional shear flow and to provide a convincing evidence to directly address this problem.

5.2 Methods

5.2.1 Selection of the geometry

Before the experimental system is designed, one needs to consider carefully about the geometry on which one performs measurements. For example, the effective dimensionality changes the expected value of exponents and thereby practical difficulty for reliable measurements. Although pipe flow might be a natural choice considering the recent development in experiments, it is disadvantageous for measuring the critical exponents because of its quasi-one-dimensional character: In spatially one-dimensional system, the critical exponent $\beta/\nu_{||}$ of the DP universality class associated with the power-law decay of the order parameter with respect to the distance from the active wall is very small (see also Chapter 4):

$$\beta^{\mathrm{1DDP}}/\nu_{||}^{\mathrm{1DDP}} = 0.159464(5) \quad (\beta^{\mathrm{2DDP}}/\nu_{||}^{\mathrm{2DDP}} = 0.4504(10)) \tag{5.1}$$

This means that one has to measure the order parameter over six orders of magnitude just in order to observe a decay in one order of magnitude, which is obviously infeasible. Hence it is desirable to perform measurements in quasi-two-dimensional system for our purpose, and then channel flow becomes a natural choice.

5.2.2 Construction of the channel

In order to make the system as close to thermodynamic limit as possible, we constructed a huge experimental channel (Fig. 5.1a, 5.1b). The channel comprised 3 pieces of slots (see

Fig. 5.1c) with streamwise length of 1,960 mm and spanwise width of 1,000 mm. Both ends of each slot were reinforced by welding 50-mm-thick flanges to ensure the precision of joint between two slots using O-ring. The channel walls were made of 25-mm-thick Polymethyl methacrylate (PMMA) glass plates of optical surface quality. The side walls were made of PMMA strips of 50 mm$\times$1000 mm$\times$5 mm. When constructed in this way, the precision of the depth was $\pm$0.1 mm. Gap width of the channel needs to be as small as possible, but if it is too small then relative inhomogenity of the gap width due to spatial variety in the thickness of the wall becomes larger, which may work as a quenched disorder and thereby affect the resulting critical phenomena. As an acceptable compromise, the gap width was chosen to be 5 mm. Thus, the aspect ratio of the channel was $2352h \times 360h \times 2h$, which is much larger than what was used in previous studies in this context, e.g. in Bottin *et al.* [11, 12].

To avoid further deflection due to static pressure load in the channel, cross-braces were placed at 425-mm intervals along the channel. The working fluid is water. The channel inlet was connected to a buffering box via a smoothly curved contracting joint whose area contraction ratio was 1:20. To set a turbulent boundary condition, we placed a grid near the inlet. (When the grid is covered with 7 layers of mesh screens, the flow remained laminar in a whole channel at least up to $\mathrm{Re} = 1,400$. Since the covering by mesh screen was not sufficient at the edge, turbulent flows did not decay near the both ends of the buffering box near $z = 0$ mm and $z = 900$ mm at $\mathrm{Re} = 1400$. Those turbulent flows injected from the inlet gradually grew and spread. Even in that case, no spontaneous nucleation of turbulent spot from the laminar state in the middle of the channel was confirmed.) Velocity control was attained by electronically controlling the speed of pump and the opening of the valve. The flow rate Q was measured by a flow meter (FD-UH40G, Keyence) and the Reynolds number Re was estimated by

$$\mathrm{Re} = \frac{3Q}{4h\nu_K}, \tag{5.2}$$

where ν_K denotes the kinematic viscosity of the water. Note that this Reynolds number coincides with the Reynolds number defined in terms of centerline velocity if the flow is completely laminar. The temperature of the water was controlled at 25 °C within the accuracy of $\pm$0.1 °C.

5.2.3 How to visualize the flow

There are four representative ways to experimentally study the transitional shear flow, namely hot-wire anemometry, laser Doppler velocimetry, particle image velocimetry and flow visualization by reflective flakes. Hot-wire anemometry and laser Doppler velocimetry measure the velocity of the fluid at the certain point, using respectively change in electrical resistance due to cooling by the flow [77, 86, 87] and the Doppler shift caused by particles passing through interference fringe of two coherent lasers [86, 90, 104]. Meanwhile

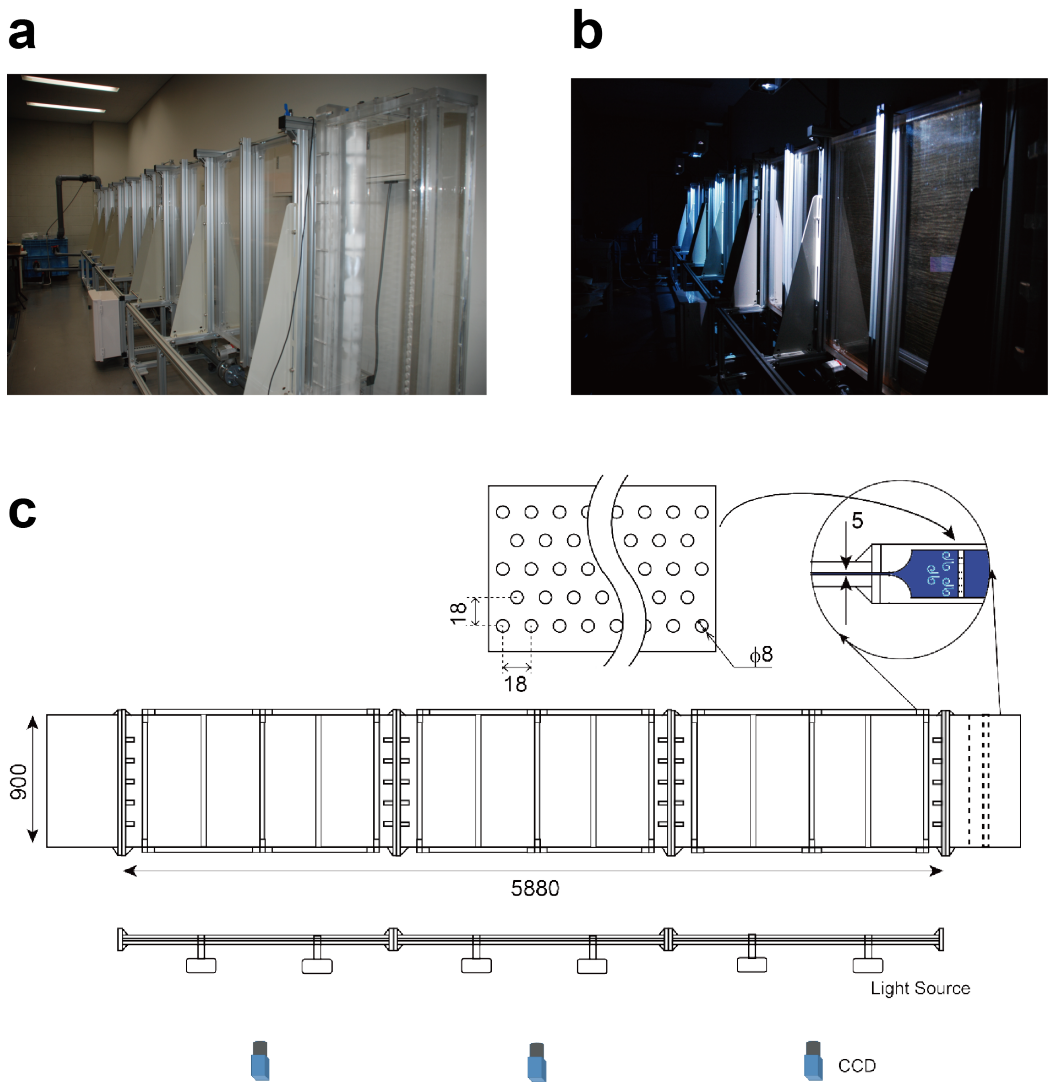

Figure 5.1: Large experimental channel used in this work. **a**: A picture of the experimental channel. **b**: The experimental channel illuminated by a light source. **c**: The figure is reproduced and modified from Supplementary Information of Ref. [84].

particle image velocimetry and flow visualization by reflective particles are used to extract information about two-dimensional (or possibly three-dimensional) flow field by making use of so-called tracer particles. Since we are interested in characterizing the dynamics of spatially localized turbulent spot, methodologies in the latter category are more favorable and hence we will describe them in some more detail in the following.

Particle image velocimetry (PIV) is an optical technique where the working fluid is seeded with small spherical particles and one tracks the motion of the particles, assuming that these particles faithfully follow the velocity field of the fluid[1]. Standard procedure for PIV is as follows:

1. Immerse moderate amount of seeding particles into the working fluid so that one can find sufficiently large number of particles within small regions on average and yet each individual particle is identifiable.

2. Illuminate the system with light sheet and take two successive images within reasonably short time spacing.

3. Split the acquired image into many small windows (often referred to as "interrogation windows") and then compute the displacement vector for each interrogation window with help of autocorrelation.

Unfortunately, up to the current technology, light sheet with a width of about 6 m is not available. What is worse, one of the key tasks in the present study is to probe spatiotemporal correlation of the system, and hence the measurement must be also resolved in time. This is in a sharp contrast with conventional usage of PIV, where one takes a single snapshot or accumulate an ensemble of independent snapshots (by taking each snapshots with sufficiently long time spacing) to compute statistical quantities. Although there indeed is a work by Lemoult *et al.* which performed time-resolved PIV for short period of time (100 advective time units, that is, $100H/u_{\mathrm{cl}}$ where $H(=2h)$ is a gap width and u_{cl} is a centerline velocity of the flow) to investigate the detailed inner structures of the turbulent spots in channel flow [60, 61], the time-resolved PIV is infeasible in the present study considering the amount of statistics needed for reliable measurements of the critical exponents.

Flow visualization by reflective flakes, which we employed in the present work, is a substantially different method from PIV, although it may look quite similar at first glance. Contrary to PIV where the displacement of the spherical particles are assumed to be related to the velocity field, visualization by reflective flakes utilizes the orientation of the platelets. Procedure of the flow visualization by reflective flakes is as follows:

[1]In reality, great care has to be paid to ensure the assumption is indeed valid. For example, the density of the particles must be close to that of the working fluid, and the size should be small enough to quickly follow the flow field and yet large enough so that sufficient amount of illuminating light is scattered by particles.

1. Immerse sufficient amount of seeding particles into the working fluid. In this case, individual particles do not have to be identifiable from the image, although putting too much tracers into the fluid may affect the resulting flow field.

2. Illuminate the system with light sheet and record images at an appropriate frame rate so that the desired time resolution is achieved.

3. Perform a sensible image analysis to distinguish between laminar flow and localize turbulent spots.

Thus the experimental procedure and accumulation of statistics is simpler than PIV. A price to pay for this advantage is that it is not straightforward how the resulting orientations of particles are related to the flow field of interest, as Gauthier *et al.* points out [36]: There have been very few published works which are concerned with this issue, one of the exceptions being the work by Savas [85]. Lack of systematic studies on flow visualization by reflective flakes presumably stems from the fact that one has to consider a motion of ellipsoid in general and thereby the governing equation becomes complicated, although one can still solve it analytically in a very simple case of plane Couette flow [52]. Nevertheless, the visualization by the reflective flakes is indeed effective as we will see below, and one could argue, at least qualitatively, that the particles align themselves onto the "stream surfaces" [85].

In the present study, Iriodin 323 (Merck) was used as a tracer particle. Iriodin 323 is mica platelets coated with titanium dioxide (10-20 μm in diameter and 3 μm in thickness, Iriodin, Merck). The concentration of the tracer was reduced to 0.04% in weight to keep the change of viscosity negligible (<0.1% according to Einstein's law [20]). Thin platelets tend to align perpendicular to shear stress which is parallel to the x-z surface in laminar flow states while they rotate in turbulent spots. The grazing angle illumination brought moderate light reflections from the laminar regions to the front, while scattering from the turbulent spots is omni-directional and its intensity deviated significantly from that of laminar regions (see Fig. 5.1b). Six commercial projectors (PJ4114NW, 3000 lumen, Ultra-short focal length, Ricoh) were attached 300 mm above and 250 mm apart from the (x, z) surfaces to illuminate the channel surface with a grazing angle to attain reasonably uniform intensity of illumination. With this setup, we obtained a clear visualization of localized turbulent spots, as shown in Fig. 5.2c.

5.2.4 Acquisition of statistics

Three monochrome CCD cameras (B1620M, Imperx, 1608 pixels 1208 pixels, 10 frames/sec) facing the center of the x-z plane of each slot synchronously captured movies of spatio-temporal dynamics of the flow of each slot. For the evaluation of the turbulent fraction, $\rho(x)$

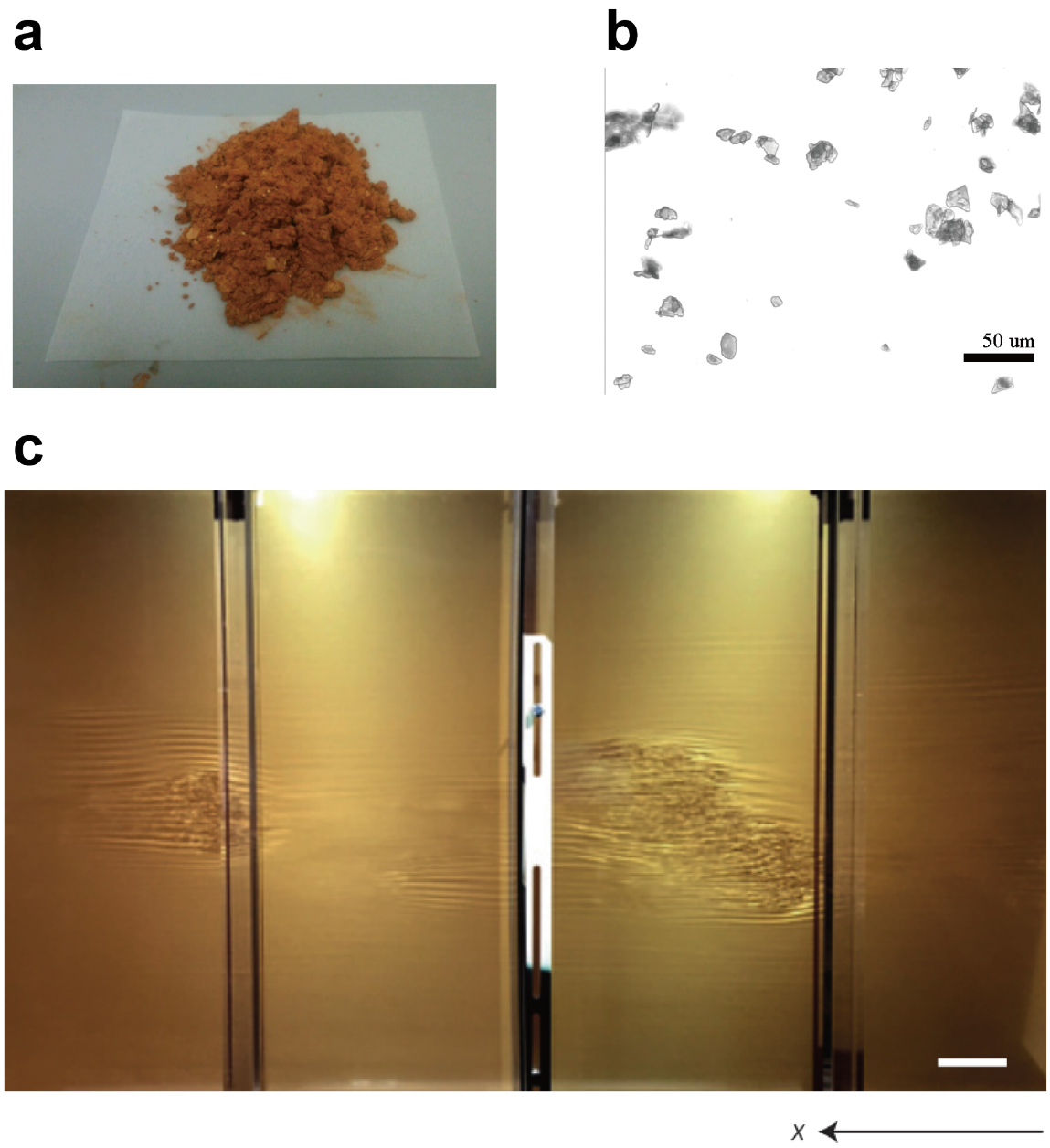

Figure 5.2: Flow visualization by reflective flakes. **a**: Raw image of the tracer particles we used in the present study, Iriodin 323. **b**: A photomicrograph of the tracer particles. The scale bar corresponds to 50 μm. **c**: Typical snapshot of the visualized flow. The picture is adapted from Ref. [84].

was measured at 6 positions (x =0.65 m ($= 260h$), 1.27 m ($= 508h$), 2.68 m ($= 1072h$), 3.23 m ($= 1292h$), 4.70 m ($= 1880h$), 5.24 m ($= 2096h$)) where the incident angle from each of 6 light sources to each measuring position in the channel are almost equal, simultaneously the reflection angle from the measuring position to each of 3 CCD cameras are almost equivalent. This choice was made to avoid unwanted inhomogeneity in the turbulent fraction $\rho(x)$ due to anisotropic effect of the scattered light from the platelets.

5.2.5 Image analysis

To obtain a background profile, the spatial profile of the scattered light intensity for the laminar state $I_{\mathrm{lam}}(x, z, t)$ was captured at $\mathrm{Re} \sim 600$ as movies for 100 sec just before and after every series of measurements was performed. Then the acquired background $I_{\mathrm{lam}}(x, z, t)$ was averaged over time, and the resulting image $I_0(x, z) = \langle I_{\mathrm{lam}}(x, z, t)\rangle_t$. For every image $I(x, z, t)$, the image is divided by the average of the background to obtain the normalized image $N(x, z, t)$:

$$N(x, z, t) := \frac{I(x, z, t)}{I_{\mathrm{lam}}} \tag{5.3}$$

This procedure was useful for suppressing the spatial inhomogenity of the image due to the illumination, as demonstrated in Fig. 5.3c. Since the observed light intensity is not constant but rather fluctuates in time even at laminar flow, we first quantified the fluctuation by studying the normalized image of the background itself:

$$N_{\mathrm{lam}}(x, z, t) := \frac{I_{\mathrm{lam}}(x, z, t)}{I_0(x, z)}. \tag{5.4}$$

It turned out that the fluctuation property of the background can be well approximated by a Gaussian distribution (black curve in Fig. 5.4). Given this observation, we computed the standard deviation $\sigma(x, z)$ of $N_{\mathrm{lam}}(x, z, t)$ and regarded the resulting $\sigma(x, z)$ as a characteristic amplitude of the fluctuation. Near the onset of sustained turbulence, where we are most interested in, the distribution of the value of $N(x, z, t)$ began to deviate from the Gaussian distribution at

$$|N(x, z, t) - N_{\mathrm{mode}}(x, z)| \gtrsim 3\sigma, \tag{5.5}$$

as suggested by red curves in Fig. 5.4. Hence, we regarded the pixel (x, z, t) as in a turbulent state if the normalized intensity $N(x, z, t)$ satisfies the above condition. A few comments are in order: First, the choice of the coefficient in a right hand side of (5.5) does not affect the result of binarization so much, although the best visual correspondence was obtained if we chose it to be 3. Second, in the left hand side of (5.5), we used mode value instead of just a unity to take systematic variation due to sedimentation of the particles into account.

Still at this stage, erronous detection of a turbulent state is possible, which may drastically affect the measurements of laminar interval distributions. In order to remove the erroneous

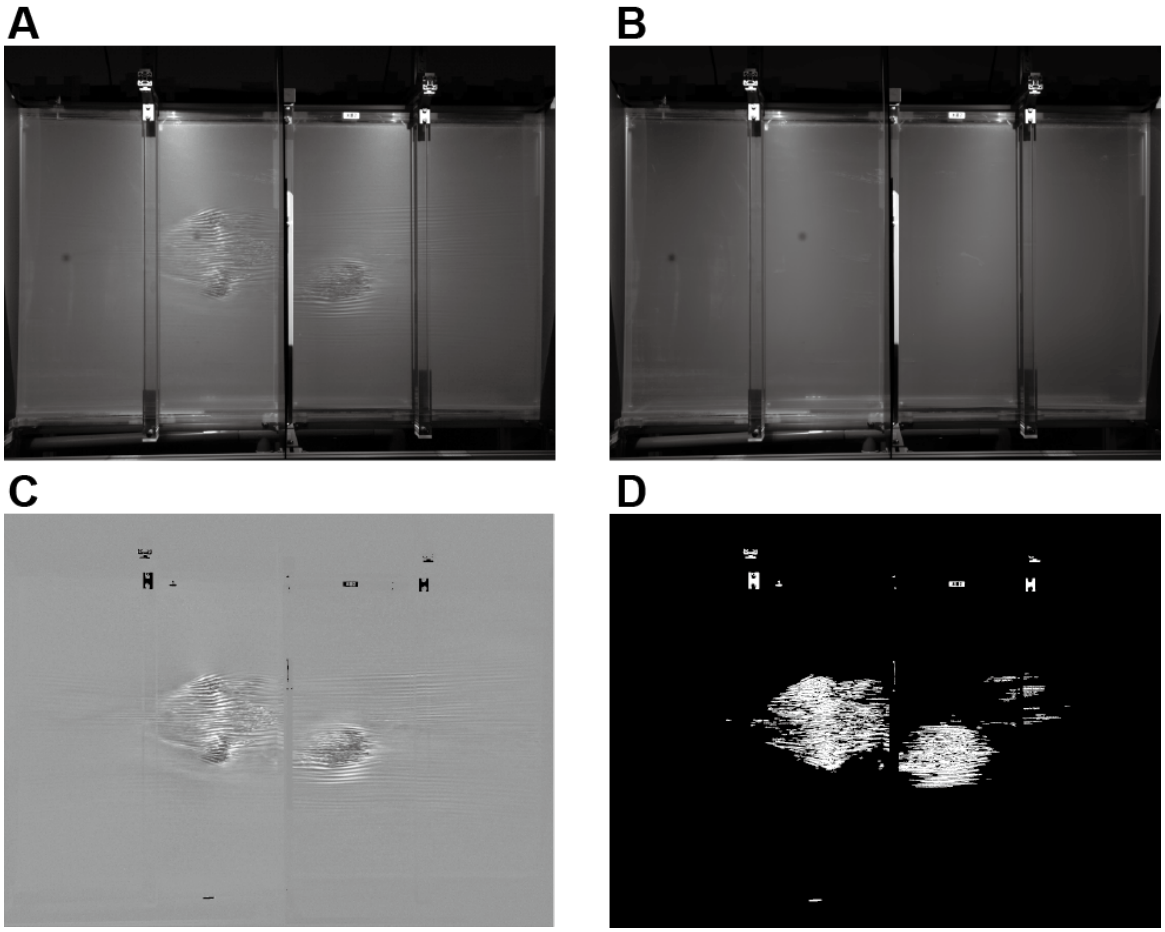

Figure 5.3: Procedure of binarization. **a**: Original image (3 illuminating projectors are used in this sample.). **b**: Background image taken at $\mathrm{Re} \sim 600$ and averaged in time. **c**: Normalized image divided by the background image. **d**: Binary image showing detected turbulent regions which exceed more than $3\sigma(x, z)$ at each pixel. The picture is adopted from Ref. [84].

detection, we excluded clusters of turbulent state whose size was smaller than h^2, assuming that turbulent eddies at moderate Reynolds number cannot be smaller than the gap width. Typical results of the binarization is shown in Fig. 5.3d, and the results are used to calculate the quantities of interest in what follows.

One may notice in Fig. 5.3d that the turbulent spot is not completely filled with the turbulent (white) pixels but it contains some laminar (black) pixels inside it. This is presumably due to the erroneous nondetection which may happen when turbulent fluctuation is within 3σ from the laminar profile by chance, and this can indeed cause overestimation of the laminar interval distribution for short intervals. Typically, the time it takes for individual turbulent spot to pass through a probe at fixed position is about 1 second, and hence the interpretation of the interval distribution should be performed in terms of statistical mechanics only when this criterion is fulfilled.

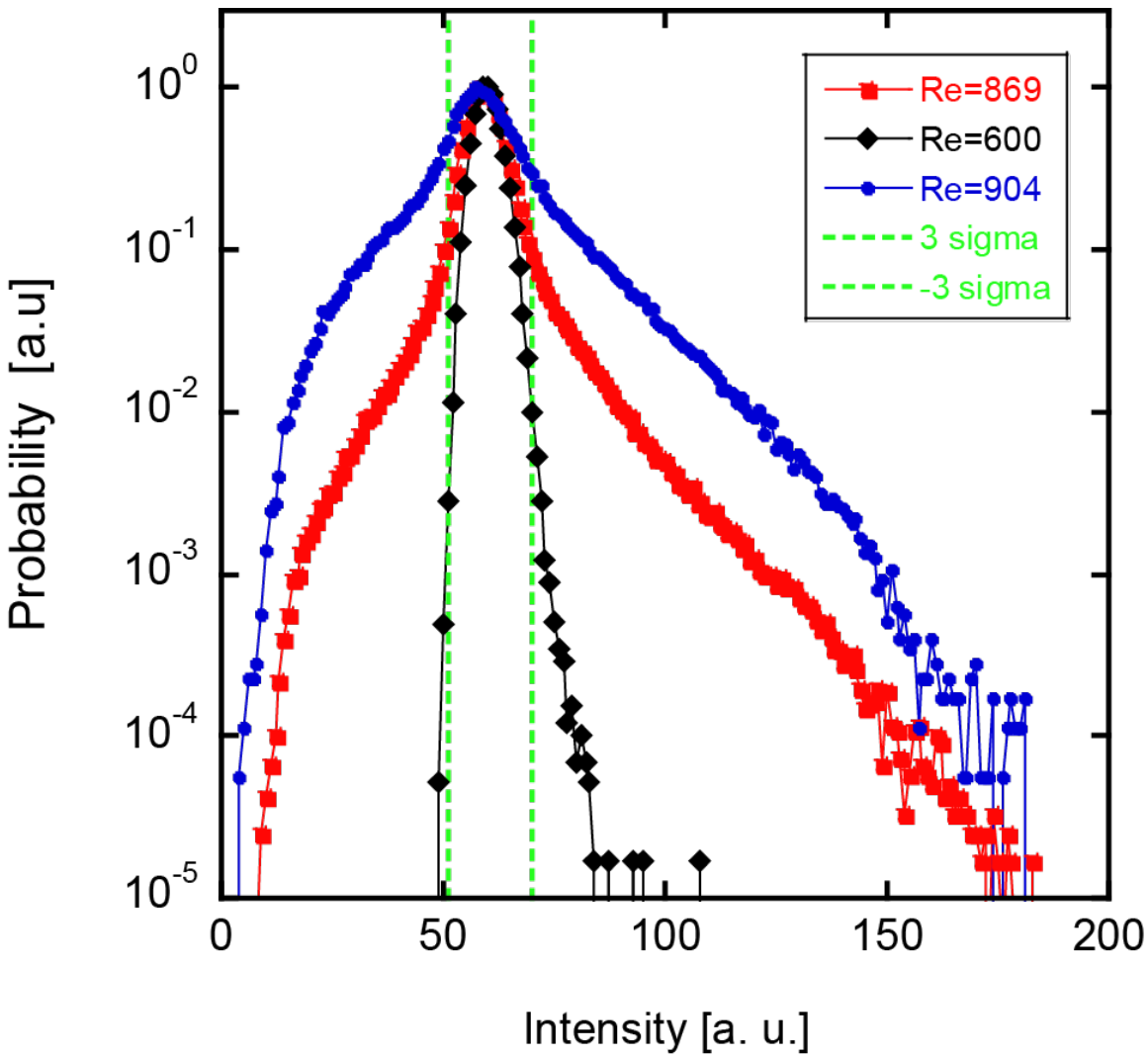

Figure 5.4: Typical probability distribution functions (PDF) of image intensity fluctuations measured at a fixed location ($x \sim 3.2$ m) in a small region (25 mm $\times$ 25mm) and accumulated for 1,000 frames. All movies were normalized by a time averaged background image taken for a laminar state ($\mathrm{Re} \sim 600$), then histogram was accumulated for the normalized images. Black symbol represents PDF of intensity fluctuations in a laminar state (black), PDF is close to a Gaussian distribution. As Re increases to $\mathrm{Re} = 869$ (red) and $\mathrm{Re} = 904$, the turbulent spots gradually increase. Accordingly, intensity fluctuations show large deviations from the Gaussian both to brighter and darker sides. Note that PDF is a superposition of a narrow Gaussian originated from laminar states and a broad distribution with large skewed wings originated from turbulent spots. Large deviations which exceed 3σ (green dashed line) from the mean laminar intensity were regarded as the turbulent state. This figure is adopted from the Supplementary Information of Ref. [84].

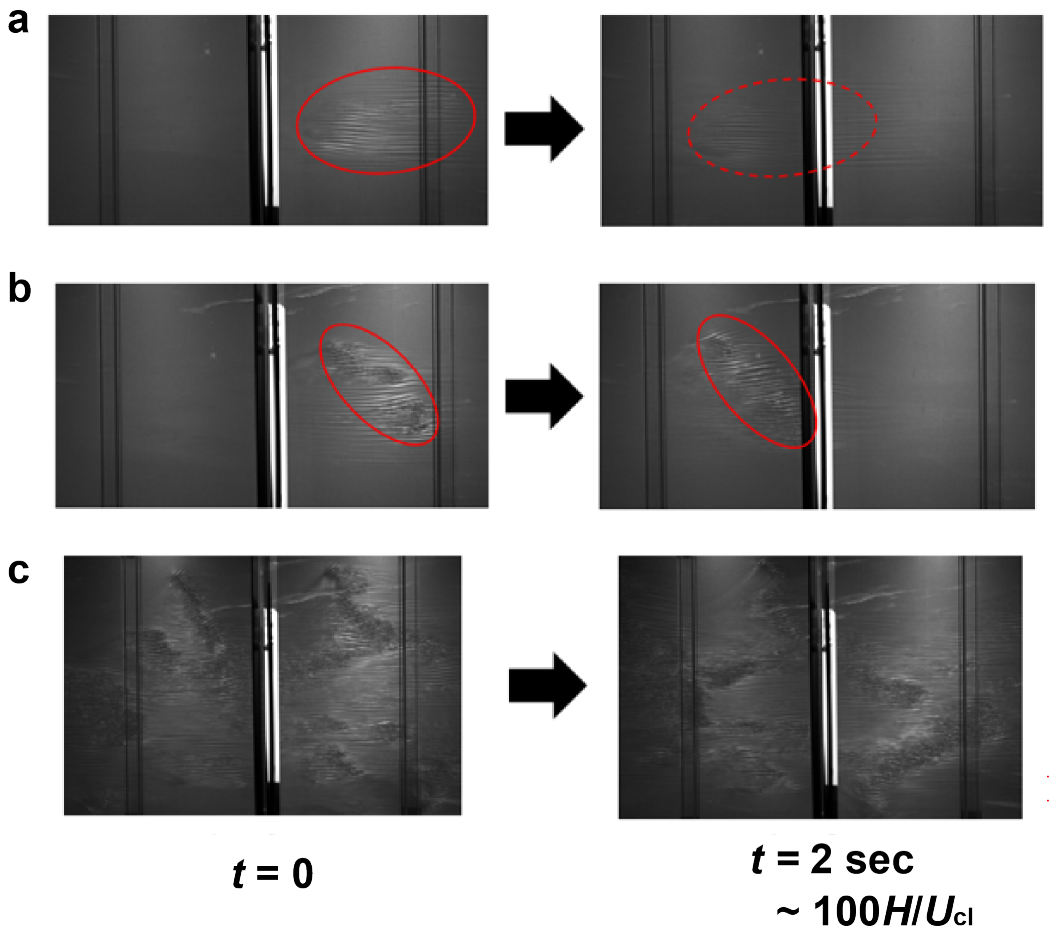

Figure 5.5: Typical dynamics of the turbulent spots. Pictures were taken at $x = 3.23$ m by the monochrome CCD camera. **a**: $\mathrm{Re} \sim 800$, **b**: $\mathrm{Re} \sim 830$, **c**: $\mathrm{Re} \sim 900$

5.3 Experimental results

5.3.1 Qualitative observation

Results of the qualitative observation for various Reynolds number is shown in Fig. 5.5. If the Reynolds number is small, the localized turbulent rarely enters the observation region, and spot would eventually decay into laminar state even if entered (Fig. 5.5a). Near the onset of sustained turbulence, the turbulent spots enters the observation region intermittently, and it can sometimes decay or sometimes split (Fig. 5.5c). If the Reynolds number is high, the observation region is filled with turbulent patterns (Fig. 5.5c).

Normalized image we obtained in Section 5.2.5 enabled us to perform the qualitative analysis for the entire channel. The results shown in Fig. 5.6 suggests the system indeed possesses the distinct transition from decaying turbulence to sustained turbulence. Meanwhile, we also found from Fig. 5.6 that the flow tends to be laminar near the sidewall even if the Reynolds number is sufficiently high, presumably due to dissipative friction at the wall. Since we are interested in a bulk property of the flow, hereafter we restricted our analysis

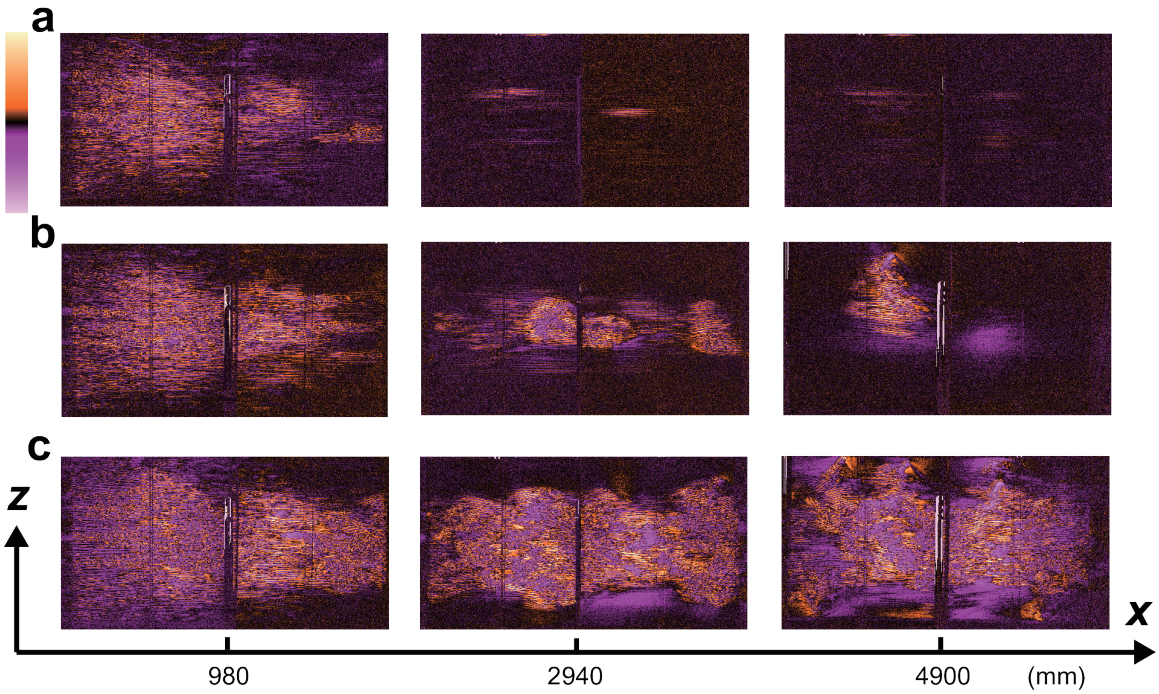

Figure 5.6: Spatial variation of the flow across the transition. **a**: Snapshots taken by three CCD cameras from left to right, respectively, at $\mathrm{Re} = 798$. Quick decay of turbulent flow is evident. Colour represents the normalized image intensity. A black colour is assigned to the point where the image intensity is close to the laminar state (see the colour map). **b**: Snapshots at $\mathrm{Re} = 842$. The intermittent nature of the turbulent spots can be seen. **c**: Snapshots at $\mathrm{Re} = 1,005$. Saturation of the turbulent fraction is evident This figure is reproduced from Ref. [84].

within a half span width around the mid-height.

5.3.2 Turbulent fraction

In order to characterize the transition, we performed a steady-state measurement of the area fraction of the turbulent region (hereafter referred to as "the turbulent fraction" ρ) for various values of x. The value of ρ, estimated by measuring the time fraction occupied by turbulent flow averaged over a protracted time period (approximately 40 min; that is, 100 times the length of the flow circulation time), was found to saturate to finite value $\rho_0(\mathrm{Re})$ for higher Reynolds number and for larger x, as shown in Fig. 5.7b. The saturation motivated us to measure $\rho_0(\mathrm{Re})$ as a function of Re at several distant locations x (namely, $x/h = 1292, 1880, 2096$). Since ρ_0 is a natural candidate for an order parameter in a context of DP-class transition which increases continuously from zero to positive values, the curves in Fig. 5.7a are fitted by the function

$$\rho_0(\mathrm{Re}) \sim (\mathrm{Re} - \mathrm{Re}_c)^{\beta}. \tag{5.6}$$

As a result, we obtained the following estimates for the critical exponent β and the critical Reynolds number Re_c:

$$\mathrm{Re}_c = 830(4), \quad \beta = 0.58(3), \tag{5.7}$$

which is in a reasonable agreement with the spatially two-dimensional DP universality class. Note that, since the choice of the region for fitting is a delicate issue, we varied the range for fitting variously to estimate the uncertainty. Also, the critical Reynolds number Re_c is fixed hereafter to prevent further arbitrariness from involving.

The above results encouraged us to measure $\rho(x)$ as a function of the distance from the grid for $\mathrm{Re} < \mathrm{Re}_c$. As shown in Fig. 5.7b, $\rho(x)$ showed clear exponential decay for $\mathrm{Re} < 803$, enabling us to define a decay length L by

$$\rho(x) \sim \exp(-x/L). \tag{5.8}$$

We investigated L as a function of Re, as shown in the inset of Fig. 5.7, and the result suggested that L shows power-law divergence with

$$L \sim (\mathrm{Re}_c - \mathrm{Re})^{-\nu}. \tag{5.9}$$

with the exponent of $\nu = 1.1(3)$ as the best fit. This value is consistent with the critical exponent $\nu_{||}$ of the DP universality class, although the uncertainty is large.

5.3.3 Laminar interval distribution

Given the difficulty to judge the order of the transition from qualitative behavior of the system and from the empirical measurements of the turbulent fraction, crucial difference between first-order phase transitions and second-order ones is whether the system exhibits divergence of the correlation length as approaching to the critical point. The results shown in Chapter 4 indicate that measuring the temporal interval distribution $P(\tau)$ of laminar state at fixed downstream locations for $\mathrm{Re} > \mathrm{Re}_c$ provides a good opportunity to address this question: If the system can be described as the DP with an active wall and advection, the following universal scaling ansatz is expected to hold:

$$P(\tau) \sim \tau^{-(2-\beta/\nu_\perp)} f(\varepsilon^{\nu_\perp}\tau). \tag{5.10}$$

To check whether this is indeed the case for channel flow, the distributions $P(\tau)$ at 3,200 mm away from the grid were accumulated for 40 different spanwise positions within a half span width around the mid-height. First, Therefore, the distributions $N(\tau)$ at $x = 3,200$ mm were accumulated for 40 different z-positions within a half-span width ($\pm$225 mm) around the mid- height. For small τ, a power-law distribution is expected near $\mathrm{Re} = \mathrm{Re}_c$. Fig. 5.8a shows the resulting $P(\tau)$ for several different Reynolds numbers. We fit this by the power law

$$P(\tau) \sim \tau^{-\mu_\perp} \tag{5.11}$$

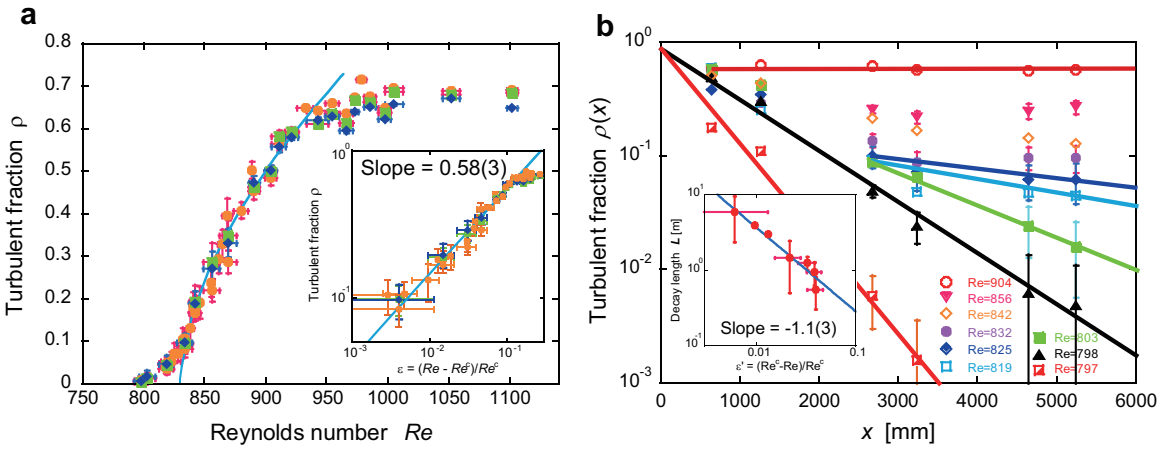

Figure 5.7: **a**: The turbulent fraction ρ versus Re is plotted at different downstream locations: $x/h = 1,292$ (orange square), $x/h = 1,880$ (blue diamond) and $x/h = 2,096$ (green square). Error bars represent standard deviation. Inset: a log-log plot of ρ as a function of reduced Reynolds number ε, where $\varepsilon := (\mathrm{Re}_c - \mathrm{Re})/\mathrm{Re}_c$, with $\mathrm{Re}_c = 830(4)$. The solid blue lines are the best fit, ε^β with $\beta = 0.58(3)$, for the data in $10^{-3} < \varepsilon < 10^{-1}$. Here, numbers in the parentheses denote 95% confidence intervals in the sense of the Student ' s t distribution. The same applies to the following. Note that data points below Re_c are removed for fitting. A non-vanishing order parameter below Re_c due to a finite size effect exists as usual; however, relatively small systems can show remarkably clear power-law behaviour in numerical models exhibiting a DP transition. **b**: The turbulent fraction as a function of the distance x from the inlet where turbulence is created by a grid. Measurements were performed for six different x where the incidence angles and the reflected angles of the light were identical. The solid lines show the exponential fittings, $\rho(x) \sim \exp(-x/L)$, applied for the data satisfying $x/h > 1,040$. Error bars represent standard deviation. Inset: log-log plot for L versus ε. Error bars of the fitted values L are 95% confidence limits. The solid line is the best fit, $L \sim |\varepsilon|^{-\nu_{||}}$ with $\nu_{||} = 1.1(3)$. The figure is adapted from Ref. [84].

and found $\mu_\perp = 1.25(5)$, as the best fit. This is close to the universal exponent in the DP universality class: $\mu = 1.204(2)$.

To observe the tail of the distributions, a complementary cumulative probability,

$$R(\tau) := \int_\tau^\infty P(t)\mathrm{d}t \tag{5.12}$$

was estimated using the empirical estimator (3.30), as shown in Fig. 5.8b. We defined the characteristic time, ξ, by fitting the tail of $R(\tau)$ with an exponential function

$$R(\tau) \sim \exp(-\tau/\xi). \tag{5.13}$$

and we found that ξ as a function of ε shows power-law divergence

$$\xi \sim \varepsilon^{-\nu_\perp}, \tag{5.14}$$

although deviation from the power law is found at large ε as expected. Fitting the data with a power law in a region where $\xi \gtrsim 1$ (sec) is achieved (keeping the argument in Section 5.2.5 in mind), we find the following estimate of the critical exponent (Fig. 5.8c):

$$\nu_\perp = 0.72(6). \tag{5.15}$$

Although the range of the power law is limited owing to the finite size of the system, the resulting exponents $\beta, \nu_\perp, \mu_\perp$ satisfies the following scaling relation (which follows from (5.10)) within experimental accuracy:

$$\mu_\perp = 2 - \beta/\nu_\perp. \tag{5.16}$$

As such, these results encourage the further exploration of universal features for the subject phenomena: We rescaled a universal scaling hypothesis (5.10). Note that, in contrast with fitting, no free parameter is involved in this scaling analysis, as long as we fix the critical point Re_c and we use the theoretical value of the DP universality class for the rescaling. We found that several curves overlap, as shown in Fig. 5.8d. It is important to emphasize that it is the first time that the scaling collapse of the experimental results on steady-state measurements have been performed in a context of absorbing phase transitions. All these results support that the transition to turbulence in channel flow can be understood as a critical phenomena of DP subject to advection by a mean flow.

5.4 Discussions

The critical exponents estimated in the experiments, along with the theoretical value of the spatially two-dimensional DP universality class is summarized in Tab. 5.1. This result supports the long-standing conjecture that transition to turbulence falls into the DP universality class. Although our finding described in this Chapter should be substantiated by theory or numerical evidences, our results suggest some relevant implications. Examples of the implications are listed up in the following:

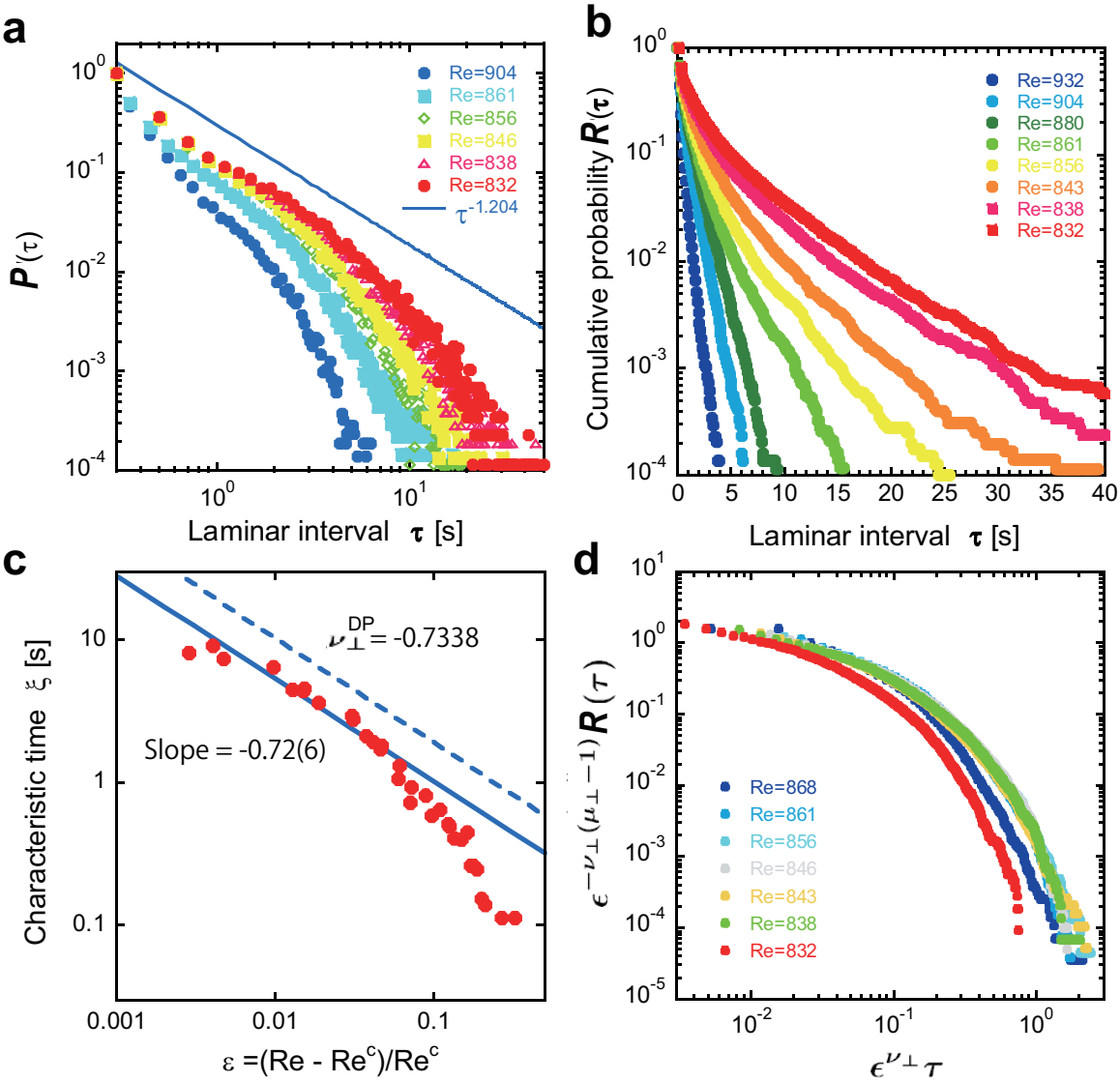

Figure 5.8: Critical behavior of correlation length and universal scaling. **a**: Laminar interval distribution $P(\tau)$ measured at a fixed downstream location ($x/h \sim 1280$) for various Reynolds number Re. The solid blue line corresponds is a guide-to-eye for $\tau^{-\mu_\perp}$. **b**: Complementary cumulative laminar interval distribution $R(\tau)$ for various Re. **c**: The characteristic time ξ as a function of reduced Reynolds number $\varepsilon := (\mathrm{Re} - \mathrm{Re}_c)/\mathrm{Re}_c$. The solid line is the best fit with slope of 0.72(6). The dashed line is a guide-to-eye for $\xi \sim \varepsilon^{-\nu_\perp}$. **d**: Data in **b** is rescaled according to the universal scaling hypothesis (5.10), where we substituted the estimated critical Reynolds number into Re_c and the theoretical value for the $(2+1)$-dimensional DP universality class into $\nu_\perp, \mu_\perp$. This figure is reproduced from Ref. [84].

Table 5.1: Summary of the critical exponents measured in this experiment. The row entitled "Theory" shows the theoretical value of the DP universality class up to the digit where comparison with experimental results is meaningful (see Tab. 2.1 for more precise value).

$d = 2$	β	$\nu_\perp$	$\nu_{\|\|}$	$\mu_\perp$
Our results	0.59(4)	0.75(6)	1.29(11)	1.25(5)
Theory	$\sim$0.58	$\sim$0.73	$\sim$1.30	1.204(2)

- The fact that the transition to turbulence in channel flow falls into DP universality class means that the competition between decaying and splitting of the turbulent spots is the most relevant process for the transition, just as in a case with pipe flow.
- The fact that the spatially *two*-dimensional DP universality class is observed in this system (given a rather limited size in spanwise direction) means that experimental realization of the DP universality class does not necessarily require extremely large system, although in principle the system should be as close to as the thermodynamic limit as possible.
- In contrast with turbulent liquid crystals, the absorbing phase in this system is laminar. Hence it might be unnecessary for a system to have a turbulent absorbing state so that it falls into the DP universality class.

To sum up, our finding suggests the possibility that transitions to turbulence in shear flow allows a room for simple and universal description and that the DP universality may be realized in wider subsets of absorbing phase transitions in reality (than it had been considered to be, at least).

Chapter 6

Conclusions and Perspectives

Throughout this thesis, we aimed to clarify to what extent the notion of the universality of absorbing phase transition is relevant for understanding natural phenomena and to examine whether a transition to turbulence in channel flow exhibits universal features so that it can be described in terms of an absorbing phase transition. In particular, we pointed out that the apparent "fragility" of the most fundamental universality class of absorbing phase transitions may simply stem from the fact that we were actually ignorant of how should we analyze the data (in Chapter 3), and provided experimental results which suggest that the transition to turbulence in channel flow falls into the universal scenario of the directed percolation (in Chapter 5).

It is worthwhile to re-emphasize here that the notion of universality in absorbing phase transitions possesses a strong potential of providing us a universal description of considerable amount of spatiotemporally complex phenomena. By focusing on a statistical features of macroscopic characterizers (e.g. whether the flow is locally laminar or turbulent) while skipping other features (e.g. detailed velocity field of the flow), one may be able to find a universal law in that coarse-grained scale even though the equation governing the microscopic dynamics are very complex and has chaotic solutions. The author believes that the notion of universality can be used (a) to create a predictive theory on a certain phenomenon by establishing a link between (universal) macroscopic features and (system-specific) microscopic dynamics, and (b) to describe various systems in a unified way (e.g. the effective Langevin equation (2.33),(2.34) with system-specific parameters $\varepsilon, \lambda, D, \Gamma$).

Given this, let us discuss some possible directions for future studies:

- Extensive work which shows the transition to sustained turbulence in narrow Taylor–Couette flow falls into the DP universality class was published [59] at the same time as ours. More recently, numerical evidences that the transition in model shear flow also falls into the DP universality class was reported [21]. Now it is high time, in the author's opinion, to go one step forward and clarify the relation between a description in terms of non-equilibrium phase transitions and a conventional approach

of dynamical systems. A work by Shih *et al.*, in which dynamics among laminar flow, turbulent flow, and so-called zonal flow are represented by predetor-prey model [89], might be a sensible clue in this direction.

- Although the author believes that the robustness of the DP universality class had been "underestimated" in experiments, the author is also aware that an absorbing phase transition in reality is not necessary so simple as stochastic models, recalling that even transitions to an absorbing phase in deterministic models are substantially more complicated than those in stochastic models. Hence, the robustness of the DP universality class in reality should be re-examined and estimated properly, based on quantitative and reliable evidences.

Considering these, it could be said that a series of works presented in this thesis is just the first step along a long and winding road to complete understanding of transitions to turbulence and of the universality of absorbing phase transitions. Nevertheless the author does hope that the methodology and experimental results provided in this work play a significant role to promote an effort to gain a universal insight into spatiotemporally complex phenomena such as turbulence.

Bibliography

[1] V. Ahlers and A. Pikovsky. Critical Properties of the Synchronization Transition in Space-Time Chaos. *Phys. Rev. Lett.*, **88**, 254101, 2002.

[2] E. V. Albano. Irreversible phase transitions into non-unique absorbing states in a multicomponent reaction system. *Physica A*, **214**, 426–434, 1995.

[3] K. Avila, D. Moxey, A. de Lozar, M. Avila, D. Barkley, and B. Hof. The onset of turbulence in pipe flow. *Science*, **333**, 192–196, 2011.

[4] M. Avila, A. P. Willis, and B. Hof. On the transient nature of localized pipe ïňĆow turbulence. *J. Fluid. Mech.*, **646**, 127–136, 2010.

[5] V. S. Barbu and N. Limnios. *Semi-Markov Chains and Hidden Semi-Markov Models toward Applications*. Springer, 2008.

[6] L. Baroni, R. Livi, and A. Torcini. Transition to stochastic synchronization in spatially extended systems. *Phys. Rev. E*, **63**, 036226, 2001.

[7] A. A. Belavin, A. M. Polyakov, and A. B. Zamalodchikov. Infinite conformal symmetry in two-dimensional quantum field theory. *Nucl. Phys. B*, **241**, 333–380, 1984.

[8] E. Ben-Naim and P. L. Krapivsky. Cluster approximation for the contact process. *J. Phys. A.: Math. Gen.*, **27**, L481–L487, 1994.

[9] C. M. Bender and S. A. Orszag. *Advanced mathematical methods for scientists and engineers*. McGraw-Hill, 1978.

[10] R. A. Blythe. *Nonequilibrium phase transitions and dynamical scaling regimes*. PhD thesis, The University of Edinburgh, 2001.

[11] S. Bottin and Chaté. Statistical analysis of the transition to turbulence in plane Couette flow. *European Physical Journal B*, **6**, 143–155, 1998.

[12] S. Bottin, F. Daviaud, P. Manneville, and O. Dauchot. Discontinuous transition to spatiotemporal intermittency in plane Couette flow. *Europhys. Lett.*, **43**, 171–176, 1998.

[13] C. Brezuidenhout and G. Grimmett. The critical contact process dies out. *Ann. Prob.*, **18**, 1462–1482, 1990.

[14] S. Broadbent and J. Hammersley. Percolation processes I. Crystals and mazes. *Proceedings of the Cambridge Philosophical Society*, **53**, 629–641, 1957.

[15] J. B. Bronzan and J. W. Dash. Erratum: Higher-order ϵ terms in Reggeon field-theory. *Phys. Rev. D*, **12**, 1850, 1974.

[16] J. B. Bronzan and J. W. Dash. Higher-order ϵ terms in Reggeon field-theory. *Phys. Rev. D*, **10**, 4208–4217, 1974.

[17] S. V. Buldyrev, A.-L. Barabási, F. Caserta, H. E. Stanley, and T. Vicsek. Anomalous interface roughening in porous media: Experiment and model. *Phys. Rev. A*, **45**, R8313–R8316, 1992.

[18] J. L. Cardy and R. L. Sugar. Directed percolation and Reggeon Field Theory. *J. Phys. A: Math. Gen.*, **13**, L423–L427, 1980.

[19] J. L. Cardy. Conformal invariance and surface critical behavior. *Nucl. Phys. B*, **240**, 514–532, 1984.

[20] D. R. Carlson, S. E. Widnall, and M. F. Peeters. A flow-visualization study of transition in plane Poiseuille flow. *J. Fluid. Mech.*, **121**, 487–505, 1982.

[21] M. Chantry, L. S. Tuckerman, and D. Barkley. Universal continuous transition to turbulence in a planar shear flow. *J. Fluid. Mech.*, **824**, R1, 2017.

[22] C.-C. Chen, H. Park, and M. den Nijs. Active width at a slanted active boundary in directed percolation. *Phys. Rev. E*, **60**, 2496–2500, 1999.

[23] S. Ciliberto and P. Bigazzi. Spatiotemporal Intermittency in Rayleigh-Bénard Convection. *Phys. Rev. Lett.*, **60**, 286–289, 1988.

[24] A. Costa, R. Blythe, and M. R. Evans. Discontinuous transition in a boundary driven contact process. *J. Stat. Mech.*, **2010**, P09008, 2010.

[25] F. Daviaud, M. Bonetti, and M. Dubois. Transition to turbulence via spatiotemporal intermittency in one-dimensional Rayleigh-Bénard convection. *Phys. Rev. A*, **42**, 3388–3399, 1990.

[26] M. M. Degen, I. Mutabazi, and C. D. Andereck. Transition to weak turbulence via spatiotemporal intermittency in the Taylor-Dean system. *Phys. Rev. E*, **53**, 3495–3504, 1996.

[27] R. Dickman and M. Martines de Oliveira. Quasi-stationary simulation of the contact process. *Physica A*, **357**, 134–141, 2005.

[28] H. W. Diehl. The Theory of Boundary Critical Phenomena. *Int. J. Mod. Phys. B*, **11**, 3503–3523, 1997.

[29] E. Domany and W. Kinzel. Equivalence of cellular automata to Ising models and directed percolation. *Phys. Rev. Lett.*, **53**, 311–314, 1984.

[30] Y. Duguet, P. Schlatter, and D. S. Henningson. Formation of turbulent patterns near the onset of transition in plane Couette flow. *J. Fluid. Mech.*, **650**, 119–129, 2010.

[31] R. Durrett and Griffeath. Contact process in several dimensions. *Z. für. Wahrsch*, **59**, 535, 1982.

[32] M. J. Feigenbaum. Quantitative Universality for a Class of Non-Linear Transformations. *J. Stat. Phys.*, **19**, 25–52, 1978.

[33] C. M. Fortuin. On the random cluster model. II. The percolation model. *Physica*, **58**, 393–418, 1972.

[34] C. M. Fortuin and P. W. Kasteleyn. On the random cluster model. I. Introduction and relation to other models. *Physica*, **57**, 536–564, 1972.

[35] P. Fröjdh, M. Howard, and K. B. Lauritsen. Directed Percolation and Other Systems With Absorbing States: Impact of Boundaries. *Int. J. Mod. Phys. B*, **15**, 1761–1797, 2001.

[36] G. Gauthier, P. Gondret, and D. Rabaud. Motions of anisotropic particles: Application to visualization of three-dimensional flows. *Phys. Fluids*, **10**, 2147–2154, 1998.

[37] J. Gleick. *Chaos: Making a New Science*. Viking Books, 1987.

[38] P. Grassberger and A. de la Torre. Reggeon field theory (Schlögl's first model) on a lattice: Monte Carlo calculations of critical behaviour. *Ann. Phys.*, **122**, 373–396, 1979.

[39] P. Grassberger. On phase-transitions in Schlögl's second model. *Z. Phys. B*, **47**, 365–374, 1982.

[40] G. Grimmett and P. Hiemer. Directed percolation and random walk. In V. Sidoravicius, editor, *In and Out of Equilibrium*. Birkhäuser, 2002.

[41] G. Grinstein, Z.-W. Lai, and D. A. Browne. Critical phenomena in a nonequilibrium model of heterogeneous catalysis. *Phys. Rev. A*, **40**, 4820–4823, 1989.

[42] T. E. Harris. Contact interactions on a lattice. *Annals of Probability*, **2**, 969–988, 1974.

[43] M. Henkel. *Conformal Invariance and Critical Phenomena*. Springer, 1999.

[44] M. Henkel, H. Hinrichsen, and S. Lübeck. *Non-Equilibrium Phase Transitions Volume 1 - Absorbing Phase Transitions*. Springer, 2008.

[45] H. Hinrichsen. Non-equilibrium critical phenomena and phase transitions into absorbing states. *Advances in Physics*, **49**, 815–958, 2000.

[46] H. Hinrichsen. Non-equilibrium phase transitions. *Physica A*, **369**, 1–28, 2006.

[47] M. Howard, P. Frojdh, and K. B. Lauritsen. Surface critical behavior in systems with nonequilibrium phase transitions. *Phys. Rev. E*, **61**, 167–183, 2000.

[48] M. Hoyuelos, E. V. Albanod, and H. O. Mártin. A multilayer contact process. *J. Phys. A: Math. Gen.*, **30**, 431–443, 1997.

[49] C.-Y. Huang and M.-C. Wang. Nonparametric Estimation of the Bivariate Recurrence Time Distribution. *Biometrics*, **61**, 392–402, 2005.

[50] H.-K. Janssen. On the nonequilibrium phase transition in reaction-diffusion systems with an absorbing stationary state. *Z. Phys. B*, **42**, 151–154, 1981.

[51] H. K. Janssen. Renormalized field theory of the Gribov process with quenched disorder. *Phys. Rev. E*, **55**, 6253–6256, 1997.

[52] G. B. Jeffery. The motion of ellipsoidal particles immersed in a viscous fluid. *Proc. R. Soc. Lond. Ser. A*, **102**, 161–179, 1922.

[53] I. Jensen. Temporally Disordered Bond Percolation on the Directed Square Lattice. *Phys. Rev. Lett.*, **77**, 4988–4991, 1996.

[54] I. Jensen. Low-density series expansions for directed percolation: I. A new efficient algorithm with applications to the square lattice. *Journal of Physics A: Mathematical and General*, **32**, 5233–5249, 1999.

[55] I. Jensen. Low-density series expansions for directed percolation: III. Some two-dimensional lattices. *J. Phys. A: Math. Gen.*, **32**, 6899–6915, 2004.

[56] I. Jensen and R. Dickman. Time-Dependent Perturbation Theory for Nonequilibrium Lattice Models. *J. Stat. Phys.*, **71**, 89–127, 1992.

[57] I. Jensen, H. C. Fogedby, and R. Dickman. Critical exponents for an irreversible surface reaction model. *Phys. Rev. A*, **41**, 3411–3414, 1990.

[58] E. L. Kaplan and P. Meier. Nonparametric Estimation from Incomplete Observations. *J. Am. Stat. Assoc.*, **53**, 457–481, 1958.

[59] G. Lemoult, L. Shi, K. Avila, S. V. Jalikop, M. Avila, and B. Hof. Directed percolation phase transition to sustained turbulence in Couette flow. *Nat. Phys.*, **12**, 254–258, 2016.

[60] G. Lemoult, J.-L. Aider, and J. E. Wesfreid. Experimental scaling law for the subcritical transition to turbulence in plane Poiseuille flow. *Phys. Rev. E*, **85**, 025303, 2012.

[61] G. Lemoult, J.-L. Aider, and J. E. Wesfreid. Turbulent spots in a channel: large-scale flow and self-sustainability. *J. Fluid. Mech.*, **731**, R1, 2013.

[62] V. Lepiller, A. Prigent, F. Dumouchel, and I. Mutabazi. Transition to turbulence in a tall annulus submitted to a radial temperature gradient. *Phys. Fluids*, **19**, 054101, 2007.

[63] A. Libchaber, C. Laroche, and S. Fauve. Period doubling cascade in mercury, a quantitative measurement. *J. Phys. Lett.*, **43**, 211–216, 1982.

[64] T. M. Liggett. *Interacting particle systems*. Springer-Verlag, 1985.

[65] E. N. Lorenz. Deterministic Nonperiodic Flow. *J. Atmos. Sci.*, **20**, 130–141, 1963.

[66] J. Marro and R. Dickman. *Nonequilibrium Phase Transitions in Lattice Models*. Cambridge University Press, 1999.

[67] J. Maurer and A. Libchaber. Rayleigh-Bénard experiment in liquid helium ; frequency locking and the onset of turbulence. *J. Physique Lett.*, **40**, L419–L423, 1978.

[68] P. Meakin and D. J. Scalapino. Simple models for heterogeneous catalysis: Phase transition-like behavior in nonequilibrium systems. *J. Chem. Phys.*, **87**, 731–741, 1987.

[69] A. G. Moreira and R. Dickman. Critical dynamics of the contact process with quenched disorder. *Phys. Rev. E*, **54**, R3090–R3093, 1996.

[70] M. Mosche. Recent developments in Reggeon field theory. *Phys. Rep.*, **37**, 255–345, 1978.

[71] M. A. Muñoz, G. Grinstein, and R. Dickman. Phase structure of systems with infinite numbers of absorbing states. *J. Stat. Phys.*, **91**, 541–569, 1998.

[72] M. A. Muñoz, G. Grinstein, R. Dickman, and R. Livi. Critical Behavior of Systems with Many Absorbing States. *Phys. Rev. Lett.*, **76**, 451–454, 1996.

[73] H. Nishimori and G. Ortiz. *Elements of Phase Transitions and Critical Phenomena*. Oxford University Press, 2011.

[74] G. Ódor. Universality classes in nonequilibrium lattice systems. *Rev. Mod. Phys.*, **76**, 663–724, 2004.

[75] S. A. Orszag. Accurate solution of the Orr–Sommerfeld stability equation. *J. Fluid. Mech.*, **50**, 689–703, 1971.

[76] H. Park, J. Kohler, I.-M. Kim, D. ben Avraham, and S. Redner. Excluded volume effects in heterogeneous catalysis: reactions between 'dollars' and 'dimes'. *J. Phys. A: Math. Gen.*, **26**, 2071–2079, 1993.

[77] V. C. Patel and M. R. Head. Some observations on skin friction and velocity profiles in fully developed pipe and channel flows. *J. Fluid. Mech.*, **38**, 181–201, 1969.

[78] C. Pirat, A. Naso, J.-L. Meunier, P. MaÃŕssa, and C. Mathis. Transition to Spatiotemporal Chaos in a Two-Dimensional Hydrodynamic System. *Phys. Rev. Lett.*, **94**, 134502, 2005.

[79] Y. Pomeau. Front motion, metastability and subcritical bifurcations in hydrodynamics. *Physica D*, **23**, 3–11, 1986.

[80] O. Reynolds. An Experimental Investigation of the Circumstances Which Determine Whether the Motion of Water Shall Be Direct or Sinuous, and of the Law of Resistance in Parallel Channels. *Phil. Trans. R. Soc. Lond.*, **174**, 935–982, 1883.

[81] V. A. Romanov. Stability of plane-parallel Couette flow. *Functional Analysis and its Applications*, **7**, 137–146, 1973.

[82] P. Rupp, R. Richter, and I. Rehberg. Critical exponents of directed percolation measured in spatiotemporal intermittency. *Phys. Rev. E*, **67**, 036209, 2003.

[83] H. Salwen, F. W. Cotton, and C. E. Grosch. Linear stability of Poiseuille flow in a circular pipe. *J. Fluid. Mech.*, **98**, 273–284, 1980.

[84] M. Sano and K. Tamai. A universal route to turbulence in channel flow. *Nat. Phys.*, **12**, 249–253, 2016.

[85] Ö. Savas. On flow visualization using reflective flakes. *J. Fluid. Mech.*, **152**, 235–248, 1985.

[86] M. F. Schatz, R. P. Tagg, H. L. Swinney, P. F. Fischer, and A. T. Patera. Supercritical transition in plane channel flow with spatially periodic perturbations. *Phys. Rev. Lett.*, **66**, 1579–1582, 1991.

[87] D. Seki and M. Masaharu. Experimental investigation of relaminarizing and transitional channel flows. *Phys. Fluids*, **24**, 124102, 2012.

[88] L. Shi, M. Avila, and B. Hof. Scale Invariance at the Onset of Turbulence in Couette Flow. *Phys. Rev. Lett.*, **110**, 204502, 2013.

[89] H.-Y. Shih, T.-L. Hsieh, and N. Goldenfeld. Ecological collapse and the emergence of traveling waves at the onset of shear turbulence. *Nat. Phys.*, **12**, 259–263, 2016.

[90] M. D. Stern. In vivo evaluation of microcirculation by coherent light scattering. *Nature*, **254**, 256–258, 1975.

[91] M. P. H. Stumpf and M. A. Porter. Critical Truths About Power Laws. *Science*, **335**, 665–666, 2012.

[92] K. Takeuchi, M. Kuroda, H. Chaté, and M. Sano. Directed Percolation Criticality in Turbulent Liquid Crystals. *Phys. Rev. Lett.*, **99**, 234503, 2007.

[93] K. A. Takeuchi. Scaling of hysteresis loops at phase transitions into a quasiabsorbing state. *Phys. Rev. E*, **77**, 030103(R), 2008.

[94] K. A. Takeuchi. Experimental approaches to universal out-of-equilibrium scaling laws: turbulent liquid crystal and other developments. *J. Stat. Mech.*, **2014**, P01006, 2014.

[95] K. A. Takeuchi, M. Kuroda, H. Chaté, and M. Sano. Experimental realization of directed percolation criticality in turbulent liquid crystals. *Phys. Rev. E*, **80**, 051116, 2009.

[96] G.-I. Taylor. Stability of a Viscous Liquid Contained between Two Rotating Cylinders. *Phil. Trans. R. Soc. A: Math., Phys. Eng. Sci.*, **223**, 289–343, 1923.

[97] A. Y. Tretyakov, N. Inui, and N. Konno. Phase Transition for the One-Sided Contact Process. *J. Phys. Soc. Jpn.*, **66**, 3764–3769, 1997.

[98] J. Wang, Z. Zhou, Q. Liu, T. M. Garoni, and Y. Deng. High-precision Monte Carlo study of directed percolation in $(d+1)$ dimensions. *Phys. Rev. E*, **88**, 042102, 2013.

[99] M.-C. Wang and S.-H. Chang. Nonparametric Estimation of a Recurrent Survival Function. *J. Am. Stat. Assoc.*, **94**, 146–153, 1999.

[100] R. T. Weidner and L. M. Brown. Physics. In *Encyclopædia Britannica*. Encyclopædia Britannica Inc., 1999.

[101] K. G. Wilson. Renormalization Group and Critical Phenomena. I. Renormalization Group and the Kadanoff Scaling Picture. *Phys. Rev. B*, **4**, 3174–3183, 1971.

[102] K. G. Wilson. Renormalization Group and Critical Phenomena. II. Phase-Space Cell Analysis of Critical Behavior. *Phys. Rev. B*, **4**, 3184–3205, 1971.

[103] I. J. Wygnanski and F. H. Champagne. On transition in a pipe. Part 1. The origin of puffs and slugs and the flow in a turbulent slug. *J. Fluid. Mech.*, **59**, 281–335, 1973.

[104] Y. Yeh and H. Z. Cummins. Localized fluid flow measurements with an He-Ne laser spectrometer. *Appl. Phys. Lett.*, **4**, 176–178, 1964.

[105] H. Zhu. Non-parametric Analysis of Gap Times for Multiple Event Data: An Overview. *Int. Stat. Rev.*, **82**, 106–122, 2014.

[106] J. Zhuo, S. Redner, and H. Park. Critical behaviour of an interacting surface reaction model. *J. Phys. A: Math. Gen.*, **26**, 4197–4213, 1993.